DESIGN OF SOLID STATE NEUTRON DETECTORS USING GEANT4 SIMULATION

By

MANOJ KUMAR PARIDA

Enrollment No.: ENGG02201304003

Indira Gandhi Centre for Atomic Research, Kalpakkam

A thesis submitted to the

Board of Studies in Engineering Sciences

In partial fulfillment of requirements

for the Degree of

DOCTOR OF PHILOSOPHY

Of

HOMI BHABHA NATIONAL INSTITUTE

May, 2019

Homi Bhabha National Institute

Recommendations of the Viva Voce Committee

As members of the Viva Voce Committee, we certify that we have read the dissertation prepared by **Manoj Kumar Parida** entitled **"Design of solid state neutron detectors using GEANT4 simulation"** and recommend that it may be accepted as fulfilling the thesis requirement for the award of Degree of Doctor of Philosophy.

G. Amarendra May 24, 2019

Chairman – Dr. G. Amarendra **Date:**

S. Tripura Sundari 24/5/19.

Guide / Convener – Dr. S. Tripura Sundari **Date:**

24/5/19

Examiner - Dr. Pradeep Sarin **Date:**

BPCRao 24/5/19

Member 1- Dr. B. P. C. Rao **Date:**

24 / May / 19

Member 2- Dr. S. Sivakumar **Date:**

Technology Advisor-Dr. K. Prabakar **Date:**

24/5/19

Final approval and acceptance of this thesis is contingent upon the candidate's submission of the final copies of the thesis to HBNI.

I hereby certify that I have read this thesis prepared under my direction and recommend that it may be accepted as fulfilling the thesis requirement.

Date:

S. Tripura Sundari 24/5/19

Place: Indira Gandhi Centre for Atomic research, Kalpakkam. **Guide/ Convener**

STATEMENT BY AUTHOR

This dissertation has been submitted in partial fulfillment of requirements for an advanced degree at Homi Bhabha National Institute (HBNI) and is deposited in the Library to be made available to borrowers under rules of the HBNI.

Brief quotations from this dissertation are allowable without special permission, provided that accurate acknowledgement of source is made. Requests for permission for extended quotation from or reproduction of this manuscript in whole or in part may be granted by the Competent Authority of HBNI when in his or her judgment the proposed use of the material is in the interests of scholarship. In all other instances, however, permission must be obtained from the author.

Manoj Kumar Parida

(Manoj Kumar Parida)

DECLARATION

I, hereby declare that the investigation presented in the thesis has been carried out by me. The work is original and has not been submitted earlier as a whole or in part for a degree / diploma at this or any other Institution / University.

Manoj Kumar Parida

(Manoj Kumar Parida)

LIST OF PUBLICATIONS ARISING FROM THE THESIS

Journal

a. <u>Published</u>

1. "Efficiency of depleted UO_2 based semiconductor neutron detectors in direct and indirect configuration- A GEANT4 simulation study" **<u>Manoj Kumar Parida</u>**, K.Prabakar and S.T.Sundari, **Journal of Instrumentation**, Vol. 13. P03006. 2018. doi:10.1088/17480221/13/03/P03006.

2. "Current-Voltage characteristics of Silicon PIN diodes irradiated in KAMINI nuclear reactor" **<u>Manoj Kumar Parida</u>**, S.Tripura Sundari, V. Sathiamoorthy and S.Sivakumar, **Nuclear Instruments Method in Physics Research A**, Vol.905, pp 129-137, 2018. doi.org/10.1016/j.nima.2018.07.014

b. <u>Under Revision:</u>

1. "Boric acid as converter material for semiconductor neutron detector- A GEANT4 Simulation study "
   <u>Manoj Kumar Parida</u>, S.Tripura Sundari and K.Prabakar, under revision in **Nuclear Instruments Method in Physics Research A**, journal**.**

c. <u>Patent application filing:</u>

1. "Solid state thermal neutron detector based on boron based material"
   Prof. Navakanta Bhat, Prof. S.A. Sivasankar, Dr. Ravi Naik, Dr. Vijay Mishra, Dr. S. Tripura Sundari, Dr. K. Prabakar and **<u>Manoj Kumar Parida</u>**, Patent under filling in Collaboration with IISc.

Conference/Symposium

1. "Efficiency of Depleted UO_2 Based Semiconductor Neutron Detectors- A Monte Carlo Simulation Study" **Manoj Kumar Parida**, K. Prabakar, S. Tripura Sundari and M. Raghuramaiah, AIP Conference Proceedings; (DOI: 10.1063/1.4980709.)

2. "Efficiency of Boric Acid Coated Semiconductor Neutron Detector - A Monte-Carlo Simulation Study " **Manoj Kumar Parida**, K.Prabakar, G.Prasanna and S.Tripura Sundari, 2017 14th IEEE India Council International Conference (INDICON) (DOI: 10.1109/INDICON.2017.8487978).

3. "Efficiency of ^{10}B based stacked semiconductor neutron detector - A GEANT4 simulation" **Manoj Kumar Parida** and S.Tripura Sundari, was presented in Research Scholar Meet–HBNI-2018 held at IGCAR, Kalpakkam; Received Best Research Contribution award for oral presentation.

Manoj Kumar Parida.

(Manoj Kumar Parida)

Dedicated to my beloved and loving parents and

my sister

Also like to dedicate to my Loving Grandparents.

ACKNOWLEDGEMENT

My research work could not have been realized without the support of many people. I would like to take this opportunity to express my heartfelt gratitude to all those who helped and supported me throughout my Ph.D.

First of all, I owe my deep sense of gratitude to my research supervisor and guide, **Dr. S. Tripura Sundari** (Head, EIS, IGCAR) for her magnanimity in spending her valuable time and restless effort with her invaluable guidance, critical and constructive suggestions, constant encouragement throughout my research work and in preparing this thesis and helping me to write all my journal paper manuscripts. I am very much grateful to **Dr. K. Prabakar** (SO/F, EIS, IGCAR) for his invaluable inputs, constant encouragement, fruitful suggestion and extending his full support at each step of my research. I am also thankful to him for teaching me Photolithography technique and suggesting GEANT4 simulation in initial years of my Ph.d and also for giving corrections regarding the manuscripts and thesis.

It's my pleasure to thank my doctoral committee, **Dr. G. Amarendra** (Chairman, Director MSG), **Dr. B. P.C. Rao** (Member) for giving their valuable suggestion and feedback during the Progress meeting. I would like to give special thanks and acknowledgement to **Dr. S. Sivakumar** (Member) for giving his technical expertise in the simulation and allowing us to carry out the neutron detection and irradiation experiments. I thank all the **Professors of HBNI** who taught me various subjects during my course work in the training school. I would like to acknowledge **Dr. Sharat Chandra** for giving critical suggestion and comments for the thesis.

I am privileged to thank **Dr. A. K. Bhaduri**, (Director, IGCAR), **Dr. S. A. V. Satyamurthy** and **Dr. P. R. Vasudeva Rao,** (Ex-Director, IGCAR) for their trust and support on me. I would also like to thank both **Dr. C.S. Sundar** and **Mr. M.P.Janawadkar** (Former MSG Director) for their support and corporation. Furthermore, I sincerely thank the **Department of Atomic Energy** (DAE), India for providing the necessary financial support. I would like to sincerely express my gratitude to **Dr. M. Saibaba** (former Dean, Student affairs), **Dr. Lakshmi Narasimhan** (Dean, Student affairs), **Dr. G.Sasikala** (Dean Engineering Sciences), **Dr .N.V. Chandreskhar** (Dean Physical Science) , **Dr. Anish Kumar** (Dean Engineering Sciences) for their support and encouragement. I would also like to acknowledge the **authorities of GSO, Kalpakkam** for providing a pleasant accommodation in the enclave.

Words would be inadequate to express my gratitude to **Dr. G. Prasanna** for explaining about any research topic, electronics, alpha spectroscopy and technical inputs.

I would like to give special thanks to both **Mrs. O.K.Sheela** madam and **Mrs. Usha Rani** madam, for the help and support, also giving technical inputs about electronics during my research work. I would also like to thank **Mr. Raghu Ramiah** and **Dr.J. Jayapandian** (Former Head, EIS,) for constant encouragement. I would also like to give special thanks and acknowledgement to my lab mates **S. Balasubramanian** for critically reading my thesis, discussion we had and also **Jeevraj** and **Venkateshwara Reddy** for their helping nature. I would also thank all the project students of our lab **Sagnik** and **Vasanth.** I would also like to gratitude **Mr. N.Murali** (Former Associate Director, EIRSG) sir for giving pep talk and motivation during the first year my Ph.d.

I would like to thank **Dr. Rajaraman** (MPD, MSG) and **Dr. Abhaya** (MPD,MSG) for lending MCA card to do the experiments. I also like to acknowledge **Mr. V.Sathiamoorthy** (RPD,FBTR) and **Mrs. Radha** (RPD,FBTR) for helping to carry out the irradiation and neutron experiment. I would also thank **Mr. Jegadeesan** (MPD/MSG) for helping in installing linux platform. I would like to extend my special thanks to the **whole family of MSG** for their help and support in various ways. I would also like to thank **Mr. Ajay Rawat** (RSD,EIRSG) for his help in installing the software. I would also like to acknowledge **Mr. Krishnan** (RSD,EIRSG) for providing gamma irradiation facility to carry out the experiments. I would like to thank **Mr. Mabin Joseph** (CD, EIRSG) for helping in installing linux Operating System. I also would like to acknowledge **Mr. Kumar (**RCL) for providing Alpha Source which enabled us to carry out the alpha spectroscopy experiments.

I would also like to thank IISc CeNSE members **Prof. Navakanta Bhat**, **Prof S.A. Shivashankar, Prof. K.N.Bhat, Dr. Vijay Mishra, Dr.Prabhakara Rao** and **Dr. Ravi Naik** for helping in fabrication of detectors. I would also like to acknowledge **Dr. Poonraj** of Ideal Sensor for providing the PCB boards which helped us to carry out the measurements.

My very-special thanks to all my friends **Dr.S. Sriram Vignesh (Geek), Dr. Vikas Kumar Jha (Studious & Hard Working), Dr. Chandan Kumar Bhagat (Best cook & generous nature), Dr. Shivang Tripathi (Coolest captain), Dr. Nidhin T.S (Fitness trainer & Optimistic)**, **Dr. Nilakantha Meher (Singer), Dr. Padmalochan Panda (Comedian), Dr. Karuna Kar Mishra (Mentor), K.C.Sahoo, Anil Kumar Behera, Binay Kumar Sahu, Suman Sourav, Dr. Yadigiri, Dr. Varun Hassija, Alok, Dr.Santhosh, Dr.Parveen Malik (IIT Guhuwati) all my batch mates- Dr. Laxman, Dr. Variavel, Dr.Santhosh, Dr. Irshad, Dr. Perumalswamy, Dr. Radhikesh, Dr. Zaibudeen,** and **all the members of JRF Enclave both senior and junior** for their help, support and

enjoyable company. I would **specially thanks to Sarvajith** from bottom of my heart for critically reading my thesis umpteen times and also for giving fruitful suggestion.

I thank **all the members of Enclave cricket team** for the funny, entertaining and exciting moments we shared during Cricket matches. I would also like to express my heartfelt thanks to the **Mess Cook**, **Hostel in charge**, and especially to **cleaning staff** for making the stay at the enclave very pleasant and lovely one.

I would also like to thanks all my school and college friends. Special thanks to all the teachers in school and colleges who taught me at various stages of my life.

Finally, I would like to express my heartfelt gratitude to most important persons in my life that is **my parents**, especially to my **mother** for all the pain she took and without her support I would not be able to complete my research work. She was always there for me in tough times. My mother took lot of care for me from Lunch box preparation to all the support she could give. I also like to especially thank to my **father** for allowing me to purse research career and all the sacrifice he made for me. My parents love and caring nature, support for me during Ph.d time cannot be express in words and it is beyond the written text. The affection and sacrifice of my parents can never be repaid back. I would like to thank my beloved **sister** and other **family members** and **relatives** for their endless love, affection, support, and encouragement.

Above all, I thank **the Almighty,** for granting me wisdom, health and strength to undertake this research work and enabling me to take it to completion. He is the one who knows all the hardships, whose satisfaction and acceptance I seek the most.

Contents

SYNOPSIS

1. Introduction and Motivation-Chapter1

Neutron detectors are of prime importance in wide spheres of applications ranging from homeland security, dosimetry to monitoring of power levels in nuclear power plants [1,2]. However, neutron is uncharged and its detection relies on the measurement of secondary reaction products generated in matter, resulting either from a neutron capture (absorption) or scatter mechanism [3,4].Currently, neutron detectors deployed in these applications are based on He^3 gas, scintillators and thermo luminescent dosimeters [5]. All these detectors detect neutrons based on the ionized reaction-products produced either from transmutation, fission or recoil nuclei reactions. Detectors based on scintillators require high power photomultiplier tubes for their operation while thermo-luminescent dosimeters have inherently low detection efficiency, moderate gamma discrimination [5]. Therefore, He^3 gas based detectors which possess high efficiency are the most sought after. But, worldwide shortage of He^3 [6] has compelled the scientific community to look for other viable alternative detectors which can address these issues and are also easy to handle. Solid state semiconductor neutron detector is one such candidate which has inherent advantages such as low power requirement for its operation, easily integrable with active readout design and thus provide portability, compact size and low cost over their counterparts [7,8]. The simplest semiconductor neutron detector is of a two dimensional (2D) planar configuration. It consists of two regions (see figure.1), a neutron converter region and charge particle semiconductor detection region, wherein in the former region, the neutron interacts with the converter material producing charged particles while the latter region registers the event of interaction with converter [9]. In essence, the efficiency of neutron detection by solid state semiconductor neutron detectors is therefore dictated by two fundamental aspects - the conversion of neutron into charged particles and its detection. The converter material is integrated onto the top surface of electronic devices such as Si PIN diode by thin film technology.

The suitability of the converter material in the neutron detector for deployment in field measurements is subtly dependent on its ability to discriminate from the background radiation as well as its interaction cross section value, which in turn is dependent on incident neutron energy. Traditionally, ^{10}B, ^{6}Li and natural Gd are widely employed for detection of thermal neutrons [10]. Amongst the three, although Gd possesses the highest neutron interaction cross section value of 27000 barns, it is seldom employed owing to the generation of low energy electrons, which poses a problem for background radiation discrimination. Hence, B^{10} with neutron interaction cross section value of 3840 barns is the next best choice of converter material which has a moderate Q value of 2.73 MeV

[9, 10].

When a parallel beam of thermal neutrons is perpendicularly incident on a detector as shown in figure 1, it interacts with the converter and generates charged particles (Li^{7} and α). The depth at which the above interaction takes place in the converter region is probabilistic in nature. Subsequently, if any one of the generated charged particles viz., Li^{7} (0.839 MeV) or α (1.47 MeV), impinge on the Si layer, it creates electron-hole pairs through columbic interaction. The sweeping of electron-hole pairs through an appropriate bias voltage provided to the silicon PIN diode generates the electrical signal as an output pulse which is further processed by external charge sensitive pre-amplifier and associated nuclear read-out electronics chain.

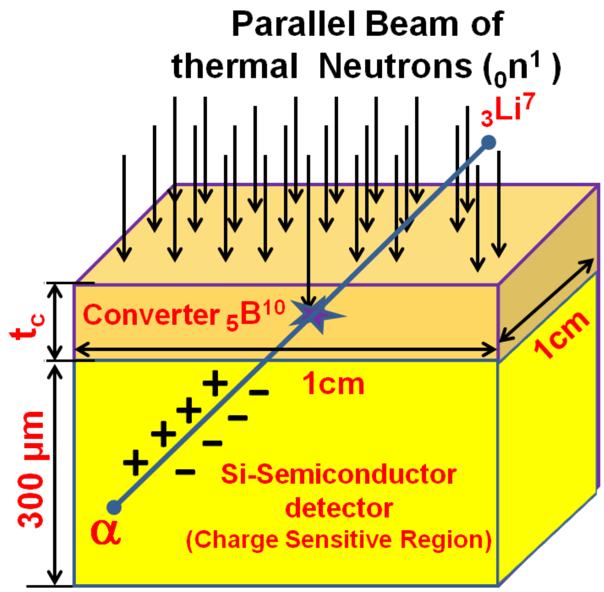

Figure 1. Planar semiconductor neutron detector configuration consists of B^{10} as converter material and Si as charge sensitive semiconductor detector region. The parallel beam of impinging thermal neutrons undergoes $B^{10}(n,\alpha)Li^7$ reaction in B^{10} converter material and produces charged particles (Li^7 and α), which will be detected in Si detector. This configuration is also known as two dimensional basic Detector Unit (DU_B).

The figure above shows a typical planar configuration detector with B^{10} as converter region and Si as charge sensitive detector region. As mentioned above, the depth or 'length' of interaction of neutron in these detectors is probabilistic. This forces an optimization for the thickness of the converter layer to a critical thickness 't_c' for maximum neutron detection efficiency (η) through simulations. For thicknesses lesser than t_c, most of the neutrons pass through the converter region, while a few interacts and which in turn generate lesser number of charged particles resulting in low η. For thicknesses larger than t_c, the generated charged particles are absorbed in the converter region itself and do not reach/ register in the silicon region, thereby leading to decrease in η. This conflicting critical thickness requirement constrains the maximum η of planar detector configuration (also known as 2D architecture). In order to overcome this problem, three dimensional (3D) architectures are adopted for the fabrication of neutron detectors [10, 11]. However, in the 3D detector also, several geometrical parameters pertaining to 'lengths' entail to be optimized from simulation to achieve maximum neutron detection efficiency.

Present thesis focuses on two aspects - GEANT4 simulation for estimating the efficiency of Semiconductor neutron detectors in various configurations (2D, 3D) with different converter materials (B^{10}, depleted UO_2) and Preliminary experimental work on the neutron sensitivity of Boron based material coated on Si PIN diode based planar neutron detector. As mentioned above, the optimum critical length is a crucial aspect in design of semiconductor neutron detector. It is prudent that prior to detector fabrication, various parameters of the detectors are warrants to be optimized for its maximum efficiency using simulation. As far as simulation in neutron detection is concerned, Monte Carlo based GEANT4 (GEometery ANd Tracking) is best known for its reliability and integrity [12]. Necessary benchmarking and validation was carried out using conventional B^{10} converter by GEANT4 simulations. Subsequent to validation with literature, extensive GEANT4 simulations were carried out for boric acid as converter material. One of the important parameters to evaluate neutron detector performance is its ability to discriminate against the background radiation. The low Q-value of neutron interaction with B^{10} sets a limitation on gamma discrimination to ~ 300 keV and therefore other converter materials such as Depleted Uranium Oxide (DUO_2) with larger gamma discriminator values ~20MeV were investigated for its efficiency in various geometers configurations. Preliminary experiments were performed to detect thermal neutrons in planar configuration using Si PIN diode coated with Boron Based material (BBM). The optimum critical coating thickness for this material was also obtained from GEANT4 simulation. All necessary precautions were taken to eliminate artefacts and minimize noises while performing the experiment on these BBM coated Si PIN diode based neutron detectors. Apart GEANT4 simulation and thermal neutron detection experiment, the present thesis also explore on the degradation in Si PIN due to neutron irradiation by I-V characteristics measurement.

2. GEANT4 Simulation Package and Experimental details - Chapter-2

The necessary theoretical background on Monte Carlo based GEANT4 simulation is outlined in chapter 2. GEANT4 is a particle tracking simulation toolkit developed by CERN with in-built physics library for the same [13, 14]. Further details like architecture of the simulation toolkit, its methodology and its adaptability to the problems addressed in the thesis are presented in this chapter. Apart from this, experimental details on the thermal neutron detection set up, alpha spectroscopy measurement and electrical characterization such as Current-Voltage (I-V) and Capacitance-Voltage (C-V) on Si PIN diodes are elucidated in detail.

It is well known that fabrication of semiconductor detectors is both time and capital intensive and therefore, it is prudent to optimize various parameters using simulations to achieve maximum detection η, prior to detector fabrication. In particular, in the design of solid state semiconductor neutron detectors, various interactions of neutrons such as scattering (elastic and inelastic) and capture with matter are random phenomena having a probabilistic distribution, which are better addressed by Monte Carlo methods. In the present thesis, extensive Monte Carlo simulations were carried out using the GEANT4 simulation toolkit for various converter materials and in different geometric configurations. In the experimental section, experimental details regarding neutron irradiation of silicon PIN diodes in KAMINI reactor and their electrical characterization (I-V and C-V) are elaborated. The details of alpha spectroscopy measurement which is mandatory for calibration of channel number to energy scale, along with details of the read-out electronics for pulse mode operation are explained. The experimental tools and procedures adopted for thermal neutron detection have also been elaborated in this chapter.

3. Benchmarking and GEANT4 Simulation of Boric acid - Chapter-3

Any simulation methodology necessitates commensurate benchmarking as a prelude for validation of results generated by the simulation. In line with this, detailed benchmarking simulations for two test problems, viz., B^{10} as converter in planar and stack configuration geometries were performed and compared with existing literature [15]. The focus on benchmarking and validation is on the determination of relevant critical 'lengths' for achieving maximum η for detection of neutrons. A typical two dimensional basic Detector Unit (DU_B) for benchmarking consists of B^{10} as converter material on top of Si detector as shown in figure 1. While the planar configuration consists of one unit of DU_B, the stack configuration was designed by replicating DU_B in the third dimension.

The results of the GEANT4 simulation (snapshot in figure 2) for planar and stack configuration are in excellent agreement with literature [15]. A maximum η for the planar configuration consisting of 100% enriched B^{10} elemental boron as converter material and Si as charged particle detector material obtained from the GEANT4 simulation was 4.01% at a critical thickness of 2.5 μm. In case of stack configuration, η was found to increase with increasing number of stacks.

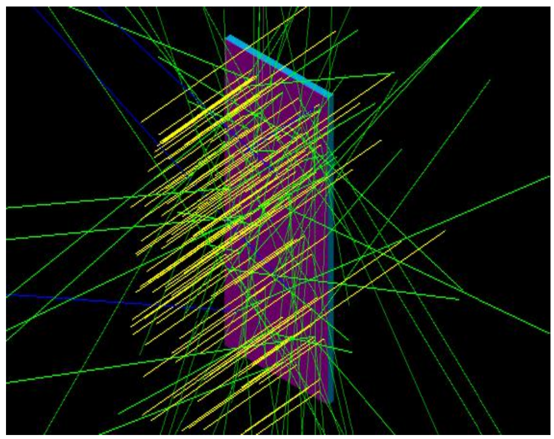

Figure 2. Snapshot of GEANT4 simulation for boron (pink color) coated on Si (Light Blue) detector in planar configuration. The yellow, green and blue lines indicate incident neutrons, emerging gamma rays and charged particles (Li^7,α), respectively.

Having validated the two test cases, the simulations were performed on boric acid as a converter material for various detector configurations like planar, stack, spherical, cylindrical perforation and cuboidal trench geometries. The choice of boric acid over conventional boron is due to its ease of handling owing its non toxic nature and coating on silicon detector. The GEANT4 simulation was carried out for different thickness of boric acid and with optimization parameters showed that a maximum detection η value of 0.73% was obtained for converter layer at critical thickness of 5 μm with 100% enriched B^{10} for planar configuration consisting of boric acid as converter material and Si as charged particle detector material.

Further, simulations pertaining to stack, sphere, cylinder and cuboid – were performed and the η were simulated for different relevant geometric 'length' parameters and B^{10} enrichments (B_E). A stack configuration detector was designed by replicating two dimensional detector units (DUs) consisting of boric acid as converter material and Si as charged particle detector material - in a third dimension. The simulation carried out for varying layer thicknesses of boric acid in stack configuration showed that η was maximum for a critical thickness (t_{sc}), but t_{sc} itself depended on the number of DUs. Detection η was also found to increase with increase in B_E and DUs. Typically, at a critical thickness of ~3.5 μm, the η for 100% B_E was found to be 15.96% for 30 DUs. For the case of sphere, cylinder and cuboids of boric acid embedded in Si, the simulations were performed for diameters and widths varying from 0.5 μm to 9.5 μm in steps of 0.5μm. In particular for cylinder and cuboid geometries, the depth was also varied from 25 μm to 275 μm with a step size of 25 μm. Although the simulated η increased with diameters and depths for sphere, cylinder and cuboids configurations, they showed a maximum η at critical dimensions between 8-9 μm of diameters and widths. Apart from the simulated η estimation, histoplots depicting the energy deposited in Si detector region by the generated charge particles (Li^7 and α) upon neutron interaction in boric acid have also been studied for various thickness, diameter and width of the detector.

4. GEANT4 simulation of Depleted UO_2 -Chapter-4

In chapter 3, boric acid was explored as converter material for the detection of thermal neutrons. However, the Q value for B^{10} interaction with neutron is ~2.7 MeV which forbids of setting Low Level Discriminator (LLD) values larger than 300 keV. Whereas, the typical energies of background gamma radiation in the nuclear reactor are in the higher range of ~ 11 MeV [16] which forbids the usage of boric acid converter material. Therefore, an alternative converter with better gamma discrimination which is of vital importance in radiation field applications is desirable. Neutron sensitive materials like the Depleted Uranium Oxide (DUO_2) which has the advantage of higher LLD setting (as high as 20 MeV) are being explored in literature [17]. Chapter 4 presents results and discussions of GEANT4 simulations for depleted DUO_2 as converter material, in both two dimensional and three dimensional (3D) configurations. In two dimensional cases, both direct and indirect configurations detectors were explored, while in the three dimensional case, cylindrical perforation and trench structure configurations were explored. As DUO_2 can be used for detection of thermal and fast neutrons, the simulations were conducted for neutrons of variable energy viz., thermal (25 meV) and fast (1 to 10 MeV). The neutrons were incident on varying thicknesses (0.25 μm to 1000 μm), diameters (1 μm to 9 μm) and widths (1 μm to 9 μm) along with depths (50 μm to 275 μm) of DUO_2 for planar, cylindrical perforated and trench structures, respectively. In the case of direct planar detectors, η was found to increase with the thickness of DUO_2 and the rate at which η increased was found to follow the macroscopic fission cross section at the corresponding neutron energy. In the case of indirect planar detector, η was lower as compared to direct configuration and was found to saturate beyond a thickness of ~3 μm. This saturation is explained on the basis of mean free path of neutrons in the DUO_2 material. For the 3D perforated silicon detectors of cylindrical (trench) geometry, backfilled with DUO_2, the η for detection of thermal neutrons ~25 meV and fast neutrons ~ typical energy of 10MeV was found to be ~0.0159% (~0.0177%) and ~0.0088% (~0.0098%), respectively. These η values were two (one) order values higher than planar indirect detector for thermal (fast) neutrons. Histogram plots were also obtained from the GEANT4 simulations to monitor the energy distribution of fission products in planar (direct and indirect) and 3D geometry (cylindrical and trench) configurations. These plots revealed that, for all the detector configurations, the energy deposited by the fission products are higher as compared to the typical gamma ray background. Thus, for detectors with DUO_2 as converter material, higher values of LLD (20 MeV) can be set, so as to achieve good background discrimination.

5. Neutron Detection Experiment- Chapter-5

This chapter describes the preliminary experimental details and results on the detection of thermal neutrons using Si PIN diode coated with Boron Based Material (BBM) in planar configuration. An experimental effort was made to fabricate a prototype thermal neutron detector in collaboration with IISc, Bengaluru, using BBM and test it for its thermal neutron detection. The BBM of optimum thickness arrived from GEANT4 simulation was coated on commercial Si PIN diodes to make a prototype test detector. The electrical characterization in the form of reverse I-V and C-V measurements were carried out on Si PIN diode prior to and after BBM coating. A typical reverse current and capacitance of 122 nA and 50 pF, respectively, were obtained at a reverse bias voltage of 100V. As I-V, C-V measurements prior to and after BBM coating did not show any significant change, it was concluded that the BBM coating has not affected the electrical behavior of diodes i.e. acts as a passive layer. The uncoated Si PIN diodes were also tested for its sensitivity to alpha particles using triple energy (Pu^{239}-5.155 MeV, Am^{241}-5.486 MeV and Cm^{244} -5.805 MeV) alpha source. The experiments revealed that the Si PIN diode had a resolution of 30 keV for the triple energy alpha source, i.e., the three peaks corresponding to their energies were resolvable. The BBM coated diode was then subjected to calibrated Am-Be neutron source which was moderated by 80 cm thick graphite [18] to generate neutrons in thermal energy range. It is to be noted that the neutron measurements were carried out in pulse mode. A standard read-out electronics chain consisting of charge sensitive preamplifier, spectroscopy amplifier and Multi Channel Analyzer (MCA) was used for acquiring the signal as counts vs channel number. Noise due to Electromagnetic Interference (EMI) was encountered in the process of data acquisition and was reduced by performing the measurements in a specially designed aluminum chamber. Moreover, the detector was operated at low reverse bias voltage to improve the gamma discrimination [19]. The uncoated Si PIN diode was also subjected to the neutron source for estimating the background contribution due to gamma radiation. The channel number to energy scale conversion was carried out using alpha spectroscopy experiment. The alpha experiment was performed on the uncoated Si PIN diode at the same electrical setting of neutron experiment, like the reverse bias supply to diode, gain and shaping time of spectroscopy amplifier. The neutron detection experiments results revealed that compared to uncoated Si PIN diode, the BBM coated Si PIN diode showed the plateau type behaviour around ~1.4 MeV energy ranges which is indeed due to the charged particles generated in B^{10} (n,α) Li^{7} reactions and hence confirms that BBM coated Si PIN diode are detecting thermal neutrons.

6. Effect of Neutron irradiation on I-V characteristics of Si PIN diode - Chapter-6.

Chapter 6 discusses the investigation of I-V characteristics of commercial planar Si-PIN diodes procured from M/s BEL Bengaluru, irradiated in a typical thermal nuclear reactor – KAMINI for neutron fluences ranging from $1x10^{14}$ to $1x10^{16}$ n/cm^2. The I-V characteristics of the virgin and neutron irradiated Si-PIN diodes are measured in ambient environment for the forward and reverse biased conditions. Analysis of forward characteristics, based on conventional diode equation in the voltage ranges below and above knee voltage, revealed increase in ideality factor from a typical value of ~2 for virgin diode to anomalous value of ~496 for the highest irradiated specimen. This increase is attributed to the damage that the diodes undergo upon irradiation. Another significant consequence of increasing the neutron irradiation fluence is the increase in knee voltage from ~ 0.5 V for virgin diode to 37.4 V for $1x10^{16}$ n/cm^2 irradiated diode specimen, without any electrical breakdown of the diode. Another consequence of the increasing neutron damage is four orders increase in the magnitude of reverse leakage current (from ~10^{-9}A to 10^{-5}A) measured under reverse bias condition. A qualitative analysis of the forward and reverse I-V characteristics, showed that the diodes change from a rectifying to ohmic behaviour with increase in fluence and this was inferred from the decrease in ‘gap’ between the forward and reverse currents in the low voltage regions. Quantitatively, the rectification ratio - ratio of the forward to reverse currents –was calculated to be 10^8 and 84 for the virgin and $1x10^{16}$ n/cm^2 irradiated specimens, respectively. The damage constant evaluated from the reverse bias I-V measurements conditions was found to be 1.7683×10^{-18} A/cm.

7. Summary, conclusions and Scope for future research –Chapter-7.

The thesis ends with the summary, conclusion and future scope which are briefly spelt out in chapter -7.

8. Organization of thesis

In summary, the findings and research contribution are documented and organized in seven chapters.

Chapter 1 introduces the motivation of the thesis along with literature on the current scenario on 1) simulation of converter materials suitable for neutron detectors using GEANT4, in particular, 2) neutron detector fabrication and detection using a boron based material and 3) neutron radiation damage on the I-V characteristics of Si PIN diodes.

Chapter 2 discusses the various simulation and experimental tools adopted during the course of research. The basics of Monte Carlo (MC) based GEANT4 simulation toolkit with a brief outline of its architecture is presented. Details of experimental tools such as current-voltage measurements (I-V), capacitance-voltage (C-V), alpha spectroscopy, neutron detection, Si PIN diode for irradiation are also discussed in this chapter.

Chapter 3 explains the details of the benchmarking procedure of GEANT4 simulations, followed by detailed simulations and optimizations of appropriate lengths for boric acid as converter material, in planar and three dimensional configurations for efficiency of neutron detection.

Chapter 4 discusses in detail optimization of the associated geometrical lengths for different configurations using GEANT4 for depleted UO_2 as a converter material in order to yield maximum efficiency for thermal and fast neutron detection. This chapter discusses the depleted UO_2 based detector in direct/ indirect and three dimensional configurations such as cylindrical perforation and cuboidal trench design structures.

Chapter 5 focuses on documenting the attempts made in fabricating thermal neutron detectors based on boron based material coated on Si PIN diode and experiments on the thermal neutrons detection.

Chapter 6 describes the changes in current voltage (I-V) characteristics on Si PIN diodes before and after neutron irradiation in a predominantly thermal nuclear reactor – KAMINI -with a particular emphasis on diode parameters such as knee voltage, ideality factor and rectification ratio.

Chapter 7 presents summary, conclusions and scope of future research.

References

[1] S. Fetter *et al.*, "Detecting nuclear warheads," *Sci. Glob. Secur.*, vol. 1, no. 3–4, pp. 225–253, 1990.

[2] C. Guardiola *et al.*, "Ultra-thin 3D silicon sensors for neutron detection," *J. Instrum.*, vol. 7, no. 03, p. P03006, 2012.

[3] J. Chadwick, “The existence of a neutron,” *Proc. R. Soc. Lond. A*, vol. 136, no. 830, pp. 692–708, Jun. 1932.

[4] P. Rinard, *Neutron Interaction with Matter-Chapter-12, Passive Nondestructive Assay of Nuclear mater*ials, US Nuclear Regulatory Commission Washington DC, Los Alamos National Lab,March 1991.

[5] G. F. Knoll, *Radiation Detection and Measurement*. John Wiley & Sons, 2010.

[6] R. T. Kouzes *et al.*, “Neutron detection alternatives to 3He for national security applications,” *Nucl. Instrum. Methods Phys. Res. Sect. Accel. Spectrometers Detect. Assoc. Equip.*, vol. 623, no. 3, pp. 1035–1045, Nov. 2010.

[7] G.Lutz, *Semiconductor Radiation Detectors: Device Physics*, Springer, (1999).

[8] A. N. Caruso, *The physics of solid-state neutron detector materials and geometries*, *J. Phys. Condens. Matter***22**, (2010) 443201.

[9] D. S. McGregor, R. T. Klann, H. K. Gersch, and J. D. Sanders, “Designs for thin-film-coated semiconductor thermal neutron detectors,” in *2001 IEEE Nuclear Science Symposium Conference Record (Cat. No.01CH37310)*, 2001, vol. 4, pp. 2454–2458.

[10] D. S. McGregor, S. L. Bellinger, and J. K. Shultis, “Present status of microstructured semiconductor neutron detectors,” *Journal of Crystal Growth*, vol. 379, no. Supplement C, pp. 99–110, Sep. 2013.

[11] R.J. Nikolic, Chin Li Chung, C.E. Reinhardt and T.F. Wang, *Roadmap for High Efficiency Solid-State Neutron Detectors*, *Proc. SPIE* **6013** (2005) 601305.

[12] C. Guardiola, K. Amgarou, F. García, C. Fleta, D. Quirion, and M. Lozano, “Geant4 and MCNPX simulations of thermal neutron detection with planar silicon detectors,” *J. Instrum.*, vol. 6, no. 09, p. T09001, 2011.

[13] S. Agostinelli *et al.*, “Geant4—a simulation toolkit,” *Nucl. Instrum. Methods Phys. Res. Sect. Accel. Spectrometers Detect. Assoc. Equip.*, vol. 506, no. 3, pp. 250–303, Jul. 2003.

[14] J. Allison *et al.*, "Geant4 developments and applications," *IEEE Trans. Nucl. Sci.*, vol. 53, no. 1, pp. 270–278, Feb. 2006.

[15] D. S. McGregor, M. D. Hammig, Y.-H. Yang, H. K. Gersch, and R. T Klann, "Design considerations for thin film coated semiconductor thermal neutron detectors—I: basics regarding alpha particle emitting neutron reactive films," *Nucl. Instrum. Methods Phys. Res. Sect. Accel. Spectrometers Detect. Assoc. Equip.*, vol. 500, no. 1, pp. 272–308, Mar. 2003.

[16] L. Jarczyk, H. Knoepfel, J. Lang, R. Müller, and W. Wölfli, "The nuclear reactor as a high intensity source for discrete gamma rays up to 11 MeV," *Nucl. Instrum. Methods*, vol. 13, no. Supplement C, pp. 287–296, Aug. 1961.

[17] C. A. Kruschwitz *et al.*, "Semiconductor neutron detectors using depleted uranium oxide," presented at the Hard X-Ray, Gamma-Ray, and Neutron Detector Physics XVI, 2014, vol. 9213, p. 92130C.

[18] I.Murataa, I.Tsudaa, R. Nakamuraa, S. Nakayamab , M. Matsumotb and H. Miyamaruc, "Neutron and gamma-ray source-term characterization of AmBe sources in Osaka University," Progress in Nuclear Science and Technology, vol. 4, pp. 345-348, April 2014.

[19] A. Singh, and A. Topkar, "Thin Epitaxial Silicon PIN Detectors for Thermal Neutron Detection with Improved Gamma (γ) Discrimination ," AIP Conference Proceedings, vol. 1731, pp. 1-3, May 2016.

List of Figures

LIST OF TABLES

Chapter-1

Introduction and Motivation

Neutron is a subatomic particle that does not carry any electric charge and therefore does not ionize matter directly [1]. It is highly penetrating and traverses considerably large distances into matter without being detected. Unlike other radiations like alpha and beta particles, the detection of neutrons poses challenges as it mainly relies on the measurement of parameters of products generated in matter by secondary reactions, resulting either from neutron capture (absorption) or scatter mechanism [2]. The design/fabrication of neutron detector warrants an understanding of neutron matter interaction and is presented in the following section.

1.1 Neutron matter Interaction

As neutron detection is strongly contingent on the mechanism of its interaction with matter, viz., capture or scattering (see figure 1.1), along with the choice of target material for its detection is also of paramount importance [2,3].

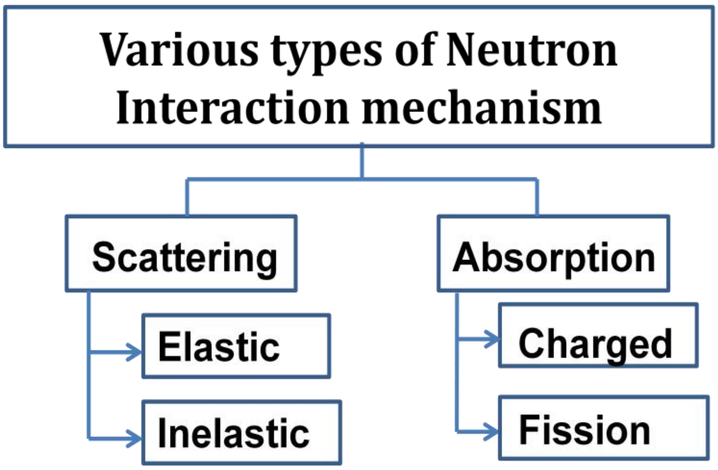

Figure 1.1. Various mechanisms of neutron interactions with matter.

In neutron capture mechanism, the incident neutrons get absorbed by atomic nucleus of target material. This causes nucleus to become unstable, which promptly decays either through the emission of charged particles such as alpha or fission into heavy ions. These emitted charge particles from neutron capture reactions are then detected by a charge sensitive detecting medium which indirectly registers the neutron's presence. In neutron scattering mechanism, the interactions are either elastic or inelastic depending on how the energy and momentum transfer of incident neutron is conveyed to the target matter. Thus, depending on the type of interaction the neutron undergoes i.e., capture or scattering, its incidence direction and energy will be changed or it can get transmuted into secondary charged particles such as alpha. A very important aspect of the type of interaction that the neutron undergoes with the matter depends on the cross sectional value or equivalently, the target area presented by the nucleus to the incident neutron, which in turn depends strongly on the energy of impinging neutron. Larger the neutron cross sectional values of matter, higher the probability of neutron interacting with that target matter. Therefore, the detection of neutron is based on the type of interaction mechanism it undergoes with matter. The following section discusses the applications of neutron detector in diverse areas and various types of neutron detectors.

1.2 Important applications and parameters of neutron detectors

Neutron detectors are of prime importance in vast spheres of applications as shown in figure 1.2.

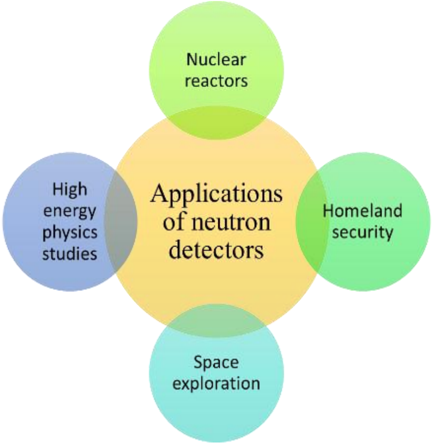

Figure 1.2. Prominent areas of applications of neutron detectors.

1. The first and foremost application is in nuclear power plants to monitor power level, as it is linearly proportional to neutron flux [3].

2. The other major application is in homeland security to prevent smuggling of special nuclear materials such as U^{235}, Pu^{239} etc. These special nuclear materials may be illicitly taken by terrorist's organization to carry out nefarious activities like building improvised nuclear weapons or dirty bombs [4].

3. Neutron detectors are also essential in space exploration/nuclear reactors to monitor the neutron dose received by astronauts/personnel in real time [5].

4. It is employed as a particle tracker in high energy physics experiments [5].

Neutron detectors employed for the above applications possess certain basic parameters/features as listed below [6].

1. Intrinsic detection efficiency: It is defined as the ratio of number of neutron interaction events recorded by the detector to the number of neutrons incident on the detector.

2. Geometric detection efficiency: It is the solid angle that the detector presents to the neutron source.

3. Absolute efficiency: It is the product of intrinsic and geometric detection efficiency. For a given geometry, it is the ratio of the number of neutrons detected to the total number of neutrons emitted by the source.

4. Gamma discrimination: It is the ability of a detector to reject the gamma radiation considered as background, vis-a-vis the radiation of interest, namely the neutrons here. This is an essential parameter because neutrons are inherently accompanied by gamma radiation [6]. This parameter is decided by a threshold voltage electronically and also by a Low Level Discriminator (LLD) value.

5. Sensitivity: It is the capability of a detector to generate a genuine and valid detector signal in response to a radiation source. Weaker the radiation source, the more sensitive should be the detector.

6. Dead time: It is the minimum time taken by a detector to recover and start processing another radiation pulse signal. The dead time characteristics are set by the associated read out electronics and detector.

Among all important parameters mentioned above, intrinsic neutron detection efficiency (η) and gamma discrimination factors are the most crucial parameters essential for the evaluation of performance of any neutron detector [6] for field applications. In the present thesis, our focus is directed towards these two aspects.

Currently, neutron detectors deployed in above mentioned applications are based on He^3 gas, scintillators and thermo luminescent dosimeters [5]. Amongst them, He^3 gas based detectors which possess the highest neutron detection efficiency are the most sought after. All these detectors detect neutrons based on ionized reaction-products produced either from transmutation, fission or recoil nuclei reactions. Detectors based on scintillators require high power photomultiplier tube, while thermo-luminescent dosimeter has inherent low neutron detection efficiency and moderate gamma discrimination [5]. Although He^3 gas based detector is the most efficient, yet worldwide shortage of He^3 [7] has compelled the scientific community to look for other viable alternative detectors which can address these issues and are also easy to handle.

Solid state semiconductor neutron detector is one such candidate which has inherent advantages such as low power requirement for its operation, easily integratable with active read out electronics design, cost effective and compact size, thus providing portability over the other [6,8,9,10]. Hence, it is imperative to discuss the semiconductor neutron detector design and its working principle, which is delineated in next section.

1.3 Semiconductor Neutron Detector - Working principle

Semiconductor neutron detector is classically conceived as a solid state ionization chamber with high density and large stopping power. It collects the electron and hole (e-h) pairs created by impinging charged particles, in much smaller volume than that needed by a gas or scintillator detector. Thus, they are compact in size. The simplest semiconductor neutron detector design is of two dimensional (2D) planar configuration type [10]. It consists of two regions (see figure 1.3), a neutron sensitive converter region comprising of the converter material and the charge particle detection region. In the former region, neutron interacts and generates charged particles while the latter region registers the event of interaction with converter. In other words, it detects the charged particles generated in the converter region.

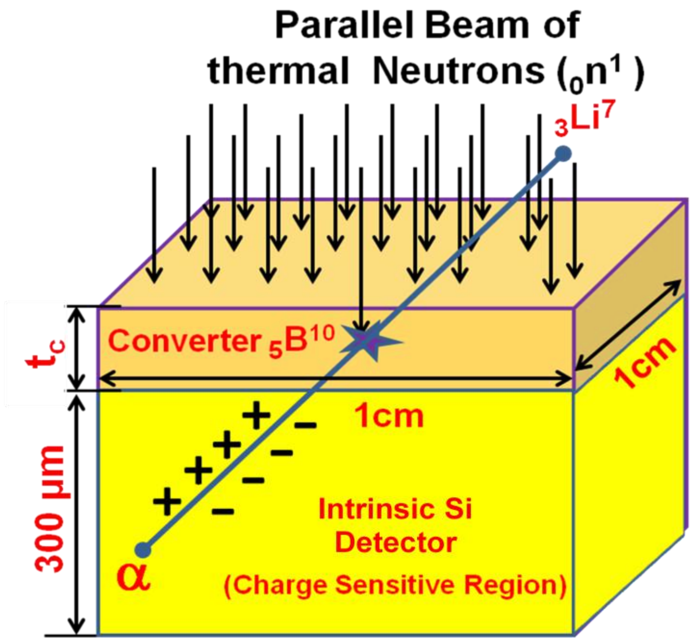

Figure 1.3. Semiconductor neutron detector in planar configuration consists of neutron sensitive converter region and charge sensitive region which is based on intrinsic type of Si.

The principle of thermal neutron detection is that, when a parallel beam of thermal neutrons are perpendicularly incident on a detector as shown in figure 1.3, it interacts with the converter material (say, ^{10}B) and generates charged particles ^{7}Li and α as depicted in equation (1) [6,10].

$$ {}^{10}_{5}\mathbf{B} + {}^{1}_{0}\mathbf{n} \rightarrow \begin{cases} {}^{7}_{3}\mathbf{Li}\ (\mathbf{0.839\ MeV}) + {}^{4}_{2}\boldsymbol{\alpha}(\mathbf{1.47\ MeV}) - \mathbf{94}\ \% \\ {}^{7}_{3}\mathbf{Li}(\mathbf{1.015\ MeV}) + {}^{4}_{2}\boldsymbol{\alpha}(\mathbf{1.78\ MeV}) - \mathbf{6}\% \end{cases} \qquad (1) $$

The depth at which the above interaction takes place in the converter region is probabilistic in nature. Subsequently, if any one of the generated charged particles impinge on intrinsic silicon (Si) region, which is a charge sensitive medium, it creates e-h pairs through columbic interaction. The total number of e-h pairs created is proportional to the energy deposited by charged particles. The e-h pairs generate an output current pulse when they are swept across by the application of appropriate reverse bias to the Si detector. The output current pulse is further processed by external charge sensitive pre-amplifier and associated read out electronics comprising spectroscopy amplifier and Multi Channel Analyzer [8].

As seen from the above the neutron converter matter interaction, i.e., the generation of charge particles has a bearing on the neutron detection efficiency which is dependent on both the converter materials and the energy of the incident neutrons. In essence, the efficiency (η) of neutron detection by solid state semiconductor neutron detector is dictated by two fundamental aspects - the conversion of a neutron into charged particles and their detection. The efficiency (η) for a semiconductor detector is defined as the ratio of number of neutrons detected (via counting the number of charged particles reaching Si detector and depositing energy greater than a set LLD value) to the number of neutrons incident on the detector.

As the suitability of converter material in the detector for field measurements is subtly dependent on energy of the background radiation, it is important to look into various types of converter materials.

1.4 Converter material

The converter materials such as ^{10}B, ^{6}Li and natural Gd are widely employed for the detection of thermal neutrons, for which the microscopic cross section and reaction products that are generated from their interaction with thermal neutrons are shown in Table 1.1 [6,10]. For the fast neutron, converter materials based on light atomic elements like H, C are preferred as their detection principle is based on proton recoil methods [11].

Table 1.1. Different converter materials for thermal neutron detection with macroscopic cross section values and their reaction products which are generated upon thermal neutron interactions [6,10].

S.No	Neutron Sensitive Converter Material	Microscopic cross section for thermal neutrons (barns)	Reaction products (Their energies)
1.	^{155}Gd,^{157}Gd	27000	Conversion electrons -29 keV to 250 keV Prompt γ-rays – up to 9 MeV
2.	^{10}B	3840	α (1.47MeV, 1.78 MeV) ^{7}Li(0.839 MeV, 1.1 MeV)
3.	^{6}Li	940	α (2.05 MeV) ^{3}H (2.73 MeV)

As seen clearly from the table 1.1, amongst the three neutron sensitive converter materials, Gd possesses the highest microscopic cross section of 27000 barns. However, it is seldom employed owing to the generation of low energy electrons in range of few keV which are comparable to background radiation energies, and therefore poses a problem for background radiation discrimination. Hence, ^{10}B with neutron interaction cross section value of 3840 barns is the next best choice of converter material which has a moderate Q- value of 2.7 MeV [6,10]. Here, the term Q-value refers to the difference in binding energies of the interacting nuclei before and after interaction.

Though boron based converter materials are widely used for thermal neutron detection, it suffers from a major drawback of a low magnitude of Low Level Discriminator (LLD) value setting. The LLD is an evaluation parameter that is used to discriminate the genuine neutron signal against the background gamma radiation. In dense radiation environments, the Q-values of ^{10}B are either lesser than or comparable to typical background radiation [12]. So, the reaction product energy (Q-value) which sets an upper bound on the setting of LLD to higher values is therefore an impediment on the detector side, to achieve 'good' background discrimination. As discussed earlier in section 1.2, among several detector characteristics, the neutron detection efficiency 'η' and gamma ray discrimination are figures of merit for performance of solid state detector which depend critically on the material parameters of the neutron sensitive converter material and the energies of the reaction products. With these considerations, uranium 'U' and its compounds are being considered as alternative converter material for solid state neutron detectors [13] which is described briefly in upcoming section.

1.5 Alternative Converter material- DUO_2

The distinct advantage of using U as a converter material over other converter materials is that the energy of fission products released is in the range of 60 to 120 MeV, which is significantly higher than the background radiation [12]. A fission reaction for neutron upon interaction with fissile materials U or Pu liberating highly energetic fission products is shown below [14].

$$\left.\begin{matrix} {}_{0}n^{1} + {}_{92}U^{235} \\ {}_{0}n^{1} + {}_{92}U^{238} \end{matrix}\right\} \longrightarrow {}_{Z1}Y1^{A1} + {}_{Z2}Y2^{A2} + x_{0}n^{1} \tag{2}$$

where Y1 and Y2 are fission products generated with atomic numbers Z1 and Z2 having atomic masses A1 and A2, respectively, while x denotes the number of neutrons generated. A major part of the fission energy (~160 MeV) manifests as kinetic energy of fission products while the rest of it is carried away by other high energy radiations such as gamma, alpha and beta [14]. This high kinetic energy of fission products permits two major advantages

(a) Effective gamma discrimination by setting higher LLD values.

(b) High signal to noise ratio as high energy fission product generates surplus electron hole pairs inside semiconducting region.

Among various compounds of Uranium, Uranium Oxide (UO_2) is known to possess semiconducting property with a band gap of 1.3 eV [15]. UO_2 also has a unique distinction of being resistant to radiation damage [15], which facilitates its operation in harsh and highly dense radiation environment. As it is ceramic in nature, it is known to withstand much higher operating temperatures (typically 2600 K), unlike other converters like B_4C, which tends to decompose at high temperatures [15]. In particular, Depleted Uranium Oxide (DUO_2) having isotopic composition as U^{235}- 0.3% and U^{238}- 99.7% is a potential candidate for semiconductor neutron detector applications owing to its lower radiological hazard nature as compared to natural and enriched Uranium [13,16]. Moreover, it is readily available as a low level radioactive waste product after enrichment of natural uranium with U^{235} for reactor fuels [15, 16]. An added advantage of DUO_2 is that it is sensitive to both thermal and fast neutrons as it has high value of fission interaction cross section for both neutron energies [6]. Therefore, a single converter material can be used for dual neutron energies.

As mentioned/discussed in section 1.3, both the converter material and the charge sensitive detection region is important for the successful functioning of a high efficient semiconductor neutron detector. Therefore, it is worthwhile to discuss briefly on the choice of Si as a semiconductor detector material. The advantages of Si semiconductor detector material over other semiconductor materials are given below:

1. Owing to low atomic number (Z) of Si, the probability of its interaction with gamma radiation by the mechanism of photoelectric effect is lesser in comparison to other semiconductor materials such as Ge and GaAs.
2. In case of Ge, a cryostat is required for its operation as radiation detector, since its reverse leakage current at room temperature is much higher than a Si semiconductor [17], thereby limiting its application at room temperature.
3. The added advantage of Si over other semiconductors is maturity in semiconductor fabrication techniques.

As the fabrication of semiconductor neutron detectors is both time and capital intensive, it is prudent that prior to detector fabrication, various parameters of the detectors are entail to be optimize for maximum efficiency of neutron detection using simulation.

It is important to note that henceforth in the thesis; Si detector refers to intrinsic type of silicon in all types of detector configurations. The Si detector is also considered to be an ideal one i.e., the energy deposited by the charged particles in the Si detector will be perfectly converted to electron-hole (e-h) pairs which result in signal generation or in other words recombination effect is neglected.

1.6 Need for simulation

As far as simulation in neutron detection is concerned, Monte Carlo technique is implemented to optimize various parameters of detectors [2]. As mentioned in section 1.3, the depth or 'length' of interaction of neutron in these detectors is probabilistic. This forces an optimization for the thickness of converter layer to a critical thickness 't_c'(see figure 1.3) for maximum neutron detection efficiency (η_{max}). For thicknesses lesser than t_c, most of the neutrons pass through the converter region, while a few interact and generate fewer charged particles leading to low η. For thicknesses larger than t_c, the generated charged particles are absorbed in the converter region itself and do not reach/ register in the detector region, thereby leading to decrease in η.

This conflicting critical thickness requirement constrains the maximum η of planar configuration detector. In order to overcome this constraint, three dimensional (3D) architectures are adopted for the fabrication of neutron detector (see figure1.4) [18].

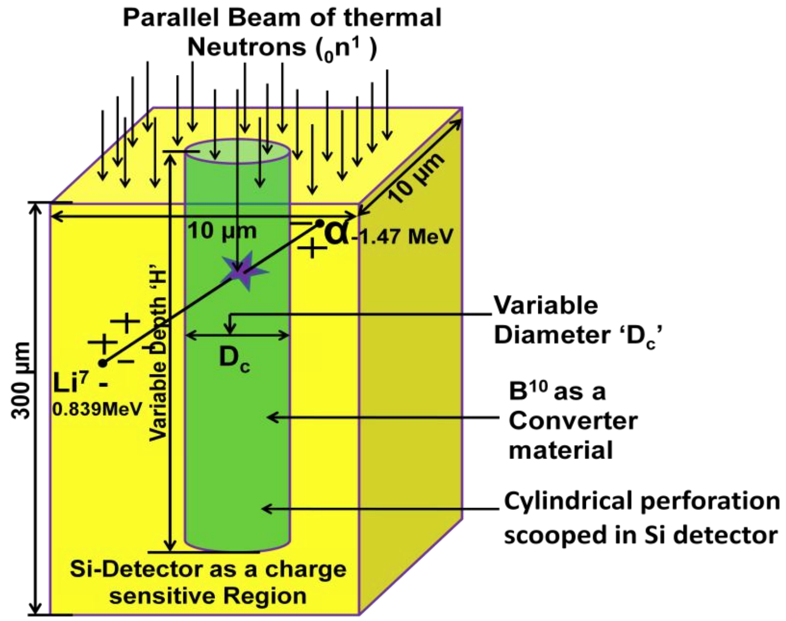

Figure 1.4. Schematic representation of a unit cell for 3D neutron detector, showing cylindrical perforations filled with converter material

However, in the 3D detector also, several geometrical parameters pertaining to 'lengths' need to be optimized from simulation so as to achieve η_{max}. GEANT4 simulation package based on Monte Carlo technique is known for its reliability and integrity [19] which is versatile and has a large repository of physics library [19,20]. It is best suited for neutron detection efficiency simulations. GEANT4 simulation toolkit is an open source and developed by CERN. Further theoretical details of GEANT4 software are elaborated in chapter 2 of this thesis.

As discussed above, simulation forms an integral core for any neutron detector fabrication. Several simulations followed by detector fabrication and subsequent neutron detection are reported in literature and a brief review of the same follows in the next section.

1.7 Brief review of literature on simulation, fabrication and experiments on solid state neutron detectors.

Several research works have been carried out in the design of solid state neutron detectors and are presented briefly in this section. McGregor et al. [21] have estimated the simulated thermal neutrons detection using LiF as a converter material for planar geometry which is found to be 4.6%. These authors have also reported [22] the improvement in the neutron detector efficiency experimentally by fabricating microstructures in Si detector and back filling with LiF converter material. They were able to achieve a neutron detection efficiency of 11.94%. S. Bellinger et al. [23] have demonstrated further improvement in thermal neutron detection experimentally by fabricating straight trench of 250 µm deep and filling with Li nano particles. They have reported much higher efficiency of 42%. S.Bellinger et al. [24] have also demonstrated neutron detection with LiF as converter material for different microstructure geometries such as hole, straight and sinusoidal pattern on Si detector. The obtained efficiencies are 9.7% (hole), 12.6% (straight) and 16.2% (sinusoidal) at 200 µm depth. J.Uher et al.[25] have performed Monte Carlo Simulation for LiF converter material and they reported a efficiency of 4.9% (planar), 6.3% (pyramidal dips) and 33% for 3D porus microstructures. S.Lo. Meo et al. [26] have performed GEANT4 simulation for LiF converter for sandwich stack configuration and corroborate with experiments. They have found GEANT4 simulation efficiency results are in good agreement with experiments. The neutron detection efficiency reported by them was 10%. Though LiF can be used as a converter material, it is hygroscopic in nature and also it has low neutron absorption cross section compared to B^{10} converter material. The low neutron absorption cross section of Li^6 leads to a requisite for fabrication of much deeper trench in Si detector which can pose a challenge.

C.Petrillo et al. [27] demonstrated neutron detection experiments using Gd based converter material but the major drawback in their experiment is the need of lead (Pb) to shield the detector against back gamma radiation since Gd converter material is sensitive to gamma radiation, which forces the LLD to be set at lower value.

A pyrolytic boron nitride based thermal neutron detector for direct configuration was studied by McGregor et al. [28]. However, in their studies they found that pyrolytic boron nitride material cannot be employed as a direct conversion detector owing to the charge transport problem associated with it. J.Uher et al. [29] have performed Monte Carlo simulation for boron nitride, they reported a simulated efficiency of 35%. B.W. Robertson et al. [30] have performed neutron detection experiments using boron carbon alloys as a converter material but the efficiency reported for the detector was of extremely low value ~ 1.3×10^{-3} %. R.J.Nikolic et al. [31] have reported thermal neutron detection efficiency of 7.3 % for B^{10} converter material. Q. Sao et al. [32] demonstrated a maximum efficiency of 48.5% for pillar array structure using B^{10} converter material, but LLD value in their studies was set at 30 keV. R.A. Muminov et al. [33] have experimentally shown for B^{10}, a efficiency of 40% for thermal neutron detection by fabricating rectangular micro pattern trenches in the Si detector and filling the micro pattern trenches with the B^{10}. R.Dahal et al. [34] carried out monte carlo simulation for honey comb microstructures detectors and reported a maximum efficiency of 45% for 95% enriched B^{10}. They have also carried out the experiment and found efficiency to be 4.5% for their detector. Incidentally, K.C.Huang et al. [35] have also reported neutron detection efficiency for honey comb microstructures in Si detector with B^{10} neutron converter material and they found efficiency of 26% for 2.5 mm^2 and 24% for 1 cm^2

detectors. They have also performed GEANT4 simulation for pulse height spectra which matches well with experiments. J.K. Shultis et al. [36] have performed detail Monte Carlo analysis on two perforation geometries namely circular holes and parallel trenches for both ^{6}LiF and B^{10} converter material. From their simulation studies they found that the efficiency of 16% for B^{10} converter material at a diameter of 6 µm for circular hole geometry, whereas in case of parallel trenches of 5 µm in width trench, they found the efficiency to be 19%. Adam M Conway et al. [37] have performed Monte Carlo analysis for pillar structured detector with dimension 2 µm x 2 µm for various depth of pillar and reported a maximum simulated efficiency 78% for B^{10} converter material. They have corroborated their simulation result for pillar depth 7 µm and 12 µm with experiments, which are in good agreement with each other. Attempts on designing neutron detectors based on alternate converter material such as DUO_2 by C.Krushtwexz et al. [13] have been also reported. A brief summary of literature review is given in table 1.2.

Table 1.2. Summary of brief literature review on solid state neutron detectors.

S.No	**Literature**	**Geometry , Converter material**	**Experimental (Exp.) / Simulation (Sim.) Efficiency**	**Remarks**
1.	McGregor et al.[21]	Planar, LiF	4.6% (Sim.)	Hygroscopic nature of converter
2.	McGregor et al.[22]	Micro structured, LiF	11.94% (Exp.)	Hygroscopic nature of converter
3.	S.Bellinger et al. [23]	Straight Trenches, LiF	42% (Exp.)	Hygroscopic nature of converter
4.	S.Bellinger et al. [24]	Micro structure pattern, LiF	9.7% (Hole), 12.6% (Straight) and 16.2% (Sinusoidal) – (Exp.)	Fabricating sinusoidal trenches in Si detector is a formidable task.
5.	J.Uher et al. [25]	Planar, Pyramidal and Porus micro structures, LiF	4.9% (Planar),6.3% (Pyramidal),33% (Porus structures) (Sim.)	Hygroscopic nature of converter
6.	S.Lo.Meo et al. [26]	Sandwich stack Configuration, LiF	10% (Exp.)	Hygroscopic nature of converter and Challenges in fabrication.

S.No	Literature	Geometry , Converter material	Experimental (Exp.) / Simulation (Sim.) Efficiency	Remarks
7.	C.Petrillo et al. [27]	Planar, Gd	Not reported	Low gamma to neutron rejection and low LLD value.
8.	McGregor et al.[28]	Direct configuration, Pyrolitic Boron Nitride	Not reported	Suffers from Charge transport issues.
9.	J.Uher et al. [29]	Direct Configuration, Boron Nitride	35% (Sim.)	Fabrication challenges.
10.	B.W. Robertson et al. [30]	Planar, Boron Carbon alloy	1.3 x 10^{-3} (Exp.)	Low efficiency
11.	R.J.Nikolic et al. [31]	Micro structured, B^{10}	7.3% (Exp.)	Low efficiency and coating complexity
12.	Q.Sao et al. [32]	Micro structured Pillar, material	48% (Exp.)	Coating complexity and low LLD value of 30 keV.
13.	R.A. Muminov et al. [33]	Rectangular Micro structured, B^{10}	40% (Exp.)	Coating complexity of B^{10} as handling B^{10} precursor diborane is toxic in nature.
14.	R Dahal et al. [34]	Honey Comb Micro structured, B^{10}	45% (Sim.) 4.5% (Exp.)	Challenge in designing Honey comb microstructures in Si.
15.	K.C.Huang et al. [34]	Honey Comb Micro structured B^{10}	26% for 2.5mm^2 detector and 24% for 1 cm^2 (Exp.)	Challenge in designing Honey comb microstructures in Si.
16.	J.K. Shultis et al. [34]	Parallel trenches and circular holes, B^{10}	16% (Trenches) and 20% (Holes) (Sim.)	Challenges in fabrication.
17.	Adam M Conway et al. [35]	Micro structured B^{10}	78% (Sim.)	Coating complexity of B^{10} as handling B^{10} precursor diborane toxic in nature.
18.	C.Krushtwexz et al. [36]	Direct Configuration, Depleted UO_2	Not reported	Maintaining stoichiometry

As seen from literature survey, extensive studies has been carried out using B^{10} as converter material and is conventionally deposited on Si using Chemical Vapour Deposition (CVD) technique, that uses diborane as a precursor. But, as diborane is toxic in nature [38], difficult to handle and expensive, alternative boron compounds are being explored. A scan of literature from Table 1.2 reveals that boric acid (H_3BO_3) is little studied as a converter material. Unlike B^{10}, this material has the advantage of being directly spin coated on Si PIN diodes using appropriate binders [39,40]. This motivated a GEANT4 simulation on boric acid, to explore it as a converter material in different configurations.

Although boron possesses high thermal neutron cross section and is suitable for detection of slow neutrons, its low Q value of 2.7 MeV (as mentioned in section 1.4) forbids the setting of LLD to high levels to achieve good gamma discrimination. As an alternative material, depleted UO_2 with a higher Q value of ~200MeV is known to achieve good gamma discrimination [13].

Having performed simulation on boric acid and DUO_2, an experimental endeavor was undertaken to fabricate a planar detector based on boron and tested for its neutron detection. The planar detectors were fabricated in collaboration with IISc by utilizing the commercial Si PIN diode coated with suitable boron based converter material.

As Si PIN diodes are used as charge particle detection medium, it is imperative to have a prior knowledge of the irradiation damage of the diodes per say on the neutron fluence. Also the Si PIN diodes are to be deployed in field conditions, the effect of neutron fluence on the semiconductor device is also of paramount importance. In this thesis, the effect of neutron irradiation on the electrical characteristics of Si PIN diodes is studied. The following section briefly describes the literature on neutron irradiation studies of Si PIN diodes.

1.8 Literature survey of neutron radiation damage on Si

The Si PIN diodes have been employed widely for neutron dosimetry in radiation environment owing to their insensitivity to micro-phonics and amenability to miniaturization [41]. Other distinct inherent advantages of these Si PIN diodes are fast signal response, low voltage operation and better energy resolution in terms of pulse height spectra [42]. Moreover, standardization of planar technology process with respect to Si PIN diodes has led to the exploration of a choice of geometries and sizes for optimization of sensitivity of the diode for neutron dose measurement [41]. However, the performances of these devices are susceptible to radiation damage especially from neutrons [43]. It is therefore imperative to study their electrical characteristics from current voltage (I-V) measurements to understand their behaviour in the presence of neutron field. The effects of neutron irradiation on semiconductor Si PIN diodes have been studied in the context of LHC (Large Hardon Collider) too [44].

Several extensive studies on the effect of neutron irradiation on the electrical characteristics have also been conducted as part of ROSE (R&D for Silicon for future Experiments) project [45]. Beattie et al. reported increase in forward voltage of the PIN diode from 10 V to 100 V with increasing neutron fluence [46], when irradiated with neutrons of 1 MeV energy. A similar investigation on I-V characteristics of irradiated Si detectors performed by Bosetti et al. [47] also reported the change in reverse and forward characteristics of diode in terms of rectification ratio, which changes drastically after critical fluence of irradiation. McPherson et al. [48] investigated the electrical characteristics of Si PIN diodes subjected to 1 MeV neutrons, both prior to and after irradiation. They concluded that the radiation damage occurs only up to certain neutron fluences and beyond that limit, the material becomes resistant to further damage. Additionally, commercial PIN diodes were characterized for their utilization as radiation monitors in LHC to cover 1 MeV equivalent neutrons by Ravotti et al. [49]. They also reported the shifting of the forward characteristics to higher voltages with increase in fluence. However, they obtained a 'thyristor' like behaviour for fluences more than $3x10^{13}$ n/cm^2. Irradiation studies conducted on Si detectors by Edwards et al. [43] indicated increase in the reverse leakage current of diode after exposure to neutrons. The increase in reverse leakage current is due to the formation of energy levels within the energy band gap [50], which aids in the thermal transition of carriers across the band gap. The I-V characteristics of non Si based materials like GaAs and GaN exposed to thermal neutron irradiation for fluences upto $3x10^{14}$ n/cm^2 have been studied by Fauzi et al. [51]. They concluded that the performance of diode degraded owing to the displacement damage due to neutrons and gamma ionization.

The above experiments have been conducted in controlled environments with respect to energy of the neutrons. However, there are not many studies on electrical characterization of Si PIN diodes when subjected to typical reactor operation condition. Hasegawa et al. [52] reported measurement of I-V characteristics of Si detectors under typical reactor operation conditions. The fluences in their study, however, were limited to $1x10^{14}$ n/cm^2. They have also not carried out any detailed analysis to study the variation of the associated diode parameters such as rectification ratio and ideality factor in particular, as a function of neutron fluence, in reactor field conditions. In the present thesis, effect of neutron irradiation on the electrical characteristics of Si PIN diodes for the typical reactor conditions was studied. The present study mainly focuses on the change in forward and reverse I-V measurement of Si PIN diode upon neutron exposure and the implications of the irradiation on device parameters such as ideality factor and rectification ratio.

The next section discusses the motivation and objective of this thesis.

1.9 Motivation and Objective of thesis

The thesis focuses on three aspects - GEANT4 simulation of converter materials to optimize geometrical parameters for maximum efficiency of neutron detection, design/fabrication of planar thermal neutron detector and to investigate the effect of neutron radiation damage on I-V characteristics of virgin Si PIN diodes.

1. GEANT4 Simulation

As the optimum critical length is a crucial aspect in design of semiconductor neutron detector and it is worthwhile to find out the critical length parameters in order to achieve η_{max} ahead of fabrication. The efficiency of semiconductor neutron detector in several different geometric configurations like planar, stack, embedded sphere, cylindrical perforation and cuboidal trench structures were explored for different converter material (boric acid and depleted UO_2) using GEANT4 simulation based on Monte Carlo method.

Necessary benchmarking and validation were carried out using conventional B^{10} converter by GEANT4 simulations. Subsequent to validation with literature, extensive GEANT4 simulations were carried out for estimating η with boric acid as a converter material. One of the most important parameter to evaluate neutron detector performance is its ability to discriminate against the background radiation. The low Q-value of neutron interaction with boron sets a limitation on gamma discrimination to ~ 300 keV and therefore other alternaive converter materials such as Depleted Uranium Oxide (DUO_2) with larger gamma discriminator values ~20 MeV were investigated for its efficiency in various configurations.

2. Neutron detection experiments

An attempt is also made to design and fabricate a prototype planar configuration thermal neutron detector in collaboration with IISc Benguluru. Preliminary experiments were performed to detect thermal neutrons in planar configuration, using Si PIN diode coated with Boron Based material[1] (BBM). The optimum critical coating thickness for this material was obtained from GEANT4 simulation and same was coated on Si PIN diode. All necessary precautions were taken to eliminate artefacts and minimize noises while performing the experiment on these BBM coated Si PIN diode based neutron detectors.

3. Investigation of radiation damage in virgin (uncoated) Si PIN diodes

Along with experimental detection of thermal neutrons, the present thesis also investigates the neutron radiation damage that takes place when virgin (uncoated) Si PIN diodes are exposed to varying neutron fluences. The main focus is to study the degradation in I-V characteristics of Si PIN due to neutron irradiation.

A point to be noted that the word 'neutron detector' used throughout the thesis means converter material with Si detector (i.e., indirect detector) except in direct configuration case where both the converter and detector are same. The Si detector refers to charge sensitive region i.e. it detects the charged particle. Both detector and Si detector are interchangeably used.

1.10 Organization of thesis

The work is entitled "Design of solid state neutron detectors using GEANT4 simulation". The findings and research contributions are documented and organized in seven chapters.

Chapter 1 introduces the motivation of the thesis along with literature on the current scenario on 1) simulation of converter materials suitable for neutron detectors using GEANT4, in particular, 2) neutron detector fabrication and detection using a boron based material and 3) neutron radiation damage on the I-V characteristics of Si PIN diodes.

[1] ***The details of the converter material is not disclosed in this thesis, as a patent application is being filed***

Chapter 2 discusses the various simulation and experimental tools adopted during the course of research. The basics of Monte Carlo (MC) based GEANT4 simulation toolkit with a brief outline of its architecture is presented. Details of experimental tools such as current-voltage measurement (I-V) set up, capacitance-voltage (C-V) measurement set up, alpha spectroscopy, neutron detection, Si PIN diode for irradiation are also discussed in this chapter.

Chapter 3 explains the details of the benchmarking procedure of GEANT4 simulations, followed by detailed simulations and optimizations of appropriate lengths for boric acid as converter material, in planar and three dimensional configurations for efficiency of neutron detection.

Chapter 4 discusses in detail optimization of the associated geometrical lengths for different configurations using GEANT4 for depleted UO_2 as a converter material in order to yield maximum efficiency for thermal and fast neutron detection. This chapter discusses the depleted UO_2 based detector in direct/ indirect and three dimensional configurations such as cylindrical perforation and cuboidal trench design structures.

Chapter 5 focuses on documenting the attempts made in fabricating thermal neutron detectors based on boron based material coated on Si PIN diode and experiments on the thermal neutrons detection.

Chapter 6 describes the changes in current voltage (I-V) characteristics on Si PIN diodes before and after neutron irradiation in a predominantly thermal nuclear reactor – KAMINI -with a particular emphasis on diode parameters such as knee voltage, ideality factor and rectification ratio.

Chapter 7 presents summary, conclusions and scope of future research.

References

[1] J. Chadwick, The existence of a neutron, Proc. R. Soc. Lond. A. 136 (1932) 692–708 doi:10.1098/rspa.1932.0112.

[2] P. Rinard, Neutron Interaction with Matter-Chapter-12, Passive Nondestructive Assay of Nuclear materials, US Nuclear Regulatory Commission Washington DC, Los Alamos National Lab,March 1991.

[3] S. Glasstone, A. Sesonske, Nuclear Reactor Engineering: Reactor Systems Engineering, Springer Science & Business Media, 2012.

[4] S. Fetter, V.A. Frolov, M. Miller, R. Mozley, O.F. Prilutsky, S.N. Rodionov, R.Z. Sagdeev, Detecting nuclear warheads, Science & Global Security. 1 (1990) 225–253.

[5] S.L.Bellinger, Advanced Microstructured Semiconductor Neutron detectors: Design, fabrication and performance, A Doctoral thesis submitted to Kansas State University (2011).

[6] A.N. Caruso, The physics of solid-state neutron detector materials and geometries, J. Phys.: Condens. Matter. 22 (2010) 443201. doi:10.1088/0953-8984/22/44/443201.

[7] R.T. Kouzes, J.H. Ely, L.E. Erikson, W.J. Kernan, A.T. Lintereur, E.R. Siciliano, D.L. Stephens, D.C. Stromswold, R.M. Van Ginhoven, M.L. Woodring, Neutron detection alternatives to 3He for national security applications, Nuclear Instruments and Methods in Physics Research Section A: Accelerators, Spectrometers, Detectors and Associated Equipment. 623 (2010) 1035–1045. doi:10.1016/j.nima.2010.08.021.

[8] H.Spieler, Semiconductor detector systems, Oxford University Press (2005).

[9] C. Guardiola, C. Fleta, G. Pellegrini, F. García, D. Quirion, J. Rodríguez, M. Lozano, Ultra-thin 3D silicon sensors for neutron detection, J. Inst. 7 (2012) P03006. doi:10.1088/1748-0221/7/03/P03006.

[10] D.S. McGregor, M.D. Hammig, Y.-H. Yang, H.K. Gersch, R.T. Klann, Design considerations for thin film coated semiconductor thermal neutron detectors—I: basics regarding alpha particle emitting neutron reactive films, Nuclear Instruments and Methods in Physics Research Section A: Accelerators, Spectrometers, Detectors and Associated Equipment. 500 (2003) 272–308. doi:10.1016/S0168-9002(02)02078-8.

[11] S. Tripathi, C. Upadhyay, C.P. Nagaraj, K. Devan, K. Madhusoodanan, S.A.V.S. Murty, Geant4 simulations of semiconductor detectors (SiC) for fast

neutron spectroscopy, in: 2015 Annual IEEE India Conference (INDICON), 2015: pp. 1–6. doi:10.1109/INDICON.2015.7443467.

[12] L. Jarczyk, H. Knoepfel, J. Lang, R. Müller, W. Wölfli, The nuclear reactor as a high intensity source for discrete gamma rays up to 11 MeV, Nuclear Instruments and Methods. 13 (1961) 287–296. doi:10.1016/0029-554X(61)90217-8.

[13] C.A. Kruschwitz, S. Mukhopadhyay, D. Schwellenbach, T. Meek, B. Shaver, T. Cunningham, J.P. Auxier, Semiconductor neutron detectors using depleted uranium oxide, in: International Society for Optics and Photonics, 2014: p. 92130C. doi:10.1117/12.2063501.

[14] C. Wagemans, The Nuclear Fission Process, CRC Press, 1991.

[15] T.Meek,M. Hu, M. J Haire,Semiconductive Properties of Uranium Oxide, in: Waste Management (2001) Symposium.

[16] J. L. Domingo, Reproductive and developmental toxicity of natural and depleted uranium: a review, Reprod. Toxicol. 15, (2001) 603.

[17] R.L.Boylestad, Electronic Devices and Circuit Theory, 11th edition, Pearson (2014).

[18] R.J. Nikolic,Chin Li Chung, C.E.Reinhardt ,T.F.Wang, Roadmap for High Efficiency Solid-State Neutron Detectors, Proceedings of SPIE , (2005)6013.

[19] S. Agostinelli et al.,Geant4—a simulation toolkit, Nuclear Instruments and Methods in Physics Research Section A: Accelerators, Spectrometers, Detectors and Associated Equipment. 506 (2003) 250–303. doi:10.1016/S0168-9002(03)01368-8

[20] J. Allison et al., Geant4 developments and applications, IEEE Transactions on Nuclear Science. 53 (2006) 270–278. doi:10.1109/TNS.2006.869826.

[21] D.S. McGregor, R.T. Klann, H.K. Gersch, J.D. Sanders, Designs for thin-film-coated semiconductor thermal neutron detectors, in: 2001 IEEE Nuclear Science Symposium Conference Record (Cat. No.01CH37310), 2001: pp. 2454–2458. doi:10.1109/NSSMIC.2001.1009315.

[22] D.S. McGregor, W.J. McNeil, S.L. Bellinger, T.C. Unruh, J.K. Shultis, Microstructured semiconductor neutron detectors, Nuclear Instruments and Methods in Physics Research Section A: Accelerators, Spectrometers,

Detectors and Associated Equipment. 608 (2009) 125–131. doi:10.1016/j.nima.2009.06.031.

[23] S.L. Bellinger, R.G. Fronk, W.J. McNeil, T.J. Sobering, D.S. McGregor, Improved High Efficiency Stacked Microstructured Neutron Detectors Backfilled With Nanoparticle6$LiF, IEEE Transactions on Nuclear Science. 59 (2012) 167–173. doi:10.1109/TNS.2011.2175749.

[24] S.L. Bellinger, W.J. McNeil, T.C. Unruh, D.S. McGregor, Characteristics of 3D Micro-Structured Semiconductor High Efficiency Neutron Detectors, IEEE Transactions on Nuclear Science. 56 (2009) 742–746. doi:10.1109/TNS.2008.2006682.

[25] J. Uher, C. Fröjdh, J. Jakůbek, C. Kenney, Z. Kohout, V. Linhart, S. Parker, S. Petersson, S. Pospíšil, G. Thungström, Characterization of 3D thermal neutron semiconductor detectors, Nuclear Instruments and Methods in Physics Research Section A: Accelerators, Spectrometers, Detectors and Associated Equipment. 576 (2007) 32–37. doi:10.1016/j.nima.2007.01.115.

[26] S.L. Meo, L. Cosentino, A. Mazzone, P. Bartolomei, P. Finocchiaro, Study of silicon+ 6 LiF thermal neutron detectors: GEANT4 simulations versus real data, Nuclear Instruments and Methods in Physics Research Section A: Accelerators, Spectrometers, Detectors and Associated Equipment. 866 (2017) 48–57. doi:10.1016/j.nima.2017.04.029.

[27] C. Petrillo, F. Sacchetti, O. Toker, N.J. Rhodes, Solid state neutron detectors, Nuclear Instruments and Methods in Physics Research Section A: Accelerators, Spectrometers, Detectors and Associated Equipment. 378 (1996) 541–551. doi:10.1016/0168-9002(96)00487-1.

[28] D.S. McGregor, T.C. Unruh, W.J. McNeil, Thermal neutron detection with pyrolytic boron nitride, Nuclear Instruments and Methods in Physics Research Section A: Accelerators, Spectrometers, Detectors and Associated Equipment. 591 (2008) 530–533. doi:10.1016/j.nima.2008.03.002.

[29] J. Uher, S. Pospisil, V. Linhart, M. Schieber, Efficiency of composite boron nitride neutron detectors in comparison with helium-3 detectors, Appl. Phys. Lett. 90 (2007) 124101. doi:10.1063/1.2713869.

[30] B.W. Robertson, S. Adenwalla, A. Harken, P. Welsch, J.I. Brand, P.A. Dowben, J.P. Claassen, A class of boron-rich solid-state neutron detectors, Appl. Phys. Lett. 80 (2002) 3644–3646. doi:10.1063/1.1477942.

[31] R.J. Nikolić, A.M. Conway, C.E. Reinhardt, R.T. Graff, T.F. Wang, N. Deo, C.L. Cheung, 6:1 aspect ratio silicon pillar based thermal neutron detector filled with B10, Appl. Phys. Lett. 93 (2008) 133502. doi:10.1063/1.2985817.

[32] Q. Shao, L.F. Voss, A.M. Conway, R.J. Nikolic, M.A. Dar, C.L. Cheung, High aspect ratio composite structures with 48.5% thermal neutron detection efficiency, Appl. Phys. Lett. 102 (2013) 063505. doi:10.1063/1.4792703.

[33] R.A. Muminov, L.D. Tsvang, High-efficiency semiconductor theramal-neutron detectors, Soviet Atomic Energy. 62 (1987) 316–319. doi:10.1007/BF01123372.

[34] R. Dahal, K.C. Huang, J. Clinton, N. LiCausi, J.-Q. Lu, Y. Danon, I. Bhat, Self-powered micro-structured solid state neutron detector with very low leakage current and high efficiency, Appl. Phys. Lett. 100 (2012) 243507. doi:10.1063/1.4729558.

[35] K.-C. Huang, R. Dahal, J.J.-Q. Lu, A. Weltz, Y. Danon, I.B. Bhat, Scalable large-area solid-state neutron detector with continuous p–n junction and extremely low leakage current, Nuclear Instruments and Methods in Physics Research Section A: Accelerators, Spectrometers, Detectors and Associated Equipment. 763 (2014) 260–265. doi:10.1016/j.nima.2014.06.047.

[36] J.K. Shultis, D.S. McGregor, Design and performance considerations for perforated semiconductor thermal-neutron detectors, Nuclear Instruments and Methods in Physics Research Section A: Accelerators, Spectrometers, Detectors and Associated Equipment. 606 (2009) 608–636. doi:10.1016/j.nima.2009.02.033.

[37] A.M. Conway, T.F. Wang, N. Deo, C.L. Cheung, R.J. Nikolic, Numerical Simulations of Pillar Structured Solid State Thermal Neutron Detector: Efficiency and Gamma Discrimination, IEEE Transactions on Nuclear Science. 56 (2009) 2802–2807. doi:10.1109/TNS.2009.2021474.

[38] T. Uemura, K. Omae, H. Nakashima, H. Sakurai, K. Yamazaki, T. Shibata, K. Mori, M. Kudo, H. Kanoh, M. Tati, Acute and subacute inhalation toxicity of diborane in male ICR mice, Arch Toxicol. 69 (1995) 397–404. doi:10.1007/s002040050190.

[39] Cardone, G. Cherubini, W. Perconti, A. Petrucci, A. Rosada, Neutron Imaging by Boric Acid, Scientific Research, vol. 1, pp. 30- 35, October 2013.

[40] G. Singh, A. Verma, R. Jeyakumar, Fabrication of c-Si solar cells using boric acid as a spin-on dopant for back surface field, RSC Adv. 4 (2013) 4225–4229. doi:10.1039/C3RA45746J.

[41] I. Anokhin, O. Zinets, A. Rosenfeld, M. Lerch, M. Yudelev, V. Perevertaylo, M. Reinhard, M. Petasecca, Studies of the Characteristics of a Silicon Neutron Sensor, IEEE Trans. Nucl. Sci. 56 (2009) 2290–2293. doi:10.1109/TNS.2009.2024150.

[42] S.J. Bates, D.J. Munday et al.,Recent results of radiation damage studies in silicon, Nucl. Instrum. Methods Phys. Res. Sect. Accel. Spectrometers Detect. Assoc. Equip. 344 (1994) 228–236. doi:10.1016/0168-9002(94)90675-0.

[43] M. Edwards, G. Hall, S. Sotthibandhu, Neutron radiation damage studies of silicon detectors, Nucl. Instrum. Methods Phys. Res. Sect. Accel. Spectrometers Detect. Assoc. Equip. 310 (1991) 283–286. doi:10.1016/0168-9002(91)91044-V.

[44] M. Moll, Development of radiation hard sensors for very high luminosity colliders—CERN-RD50 project, Nucl. Instrum. Methods Phys. Res. Sect. Accel. Spectrometers Detect. Assoc. Equip. 511 (2003) 97–105. doi:10.1016/S0168-9002(03)01772-8.

[45] G. Lindström, M. Ahmed, S. Albergo, et al.,Radiation hard silicon detectors—developments by the RD48 (ROSE) collaboration, Nucl. Instrum. Methods Phys. Res. Sect. Accel. Spectrometers Detect. Assoc. Equip. 466 (2001) 308–326. doi:10.1016/S0168-9002(01)00560-5.

[46] L.J. Beattie, A. Chilingarov, T. Sloan, Forward-bias operation of Si detectors:: a way to work in high-radiation environment, Nucl. Instrum. Methods Phys. Res. Sect. Accel. Spectrometers Detect. Assoc. Equip. 439 (2000) 293–302. doi:10.1016/S0168-9002(99)00840-2.

[47] M. Bosetti, N. Croitoru, C. Furetta, C. Leroy, S. Pensotti, P. Rancoita, M. Rattaggi, M. Redaelli, A. Seidman, Study of current-voltage characteristics of irradiated silicon detectors, Nucl. Instrum. Methods Phys. Res. Sect. B Beam Interact. Mater. At. 95 (1995) 219–224. doi:10.1016/0168-583X(94)00439-0.

[48] M. McPherson, B.K. Jones, T. Sloan, Effects of radiation damage in silicon p - i - n photodiodes, Semicond. Sci. Technol. 12 (1997) 1187. doi:10.1088/0268-1242/12/10/003.

[49] F. Ravotti, M. Glaser, M. Moll, F. Saigne, BPW34 Commercial p-i-n Diodes for High-Level 1-MeV Neutron Equivalent Fluence Monitoring, IEEE Trans. Nucl. Sci. 55 (2008) 2133–2140. doi:10.1109/TNS.2008.2000765.

[50] A. Ruzin, Recent results from the RD-48 (ROSE) Collaboration, Nucl. Instrum. Methods Phys. Res. Sect. Accel. Spectrometers Detect. Assoc. Equip. 447 (2000) 116–125. doi:10.1016/S0168-9002(00)00179-0.

[51] D.A. Fauzi, N.K.A.M. Rashid, J.A. Karim, M.R.M. Zin, N.F. Hasbullah, O.A.S. Fareed, Electrical performances of commercial GaN and GaAs based optoelectronics under neutron irradiation, IOP Conf. Ser. Mater. Sci. Eng. 53 (2013) 012029. doi:10.1088/1757-899X/53/1/012029.

[52] M. Hasegawa et al.,Radiation damage of silicon junction detectors by neutron irradiation, Nucl. Instrum. Methods Phys. Res. Sect. Accel. Spectrometers Detect. Assoc. Equip.277 (1989) 395 400.doi:10.1016/0168-9002(89)90768-7.

Chapter -2

GEANT4 Simulation package and Experimental details

This chapter outlines the details of methodology of GEANT4 simulation package including its architecture and process flow adopted in this thesis. It also discusses briefly the experimental aspects on fabrication of planar semiconductor neutron detector based on boron and subsequent detection of thermal neutrons. The experimental details pertaining to neutron irradiation and electrical characterization of silicon PIN diodes to investigate the effect of radiation damage are outlined.

2.1 Simulation

2.1.1 Monte Carlo method

Monte Carlo (MC) method is a stochastic process which uses random number sequence and probability statistics. This method developed by John Von Neumann and Stanislaw Ulam [1] has been widely employed to solve complex integro-diferential equation in the fields of physics and mathematics. Advancement in computer technology coupled with improved performance in its operations enabled this method to be used widely by scientists across the world.

Basically, MC methods are implemented in the form of computational algorithm that heavily rely on random sampling in order to estimate any relevant parameters of interest required for experiments. In context of particle transport in matter, it is very important to determine the most probabilistic path length which changes frequently due to a large number of possible interactions/events. So, instead of predicting or following the path of a single particle, it is indeed prudent to statistically consider large numbers particles that will undergo a specific type of interaction with help of MC techniques

[1,2]. Millions of particles can be simulated with specific energy and direction, such that they traverse some range in the matter based on their mean free path value [1,2].

In particular, for the design of solid state semiconductor neutron detectors, various interactions of neutrons with matter, such as scattering (elastic and inelastic), absorption or capture which are random phenomena are better addressed by MC methods [3,4]. In addition to its ability in handling probabilistic interactions, it is also possible to simulate experimental set-up [3], emulate the radiation source [3,4] and estimate the parameters of interest. The other major advantage of MC simulation is that it allows the optimization of detector design geometry which helps in reducing the cost, ahead of any detector fabrication.

The MC method is extremely versatile to the extent that experimental simulation of events, starting from the generation of neutrons with specific energy, direction and its distance from the intended target can be simulated [2,3]. As for tracking the neutron path, the implemented MC method takes a decision to simulate the type of interaction including that of generation of secondary particles, which is dependent on both the neutron energy and the magnitude of its interaction cross section with the material. The above steps are repeated several times until the neutron and the secondary particles which are generated on interaction, are either absorbed or escape the simulation boundaries. These simulations and calculations were traditionally based on MC technique had been carried out by D.S.McGregor et al. [5] using matlab tool for estimating efficiency of semiconductor neutron detector. Although the implementation with matlab is simpler, it gives fewer details on the type of interactions the neutrons undergo, generation of secondary particles etc. More sophisticated, dedicated and versatile software based on Monte Carlo methods such as MCNPX (Monte Carlo N-Particle eXtended) and GEANT4 (GEometry ANd Tracking) are employed extensively by researchers in the field of designing neutron detector [6,7,8,9,10,11,12]. A brief discussion on MCNPX and GEANT4 simulation is presented in following section.

2.1.2 MCNPX Simulation

MCNPX is an advanced version of MCNP (Monte Carlo N-Particle code) which was developed in Los Almos National Laboratory [13] and has been used extensively to study the transport and interaction of neutrons, photons and electrons in matter. Coded in Fortran90, it possesses the capability to simulate interaction of 34 fundamental particles, for energies ranging from meV to GeV using both nuclear library and various physics models [13]. K.Sedlackova et al.[14] and Adam et al. [15] have performed MCNPX simulations pertaining to fast neutron detection using SiC semiconductor and pillar structured solid state thermal neutron detector with boron as a converter material, respectively and showed excellent agreement with their experimentally obtained results. Although several other studies have been carried out with MCNPX - it is seldom used for tracking heavy charged particles in matter [16]. Moreover, it is a commercial software, which involves huge cost in procurement.

2.1.3 GEANT4 Simulation

In contrast to MCNPX, GEANT4 software is an open source and freely downloadable from GEANT4 website [17]. It is also a particle tracking simulation toolkit software package [9,18] which is based on Monte Carlo method, developed in CERN by worldwide collaboration of physicists and computer programming scientists. Several library functions and features are available in repository of GEANT4 toolkit, which offers user the versatility to cover all aspects of the detector simulation right from definition of detector in terms of its size, material, defining its sensitive region, projectile particle of interest, tracking of particle in detector, specific and relevant physics process of the particle, retention of data for detector response and to the visualization of detector through graphical interface [18]. Going by its versatility and modularity, it has been used in wide range of applications in domains of radiation physics for designing complex detector, for high energy physics experiments, as well as in nuclear medicine, space science and astrophysics [9,18]. The added advantage of GEANT4 is that, it is based on user friendly Application Programming Interface (API). The API is a collection of methods and subroutines with certain library functions which enable the developer to communicate between various software components through call subroutines [16]. This toolkit extensively uses object oriented concepts with C++ as programming language, thereby facilitating modularity in the design of software. In the subsequent section, a brief overview on the architecture of GEANT4 toolkit and process flow of the simulation used in the present work will be discussed.

2.1.4 Comparison of GEANT4 and MCNPX

Although both GEANT4 and MCNPX have been used by researchers around the world for studying physics problems, it is worthwhile to peep into their comparison. In one of the reports, Guardiola et al. [6] have evaluated detection efficiency of thermal neutrons for B^{10} converter material using GEANT4 (patch 4.9.2) and MCNPX (version 2.6.0) toolkit. They found that the maximum efficiency for thermal neutron detection was 3.3% and 5% with GEANT4 (patch 4.9.2) and MCNPX (version 2.6.0), respectively. The disagreement in efficiency between the two toolkits was due to implementation of physics processes differently [6]. In ref.6, the cross section value for interaction was taken from ENDF (Evaluated Nuclear Data File) B/VI version of library in GEANT4 (patches 4.9.2) which are more accurate for fast neutrons [19]. Moreover, neutron cross section data were constantly upgraded and ENDF B/VII version library is implemented in GEANT4 for patch 4.10.02 for the interaction of thermal neutrons.

ENDF B/VII has several advantages over ENDF B/V1 due to addition of new cross sections for more extensive neutron fission product cross sections, more precise standard cross sections and improved thermal neutron scattering [19,20]. Hence, in the present work, an upgraded patch of GEANT4 (4.10.02) with updated file (ENDF B/VII version) was implemented for simulation studies. Rotondwa Mudau et al. [21] have studied the comparison of GEANT4 (patch 4.9.5) with MCNPX (version 2.7) for neutron scattering, in order to validate the GEANT4 (patch 4.9.5) implementation of ENDF/B-VII database for nuclear interaction cross sections and also benchmarking this against MCNPX (version 2.7) for low energy neutron transport. They found good agreement between the results of GEANT4 (patch 4.9.5) and MCNPX(version 2.7). Incidentally, another studies by B. M.van der Ende et al. [22] have reported consistent results obtained from both GEANT4 (4.10.02) and MCNPX (version 2.7) simulation studies for Cf ^{252} and mono energetic thermal neutron sources (0.025 eV). S. Meo et al. [23] have performed GEANT4 simulation on LiF as converter material for thermal neutron detection and they corroborated their simulation efficiency results with experiments which are in close agreement with each other. The above reports reiterate that GEANT4 can be used for low energy neutron transport in any material. Based on the above reported literature, GEANT4 (patch 4.10.02) simulation package was employed for investigations in this thesis. Detailed architecture of GEANT4 simulation toolkit follows in next section.

2.1.5 Architecture of GEANT4 software

The schematic of GEANT4 toolkit package consists of 17 major class categories [18,24] as shown in figure 2.1. The architecture represents the hierarchical structure with a unidirectional flow, where the lower class category is used by higher class category. The bottom most and top most classes are the Global and GEANT4, respectively. The global category collects all classes, types, structures and constants which are needed in the GEANT4 toolkit.

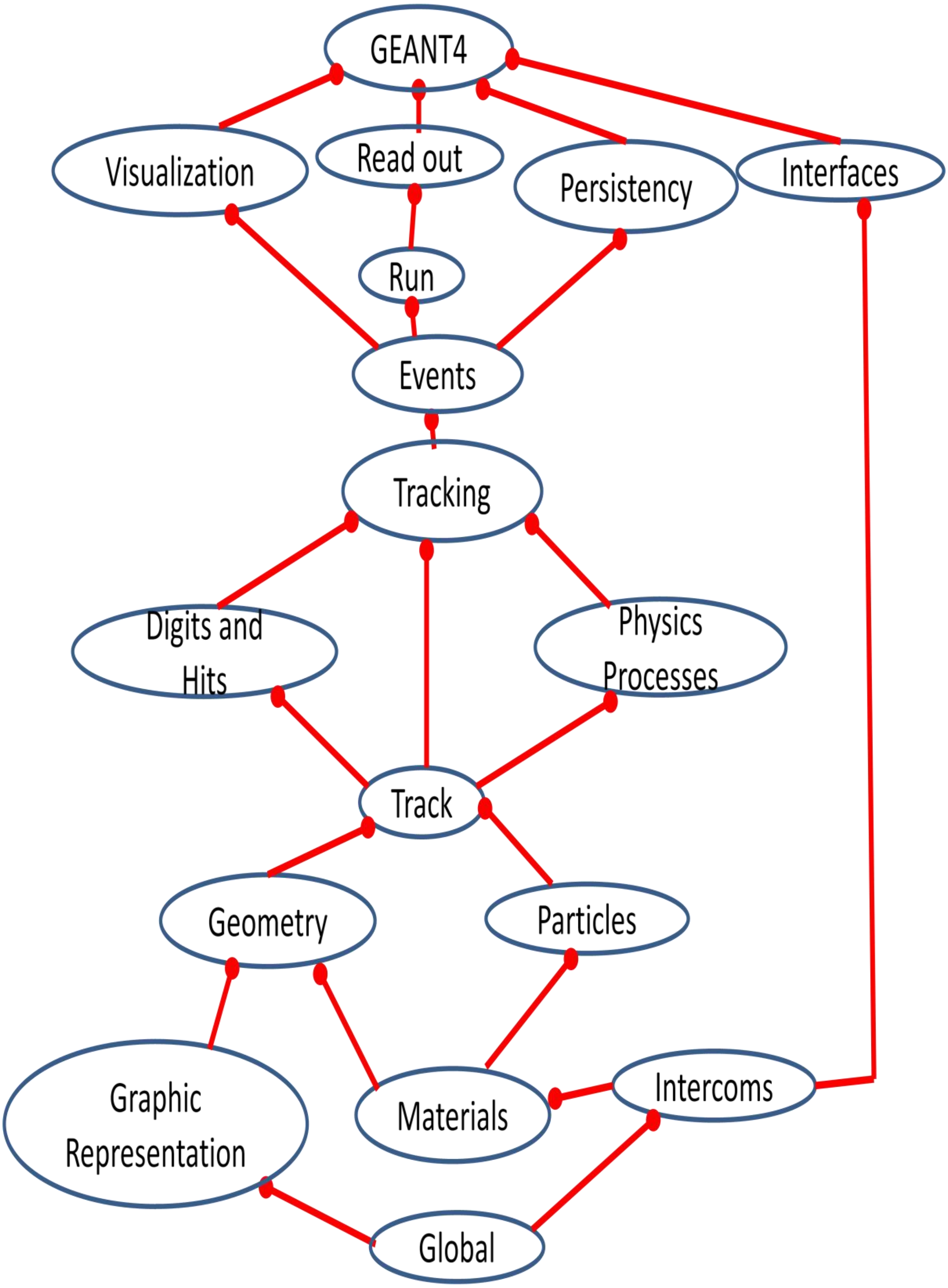

Figure 2.1. Architecture of GEANT4 simulation toolkit consisting of 17 major class categories [24].

The function of each category of toolkit is explained briefly in table 2.1 [18,24].

Table 2.1. Major functions of important category of GEANT4 Simulation toolkit.

S.No	***Category of Toolkit***	***Major Functions of Category***
1.	Geometry	• It is used to define the geometrical aspect of the detector. • In this category, the user must define the sensitive region of the detector by implementing G4VSensitive class [24]. • The other aspects of detector like dimension, orientation are also defined in the geometry category. • The detector material is defined in the geometry category using either G4Material class or NIST Material database.
2.	Particle	• It handles the definition of particles to be used in the simulation. • The user has to specify the type of particles, number of particles, position of incident particles, energy and beam direction of particles.
3.	Physics Process	• It deals with all the relevant physics processes involved in the interaction of particles in material. • The modularity of toolkit allows users to implement multiple physics models per interaction. • Physics models based on the energy range, particle type, and material can be selected.
4.	Run and Event	• It deals with the generation of events, interfaces to the event generators and any secondary particles generated in the material after interaction with the primary particle [24]. • Its specific role is to provide particles to be tracked to the tracking management category.

S.No	Category of Toolkit	Major Functions of Category
5.	Tracking and Track	• Its function is to handle propagation of a particle by analyzing the various factors which limit the step and apply appropriate physics processes. • The significant aspect of the software design is to generalize the GEANT4 physics process which could perform actions, along the tracking step, either localized in space, or in time, or distributed in space and time.
6.	Hits and Digitization	• It manages the creation of hits in the sensitive region of the detector and its use for the digitization.
7.	Visualization and Interface	• It manages the visualization of solids for detector, trajectories of particles both primary and secondary hits, which is the interaction of particles in the sensitive volume of detector and it interacts with the underlying graphical libraries. • The object oriented design of visualization component facilitates to develop several drivers independently, such as for OpenGL, Qt and OpenInventor (for X11 and windows), DAWN, Postscript (via DAWN) and VRML [18]. • The interfaces category handles the production of the graphical user interface (GUI) and the interactions with external software [18].

It is important to note that GEANT4 toolkit in itself is not a standalone application. The user must define the material, projectile and geometry parameters that are essential to carry out the simulation experiments. Moreover, the user has to write customized codes using the library resources available in the toolkit. The user initially has to define the main () function. It is an imperative function and from this function all other classes are defined and invoked.

Besides the main () function, the toolkit has two main user classes; one is mandatory /compulsory which must be defined by the user and another is an optional [24]. The mandatory class consists of user initialization classes which are used during the initialization phase of simulation. The three classes under initialization class are:

1. G4VUserDetectorConstruction

In this user initialization class, the user needs to write codes for describing the detector in terms of its size, shape and material.

2. G4VUserPhysicsList

The G4VUserPhysicsList is utilized by the user to explicitly define the relevant physics processes required for the description of the particle interaction with matter.

3. G4VUserActionInitialization.

The attributes of the projectile in terms of projectile particle, its energy, direction and number of particles are specified in the G4VUserActionInitialization class.

The optional classes are user action class, which includes five major classes:

1. G4UserStepping Action – for analyzing the steps of particles.

2. G4UserEvent Action- defines histogram and event selection.

3. G4UserTracking Action- decides whether the trajectory of particle needs to be stored or not.

4. G4UserStacking Action-storing track information.

5. G4UserRun Action- to controls the flow of simulations and store histogram.

After defining the above two classes, the user must compile the collection of GEANT4 individual files for which the GEANT4 kernel generates an executable file which is to be run to begin the simulation process [24]. A point to note is that in the present work, GEANT4 software was installed in Fedora Linux operating system.

Four important components in the execution of GEANT4 simulation are

1. Step - It is the minimum path length that particle traverses in material before interaction.

2. Track- It traces the path taken by particle or total number of all steps taken by the particle while propagating through matter.

3. Event- It stores the track history of single incident particle along with the track of all the secondary particles that are generated upon the interaction of primary particle with material.

4. Run- It is a collection of all events that share the same detector geometry, physics process and particle.

The next section briefly explains about the process flow of the GEANT4 simulation pertaining to the present neutron detector simulation work.

2.1.6 Process flow of Simulation pertaining to present work

The relevant parameters fed as input to simulation toolkit and outputs obtained from the toolkit are illustrated in figure 2.2.

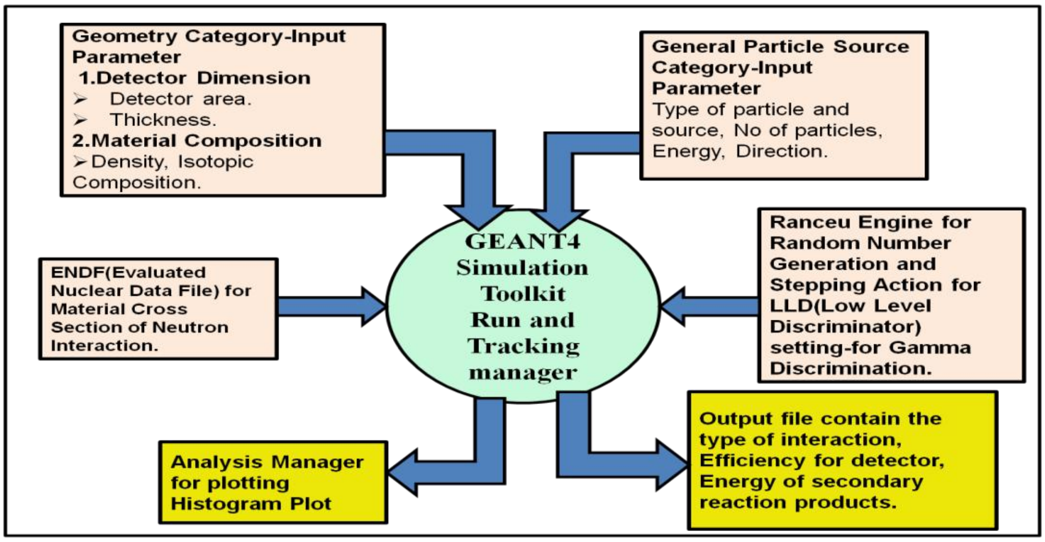

Figure 2.2. Process flow of simulation in the present work with relevant input and output parameters.

2.1.6.1 Detector definition - User input

The definition of detector to be simulated was defined in geometry category while G4Detector Construction class was used to define its dimensions. The volume of detector is expressed using the concept of logical volume and physical volume. The logical volume defines the physical attributes of the detector element including its shape and other volumes such as trenches, perforations etc enclosed in it. The physical volume specifies the spatial positioning of the detector inside the world/mother volume. The mother volume represents the experimental boundaries within which, both the projectile and the detector are defined/confined. The material of detector was defined by implementing G4Material class [24]. The graphic representation category is utilized by geometry category for the visualization of the detector. Thus, the user defines detector dimension and material composition in geometry category which was given as input parameter in the toolkit (see figure 2.2).

2.1.6.2 Particle projectile - User input

Next important category in toolkit is the particle category in which the particles to be projected on the detector are defined by user and given as input parameter in the toolkit. In this category, primary generator class is used to input the particle energy, direction, initial position, number of particles and type of the source - planar or point - source. There are two ways of defining primary particles viz., Gun particle and General Particle Source (GPS) class. The particles are shot serially one after another onto the detector front face in Gun particle class while the GPS class has a feature employing parallel source of particles. It is important to note that in present simulation work, GPS class was implemented for generating parallel beam of mono energetic neutrons [24].

2.1.6.3 Process flow in run and tracking manager

After the projectile is generated, the simulation passes on to run category which is the largest unit of simulation. This category comprises of a class known as run manager whose object needs to be defined in the main program. The run manager object initializes three mandatory user classes, namely detector construction, primary generator and physics process. Run category also manages collection of all events associated with the particles. The simulation process flow in the run, event and tracking category is depicted as flow chart (see figure 2.3) and further details are described below.

- First step is to initialization of G4Event object in G4Event Manager class.
- In the second step, G4Event object is assigned the primary particle and primary vertex.
- The G4EventManager converts the primary particles and primary vertex objects associated with the G4Event object to G4Track object which is then passed on to G4StackingManager class for storing.
- G4EventManager then serially pops one by one the G4Track object from the G4StackingManager class and sends to the G4TrackingManager class. The G4TrackingManager acts as a broker link between the Hierarchal class (that is the Event) and lower class (Track).
- G4TrackingManager gives its input to the G4Stepping Manager whose essential role is in tracking of a particle. It takes care of the entire message of passing between the objects of different categories relevant to transporting of particles.
- G4SteppingManager has public stepping method and helps in steering the particles through the medium. In GEANT4, all the particles are tracked till their kinetic energies are zero or a particle goes out of the world volume.

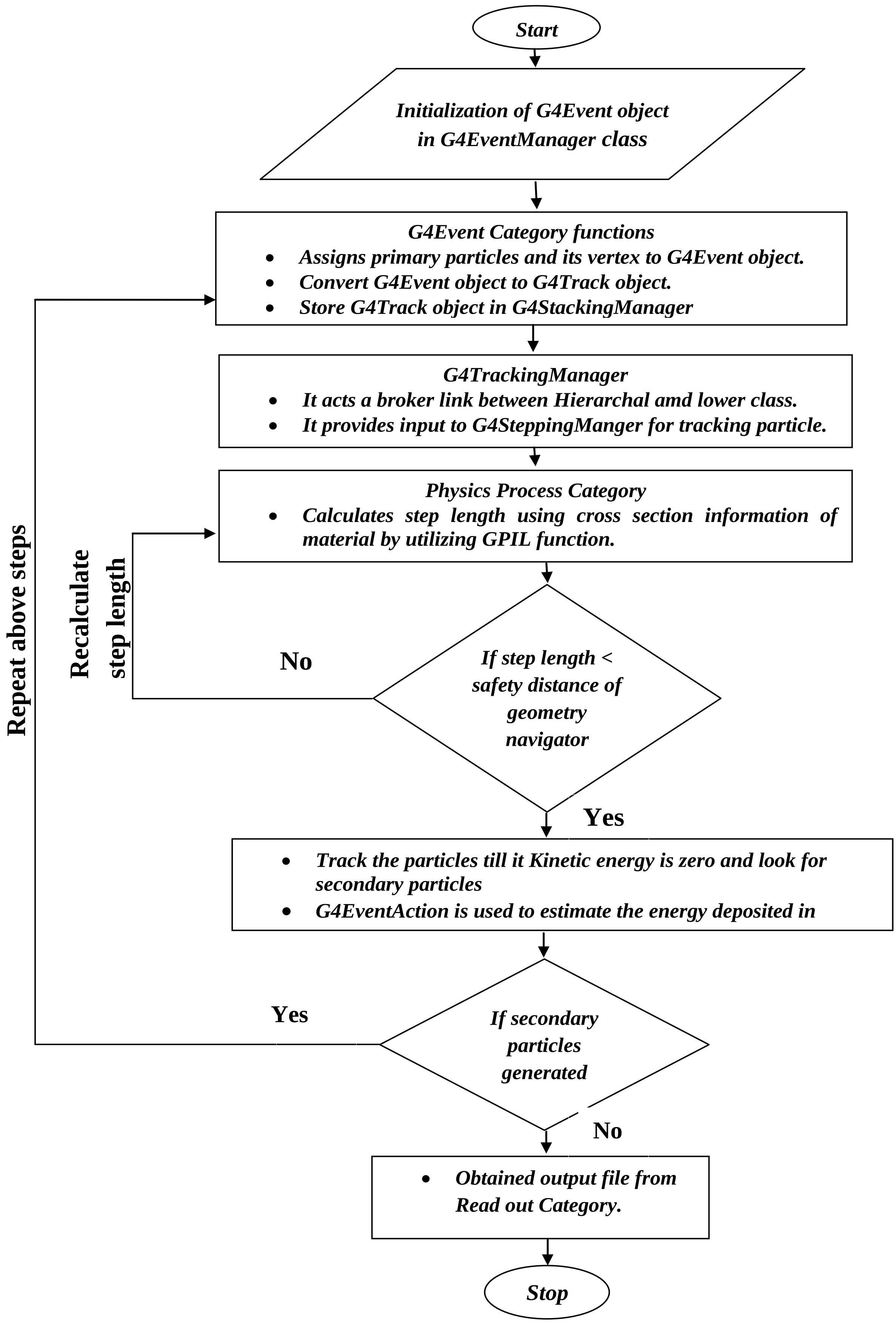

Figure 2.3. Flow chart of simulation process in run, event and tracking category.

- Subsequent to the tracking of particles, the simulation then passes on to process category which has a GPIL (Get Physical Interaction Length) method. GPIL method calculates the step length of the given particle between successive space time points - from the current space time to the next space time point - based on the interaction cross section of the projectile with the material, as dictated by physics process category.
- The physics process category decides what type of interaction the particle will undergo while it traverses through matter.
- The associated physics process gives the step length and is compared with 'safety' distance calculated by geometry navigator. 'Safety' is the length to the next volume boundary and is implicitly specified by the G4SteppingManager, so that the interaction takes place with a physical matter entity.
- If the step length provided by the process is smaller (more) than the 'safety' distance of geometry navigator, then the step length is chosen (recalculated).
- When the particle travels through the medium, all the continuous processes are invoked. The particle kinetic energy is updated only after all the invoked processes have been completed. The change in kinetic energy is the sum of the contributions from all the continuous processes.
- The secondary particles if generated in the process, are stored in the stacking manager and popped out serially one by one and tracked. The G4Step class is used to store the transient information like Pre step point and Post step point. G4Track keeps the current information about the particles, whereas, all the track information is stored in G4Event object.

- The energy deposited by particles in matter is traced by G4Event Action function. G4Event class output is fed to the run category.
- Finally, the run category input is given to the readout category to generate final simulation result output file.

The output file gives the information on the detailed analysis of the types of interactions that the particle undergoes, number of particles interacted, range of particles in detector medium and efficiency of detector etc. The energy deposited by both primary and secondary particles in detector is obtained from a histogram plot which is generated in the analysis manager [24].

In summary, general process flow of simulation was discussed. Further details of the simulation pertaining to detector geometry and material will be explained in subsequent chapters. The initial simulations were based on benchmarking the literature results which will be explained in chapter 3.

Apart from simulations, experiments were carried out for detection of thermal neutrons by boron based materials coated on silicon PIN diodes and to understand the effect of neutron irradiation on virgin (uncoated) silicon PIN diodes therefore, it is pertinent to discuss the relevant experimental details.

2.2 Experimental details

2.2.1 Si Device Information

2.2.1.1 Si-PIN diode

In the present thesis, Si PIN (P-type, Intrinsic, N-Type) diodes procured from BEL (Bharat Electronics Limited, Bengaluru) shown in figure 2.4, were used for carrying out alpha/neutron detection and irradiation damage studies.

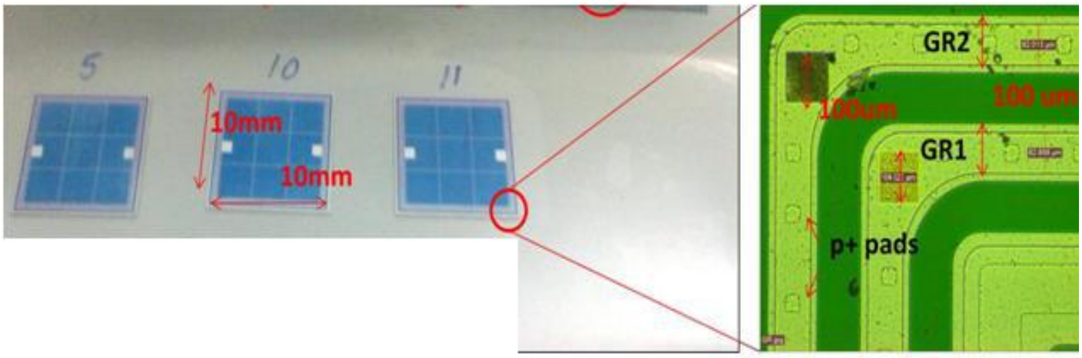

Figure 2.4. Si-PIN diodes used in experimental work [25].

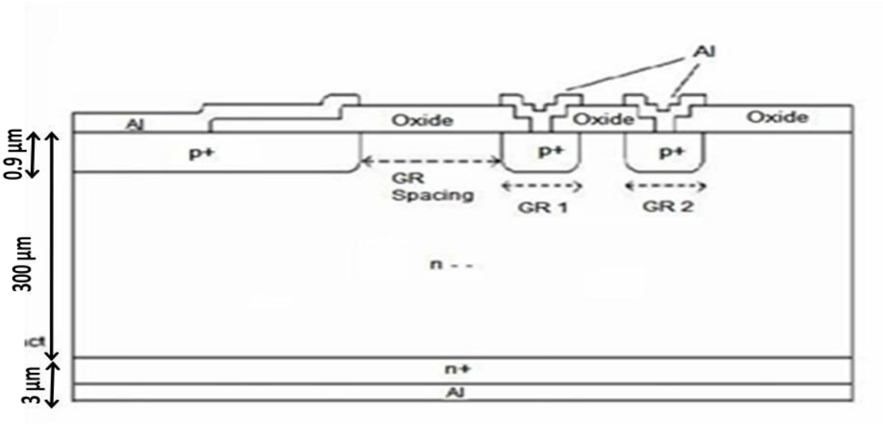

Figure 2.5. Cross sectional view of Si PIN diode [25].

The cross sectional view of Si PIN diode shown in figure 2.5 with thicknesses of P, I and N regions as - 0.9 μm, 300 μm and 3 μm, respectively. Silicon diodes with lateral dimensions of 10mm x 10mm (with active area of 94.09 mm^2) were used for alpha/neutron detection experiments while those of smaller dimensions 5mm^2 (with active area of 22.09 mm^2) devices were used for irradiation experiments to facilitate loading of diode inside the polythene vial. Two Guard Rings (GR) each of thicknesses about 100μm completely surround the active region of diode to improve its performance [26]. Aluminum metal contacts to the guard rings are 0.1mm x 0.1mm in dimension.

The p+ pads present over the guard rings are about 10μmx10μm in size. The window material made of SiO_2 on top surface of diode is 0.5 μm thick. The operating temperature range of diode is -65 °C to 125 °C.

2.2.1.2 Electrical characterization of Si-PIN diodes in terms of I-V and C-V measurements.

The electrical characterization i.e., current-voltage (I-V) and capacitance-voltage(C-V) measurements were performed on Si PIN diodes by mounting them on a specially designed PCB (Printed Circuit Board) which in turn was placed inside a light tight Aluminum chamber (see figure 2.6). This chamber shields the diode from external electrical interference, apart from providing a dark environment.

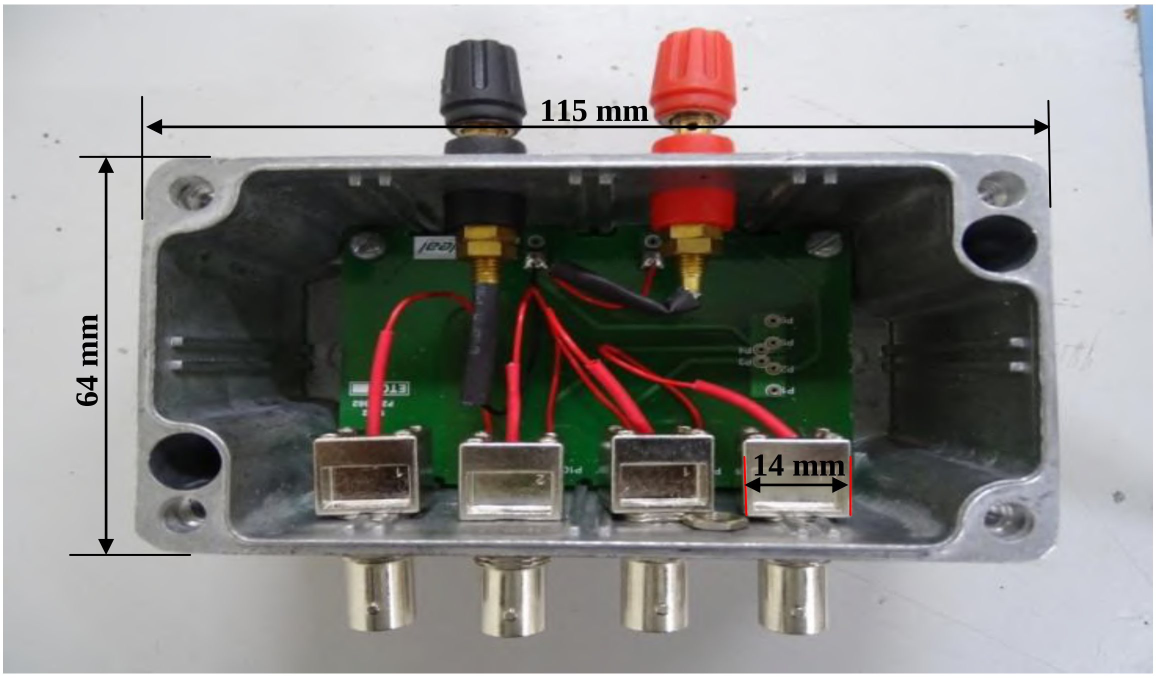

Figure 2.6. Aluminum Faraday chamber encasing PCB used in measuring the I-V and C-V characteristics of Si PIN diodes. (Top lid cover is not shown)

A Source Measurement Unit (SMU) (model- Keysight B2912A) and LCR meter (model- E4980 A) were employed for I-V and reverse C-V measurements, respectively. These measurements were automated using LabView interfacing platform and commercially available Quick I-V measurement software, so as to acquire data using a personal computer. The complete automated experimental set up for I-V and C-V measurement is shown in the figures -2.7 (a) and 2.7 (b), respectively.

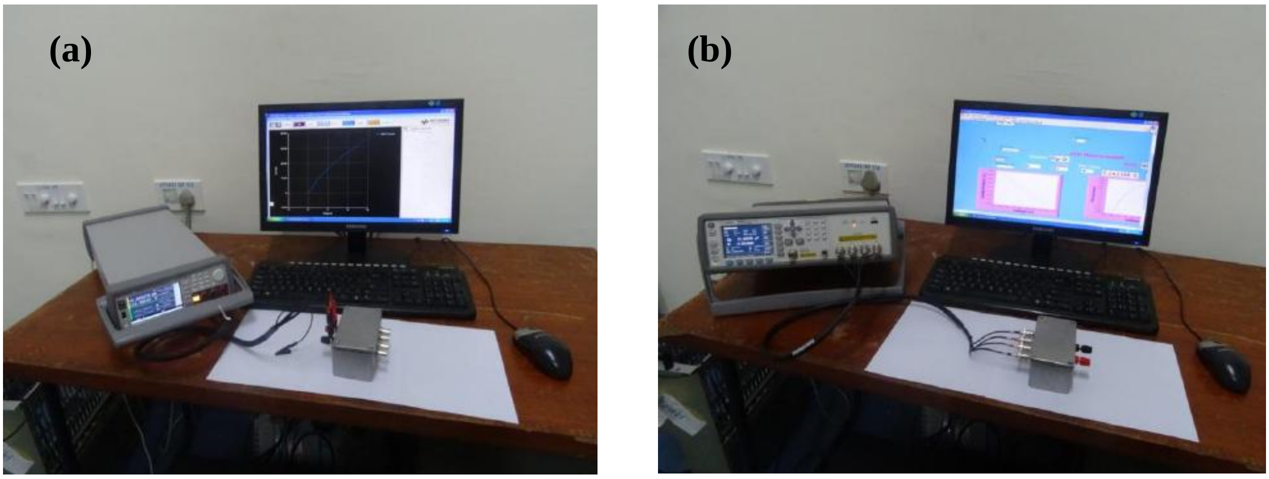

Figure 2.7. Experimental set-up used for (a) I-V and (b) C-V measurement.

2.2.2 Neutron detection experiment

2.2.2.1 Read out electronics for detection of alpha /neutrons

Before embarking on detection of neutrons, the nuclear readout chain shown in figure 2.8 [27,28], is tested for its functionality by detecting alpha particles [29]. Since the range of alpha particles in air is typically a few cms, the experiment was conducted under a vacuum of 10^{-3} torr, in a dedicated and specially designed Aluminum vacuum chamber (see figure 2.9). This consisted of grooves (see figure 2.10) to facilitate the placement of detector (Si PIN diode) and triple energy alpha source (Pu^{239} - 5.155 MeV, Am^{241}- 5.486 MeV and Cm^{244}- 5.806 MeV) in a disc form (see figure 2.11). The alpha source was placed at a distance of 1 cm from Si PIN diode inside the Aluminum chamber. It is worthwhile to note that the pulse mode of operation was used for both detection of alpha particles and neutrons. Si PIN diode was reverse biased using a high voltage power supply (model - NHQ105 M). The current pulse from Si PIN diode due to alpha exposure was measured using a charge sensitive preamplifier (model CSP-11, gain of 150 mV/pC). In order to reduce the noises arising out of parasitic capacitance, a smaller length of cable - typically 15cm - with SMA (Sub Miniature –A) and SHV (Safe High Voltage) terminators was used to connect signal output from the diode to charge sensitive preamplifier. The charge sensitive preamplifier integrates the current signal pulse i_d [27,28] from the detector, over a time t and generates a voltage output pulse V_{out} (t) as

$$\boldsymbol{V_{out}\,(t) \propto Q = \int_0^t i_d(d\tau)}$$

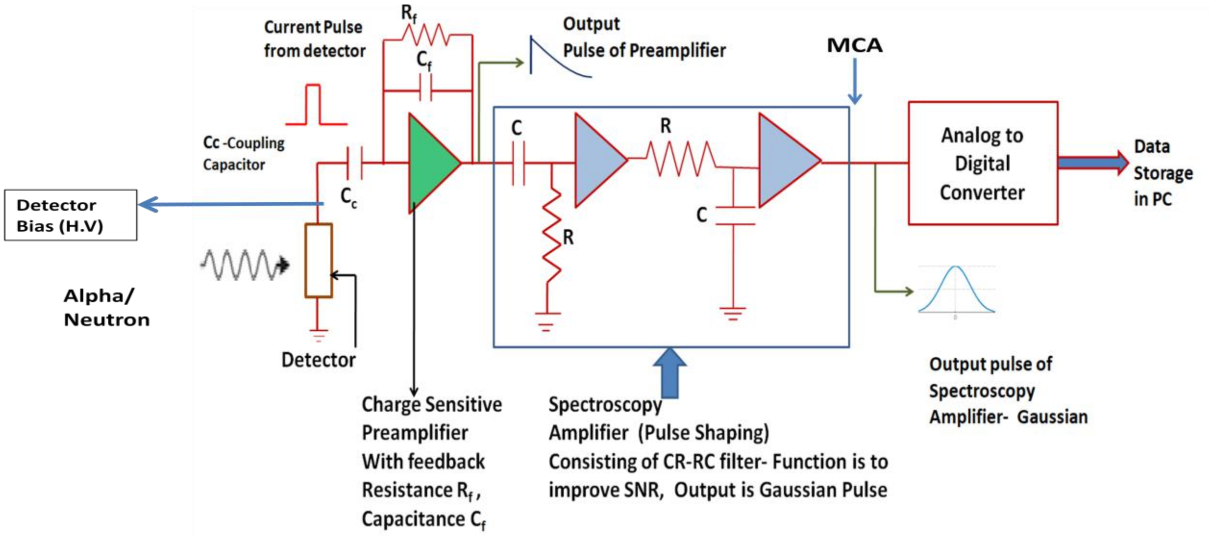

Figure 2.8. Block diagram of the read out electronics for detection of alpha particles and neutron.

Figure 2.9. Vacuum chamber with SMA (Sub Miniature –A) to SHV (Safe High Voltage) cable connection.

Figure 2.10. Aluminum holder consisting of grooves to mount silicon PIN diode and alpha source to be placed inside the vacuum chamber.

Figure 2.11. Triple energy alpha Source in disc shape.

As shown in figure 2.8, the charge sensitive preamplifier output is fed as input to a pulse shaping amplifier (also known as Spectroscopy Amplifier) which consists of integrator and differentiator circuits, to improve on signal to noise ratio [27,28]. The output pulse of spectroscopy amplifier is a gaussian pulse whose rise and fall times are dictated by time constant of integrator and differentiator circuits [27,28], respectively. In the present work, spectroscopy amplifier (model- Ortec-673) with appropriate gain settings and shaping time was used. The last stage of the read out electronics chain is a multi channel analyzer (MCA) (model-Fast Comtec MCA-3,13 Bit ADC (Analog to Digital Converter)) which converts the analog gaussian pulse to a digital one, and was interfaced with a personal computer for further data acquisition, storing and processing [27,28]. The photograph of the experimental set up for alpha detection is shown in figure

2.12. The same experimental setup is used for the detection of neutrons except that (a) the alpha source is replaced by a thermal neutron standard source, (b) Vacuum pump is not required and (c) settings of detector bias and gain parameter of spectroscopy amplifier were varied.

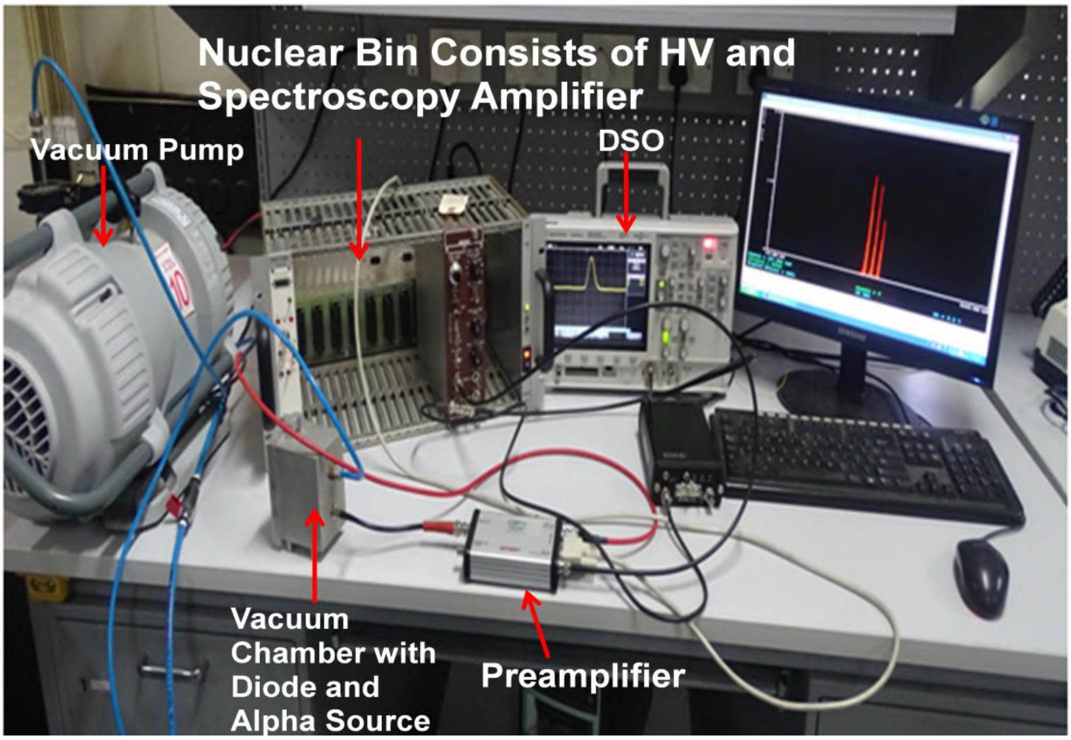

Figure 2.12. Experimental set up used in the alpha particle detection.

2.2.2.2 Detection of thermal neutrons

For the detection of thermal neutrons, a suitable converter material based on boron, herein referred to as BBM, was used. The details of the converter material and the coating procedure are not disclosed in this thesis, as a patent application is being filed. The optimum thickness of BBM coating was obtained from the GEANT4 simulation and same was coated on Si PIN diodes having an active area of 94.09 mm^2. The coating thickness was measured using a Dektak surface profilometer (model-6M Vektak, Veeco,USA). The I-V and C-V measurements were carried out on the diodes using experimental setup as shown in figure 2.7 (a) and 2.7(b), before and after the BBM coating, to ascertain the effect of the BBM coating on these measurements. The thermal neutron detection experiments were carried with a thermal neutron flux standard facility. This facility has eight Am-Be neutron sources of activity 0.5 Ci and is moderated by nuclear grade graphite [30,31]. The facility has constant neutron flux zone where flux was 7 x 10^3 n/cm^2-s. The neutron flux was estimated by foil activation method. The BBM coated Si PIN diodes were exposed to thermal neutrons by placing them inside the Aluminum chamber at constant neutron flux zone. Then the appropriate bias was applied to detector and cable connection was provided to acquire the signal. The read out electronics for the detection of neutrons is similar to the alpha experiments as shown in figure 2.12.

As is well known, devices of silicon devices like PIN diode when exposed to harsh radiation conditions undergo radiation damage [32]. Therefore, an attempt is made to examine the radiation damage in silicon PIN diodes when exposed to predominantly thermal neutrons by measuring the electrical characteristics. The details of this experimental procedure follow in the next section.

2.2.3 Neutron Irradiated experiments on Si- PIN Diodes

In order to understand the effect of neutron irradiation on the electrical I-V characteristics, the Si PIN diodes were subjected to predominantly thermal neutron source in KAMINI (KAlpakkam MINI reactor) nuclear reactor. This reactor is cooled and moderated by light water and fueled with uranium-233 metal. The KAMINI reactor generates 30 kW of thermal energy at full power [33].

The Si PIN diodes were packed in a polythene vial and transferred to the core of KAMINI reactor with a pneumatic fast transfer mechanism. The flux at the irradiation location was 6.01×10^{11} n/cm^2·s when the reactor was operated at 20 kW. The irradiation times were so chosen so as to result in neutron fluences ‘ϕ’ ranging from 1×10^{14} to

1×10^{16} n/cm^2. The neutron flux and spectrum at irradiation location have been experimentally measured by foil activation method [34]. The neutron spectrum at the irradiation location of the reactor is shown in figure 2.13. The corresponding neutron fluxes for various energy intervals are summarized in table 2.2 [34]. The ambient temperature at the irradiation location was 300 K. Post irradiation, the diodes had an activity in excess of 10 mR/h and was unsafe for handling/ carrying out any experiment. The diodes were therefore placed inside a lead pot for over a month until the activity was below 0.1mR/h and which is considered safe to be handled by personnel for further experiments. It is to be noted that diodes were also subjected to gamma rays (approx 3.14 x 10^4 Gy/h).

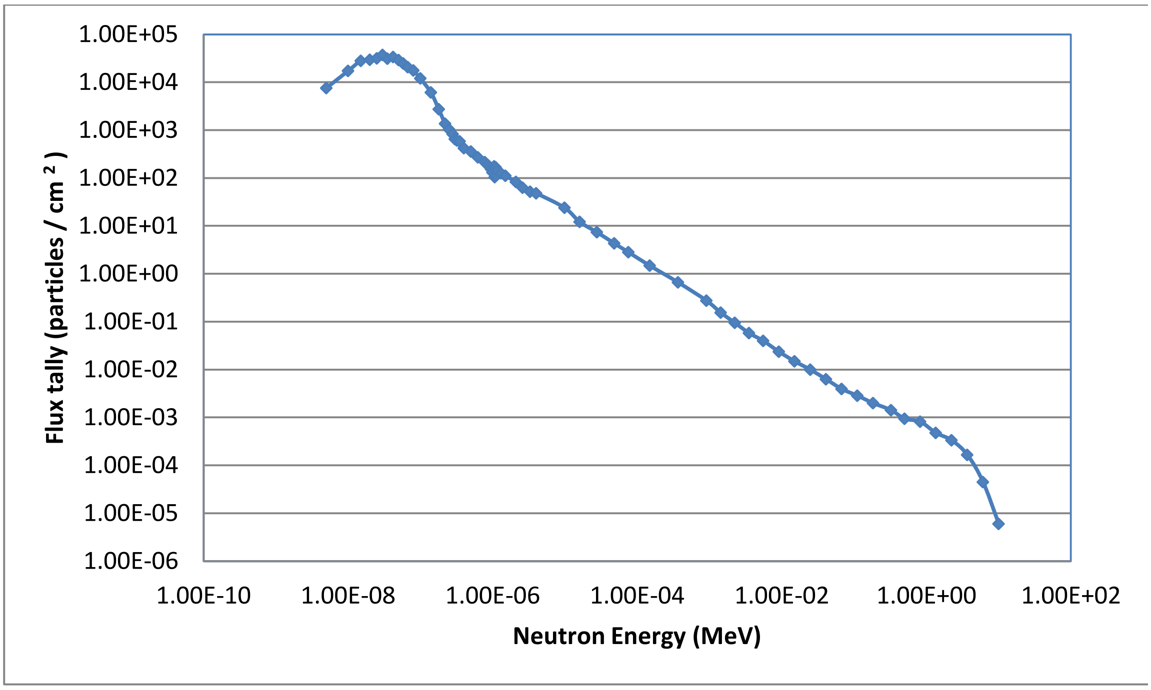

Figure 2.13. Neutron flux variation at the neutron irradiation location.

Table 2.2. Neutron energy and flux measured at neutron irradiation location [34].

Neutron Energy Interval	**Neutron Flux($cm^{-2} \cdot s^{-1}$)**
0 - 0.56 eV	3.45 $\times 10^{10}$
0.56 ev – 0.5 MeV	4.30 $\times 10^{11}$
0.5 MeV- 2 MeV	1.36 $\times 10^{11}$

The I-V characteristics in forward and reverse bias conditions were carried out for all the Si PIN diodes prior to irradiation. In case of virgin diode (i.e., on unirradiated diode), for the forward bias condition, the measurements were carried out till 0.8V with a step size of 50 mV, while for the reverse bias conditions, the measurements were carried out from 0 V till 100 V, incremented by 1 V. The experimental set up as shown in figure 2.7(a) was used for the I-V measurement. For measurements of forward current in irradiated specimens, the upper limit on forward voltage was set at a value where a sharp increase in current was obtained [35]. However, for measurements in reverse bias conditions, the upper voltage (till 100 V) was kept the same as that in the virgin case. In order to estimate the depletion width of Si PIN diode, a reverse C-V measurement was performed using the set up shown in figure 2.7 (b) from 0 V to 100V at constant frequency of 1 MHz.

Having discussed about the GEANT4 simulation and experimental details, the focus now moves to the simulation and experimental results which are presented and explained in the subsequent chapters. The next chapter discusses in detail about the GEANT4 simulation results for benchmarking with literature and employment of boric acid as a converter material.

References

[1] N.Metropolis, S. Ulam, The Monte Carlo Method, Journal of the American Statistical Association. 44 (1949) 335. doi:10.2307/2280232.

[2] S.A. Dupree, S.K. Fraley, A Monte Carlo Primer - A Practical Approach to Radiation Transport, Kluwer Academic, NY (2002).

[3] P. Rinard, Neutron Interaction with Matter-Chapter-12, Passive Nondestructive Assay of Nuclear materials, US Nuclear Regulatory Commission Washington DC, Los Alamos National Lab,March 1991.

[4] E.E. Lewis, W.F. Miller, Computational Methods of Neutron Transport, American Nuclear Society, Inc., LaGrange Park, IL (1993).

[5] D.S. McGregor, M.D. Hammig, Y.-H. Yang, H.K. Gersch, R.T. Klann, Design considerations for thin film coated semiconductor thermal neutron detectors—I: basics regarding alpha particle emitting neutron reactive films, Nuclear Instruments and Methods in Physics Research Section A: Accelerators, Spectrometers, Detectors and Associated Equipment. 500 (2003) 272–308. doi:10.1016/S0168-9002(02)02078-8.

[6] C. Guardiola, K. Amgarou, F. García, C. Fleta, D. Quirion, M. Lozano, Geant4 and MCNPX simulations of thermal neutron detection with planar silicon detectors, J. Inst. 6 (2011) T09001. doi:10.1088/1748-0221/6/09/T09001.

[7] S. Tripathi, C. Upadhyay, C.P. Nagaraj, K. Devan, K. Madhusoodanan, S.A.V.S. Murty,Geant4 simulations of semiconductor detectors (SiC) for fast neutron spectroscopy, in: 2015 Annual IEEE India Conference (INDICON), 2015: pp. 1–6. doi:10.1109/INDICON.2015.7443467.

[8] J. Uher, C. Fröjdh, J. Jakůbek, C. Kenney, Z. Kohout, V. Linhart, S. Parker, S. Petersson, S. Pospíšil, G. Thungström, Characterization of 3D thermal neutron semiconductor detectors, Nuclear Instruments and Methods in Physics Research Section A: Accelerators, Spectrometers, Detectors and Associated Equipment. 576 (2007) 32–37. doi:10.1016/j.nima.2007.01.115.

[9] J. Allison, K. Amako et al., Geant4 developments and applications, IEEE Transactions on Nuclear Science. 53 (2006) 270–278. doi:10.1109/TNS.2006.869826.

[10] S.F. Naeem, S.D. Clarke, S.A. Pozzi, Validation of Geant4 and MCNPX-PoliMi simulations of fast neutron detection with the EJ-309 liquid scintillator, Nuclear Instruments and Methods in Physics Research Section A: Accelerators, Spectrometers, Detectors and Associated Equipment. 714 (2013) 98–104. doi:10.1016/j.nima.2013.02.017.

[11] R. Lemrani, M. Robinson, V.A. Kudryavtsev, M. De Jesus, G. Gerbier, N.J.C. Spooner, Low-energy neutron propagation in MCNPX and GEANT4, Nuclear Instruments and Methods in Physics Research Section A: Accelerators, Spectrometers, Detectors and Associated Equipment. 560 (2006) 454–459. doi:10.1016/j.nima.2005.12.238.

[12] R. Dahal, K.C. Huang, J. Clinton, N. LiCausi, J.-Q. Lu, Y. Danon, I. Bhat, Self-powered micro-structured solid state neutron detector with very low leakage current and high efficiency, Appl. Phys. Lett. 100 (2012) 243507. doi:10.1063/1.4729558.

[13] J.K. Shultis, R.E. Faw, An MCNP Primer, a report submitted in Kansas state University, US,2008.

[14] K. Sedlačková, B. Zat'ko, A. Šagátová, M. Pavlovič, V. Nečas, M. Stacho, MCNPX Monte Carlo simulations of particle transport in SiC semiconductor detectors of fast neutrons, Journal of Instrumentation. 9 (2014) C05016–C05016. doi:10.1088/1748-0221/9/05/C05016.

[15] A. M. Conway, T. F. Wang, N. Deo, C. L. Cheung, and R. J. Nikolic, "Numerical Simulations of Pillar Structured Solid State Thermal Neutron Detector: Efficiency and Gamma Discrimination," *IEEE Trans. Nucl. Sci.*, vol. 56, no. 5, pp. 2802–2807, Oct. 2009.

[16] C.Guardiola Salmeron, Novel silicon sensor for neutron detection, A doctoral thesis, Autonomous University of Barcelona, Spain, 2012.

[17] GEANT4 Website- https://geant4.web.cern.ch/

[18] S. Agostinelli, J. Allison et al., Geant4—a simulation toolkit, Nuclear Instruments and Methods in Physics Research Section A: Accelerators, Spectrometers, Detectors and Associated Equipment. 506 (2003) 250–303. doi:10.1016/S0168-9002(03)01368-8.

[19] M.B. Chadwick, P. Obložinský et al., ENDF/B-VII.0: Next Generation Evaluated Nuclear Data Library for Nuclear Science and Technology, Nuclear Data Sheets. 107 (2006) 2931–3060. doi:10.1016/j.nds.2006.11.001.

[20] E. Mendoza, D. Cano-Ott, T. Koi, C. Guerrero, New Standard Evaluated Neutron Cross Section Libraries for the GEANT4 Code and First Verification, IEEE Transactions on Nuclear Science. 61 (2014) 2357–2364. doi:10.1109/TNS.2014.2335538.

[21] R. Mudau, A. Muronga, S. Connell, C. Jacobs, A Comparison of Neutron Scattering in Geant4 and MCNP, a report submitted to University of Johnesburg ,South Africa.

[22] B.M. van der Ende, J. Atanackovic, A. Erlandson, G. Bentoumi, Use of GEANT4 vs. MCNPX for the characterization of a boron-lined neutron detector, Nuclear Instruments and Methods in Physics Research Section A: Accelerators, Spectrometers, Detectors and Associated Equipment. 820 (2016) 40–47. doi:10.1016/j.nima.2016.02.082.

[23] S.L. Meo, L. Cosentino, A. Mazzone, P. Bartolomei, P. Finocchiaro, Study of silicon+ 6 LiF thermal neutron detectors: GEANT4 simulations versus real data, Nuclear Instruments and Methods in Physics Research Section A: Accelerators, Spectrometers, Detectors and Associated Equipment. 866 (2017) 48–57. doi:10.1016/j.nima.2017.04.029.

[24] Geant4 User's Guide for Application Developers, (developed in CERN). http://geant4.web.cern.ch/geant4/UserDocumentation/UsersGuides/ForApplicationDeveloper/html/index.html (accessed January 29, 2016).

[25] N. Bhat, S.A.Shivashankar, K.N.Bhat,P. Rao, V.Mishra, Final Report on Development of solid state neutron sensors, submitted to IGCAR Kalpakkam, 2016.

[26] V.Mishra, V.D.Srivastava, S.K.Kataria, Role of guard rings in improving the performance of silicon detectors, Pramana-Journal of Physics. 65 (2005) 259-272.

[27] G. F. Knoll, Radiation Detection and Measurement, John Wiley & Sons, (2010).

[28] H.Spieler, Semiconductor detector systems, Oxford University Press (2005).

[29] A. Pappalardo, M. Barbagallo, L. Cosentino, C. Marchetta, A. Musumarra, C. Scirè, S. Scirè, G. Vecchio, P. Finocchiaro, Characterization of the silicon+6LiF thermal neutron detection technique, Nuclear Instruments and Methods in Physics Research Section A: Accelerators, Spectrometers, Detectors and Associated Equipment. 810 (2016) 6–13. doi:10.1016/j.nima.2015.11.114.

[30] V.Sathiamoorthy, P.Mohanakrishnan,Characterisation of Neutron Spectrum of TNFSF, a report submitted in Indira Gandhi Centre for Atomic Research, Kalpakkam, Dec.1999.

[31] I.Murataa, I.Tsudaa, R. Nakamuraa, S. Nakayamab, M. Matsumotb and H. Miyamaruc, Neutron and gamma-ray source-term characterization of AmBe sources in Osaka University, Progress in Nuclear Science and Technology, vol. 4, pp. 345-348, April 2014.

[32] M. Hasegawa, S. Mori, T. Ohsugi, H. Kojima, A. Taketani, T. Kondo, M. Noguchi,Radiation damage of silicon junction detectors by neutron irradiation, Nucl. Instrum. Methods Phys. Res. A 277 (1989) 395–400, http://dx.doi.org/10.1016/

[33] D.K. Mohapatra, P. Mohanakrishnan, Measurement and prediction of neutron spectra in the Kalpakkam mini reactor (KAMINI), Appl. Radiat. Isot. Data Instrum. Methods Use Agric. Ind. Med. 57 (2002) 25–33.

[34] G.V.S.A. Kumar, S. Sen, E. Radha, J.S.B. Rao, R. Acharya, R. Kumar, C.R. Venkatasubramani, A.V.R. Reddy, M. Joseph, Studies on neutron spectrum characterization for the Pneumatic Fast Transfer System (PFTS) of KAMINI reactor, Appl. Radiat. Isot. 124 (2017) 49–55,http://dx.doi.org/10.1016/j.apradiso.2017.03.009.

[35] L.J. Beattie, A. Chilingarov, T. Sloan, Forward-bias operation of Si detectors: a way to work in high-radiation environment, Nucl. Instrum. Methods Phys. Res. A 439 (2000) 293–302, http://dx.doi.org/10.1016/S0168-9002(99)00840-2.

Chapter-3

Benchmarking and GEANT4 Simulation of Boric Acid

This chapter discusses benchmarking and validation of GEANT4 simulation results with literature for two test problems. It also includes result and discussion of boric acid as a converter material for thermal neutron detection in various geometries configurations such as two- dimensional (2D-planar and stack) and three dimensional (3D-spherical, cylindrical and cuboidal trenches). The aim of the GEANT4 simulations is primarily to estimate neutron detection efficiency.

3.1 Benchmarking

The reliability of any simulation package is based on its validation and benchmarking with experimental data or corroborative results [1]. As far as simulation in radiation detection field is concerned, GEANT4 is known for its reliability and integrity [2, 3]. It is also important to note that any simulation methodology necessitates commensurate benchmarking as a prelude for validation of results generated by the simulation. Therefore, prior to application of GEANT4 for simulation of detectors in the present work, suitable benchmarking and validation needs to be carried out. In present work, two test problems, viz., planar and stack geometries were selected for benchmarking with literature. The focus in benchmarking and validation is on the determination of critical thickness for achieving maximum efficiency for detection of thermal neutrons (η_{max}).

3.1.1 Planar Geometry- Benchmarking

3.1.1.1 Planar geometry detector design

A neutron detector in planar geometry also known as two dimensional (2D) configuration was designed in ‘geometry’ category of toolkit with a surface area of 1cm^2

along X-Y plane consisting of 100% enriched elemental B^{10} (neutron sensitive converter material) and Si (charged sensitive detector material) as shown in figure 3.1 (a) and (b). The Si semiconductor detector region was defined as a charge sensitive region by utilizing GV4Sensitive class [4]. The thicknesses of Si detector and B^{10} Converter Material (CM) was 300 µm and variable 't', respectively as shown in figure 3.1 (a),(b) and (c).

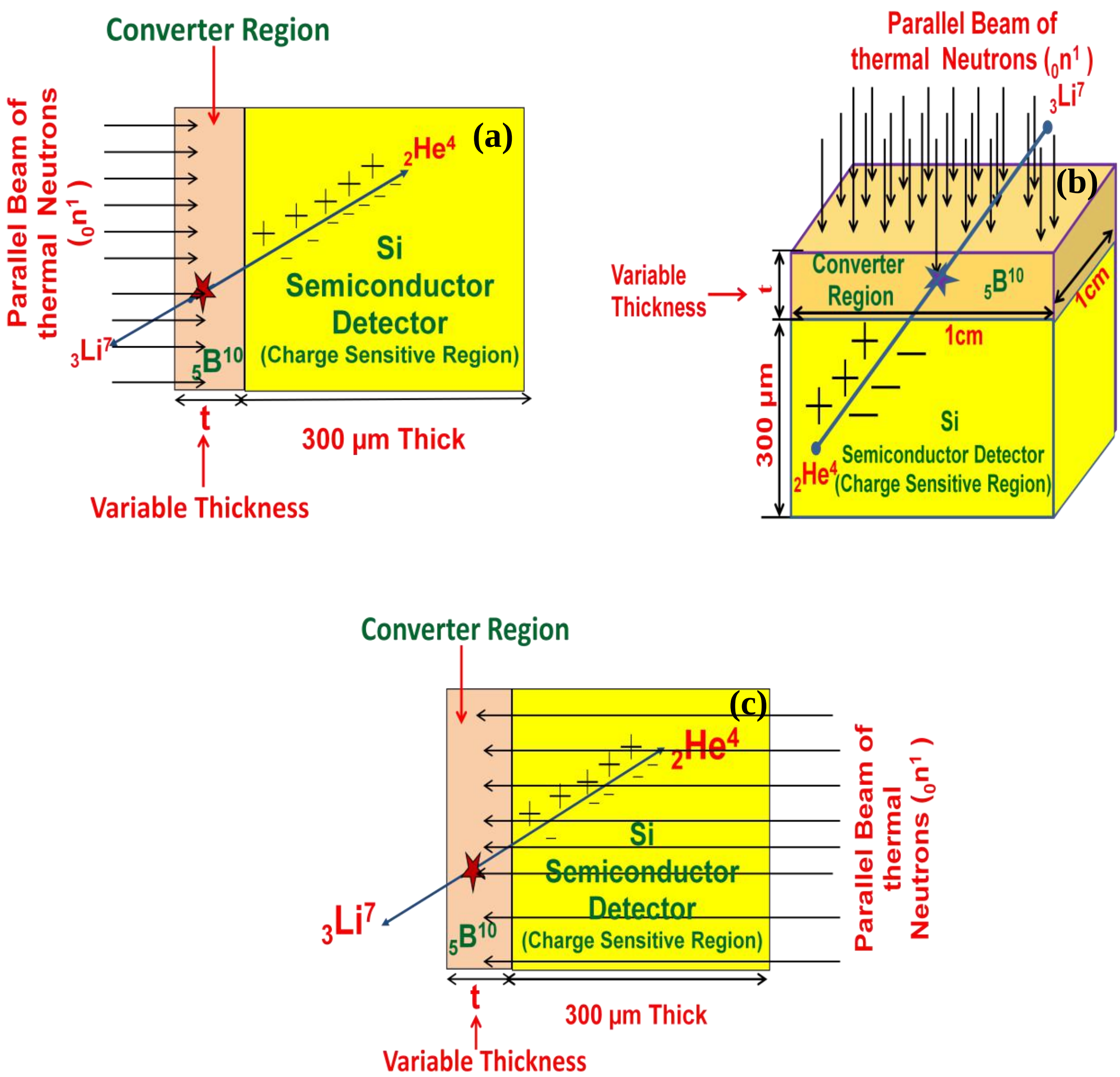

Figure 3.1. Planar detector configuration geometry consisting of elemental B^{10} as CM having variable thickness 't' on top of Si detector (300 µm), as shown for front irradiation (a) Side view (b) Top view and (c) Back irradiation.

G4Placement function was implemented to define the position of detector with respect to mother volume. The mother volume is an experimental boundary region in the simulation with a volume cube of dimension 1000 cm^3. Requisite material parameters, like density, isotope composition and constituent number of elements in a compound were given as input parameter by the user in the toolkit, while other parameters like the atomic number and mass were taken from material library database of National Institute of Standards and Technology (NIST) of GEANT4 [4]. In the present simulation, density for 100% enriched elemental B^{10} and Si materials were given as 2.34 g/cm^3 and 2.32 g/cm^3, respectively.

3.1.1.2 Simulation methodology

A typical simulation begins with a parallel beam of 10^8 mono energetic thermal (25 meV) neutrons emanating from a planar source incident perpendicularly on the front face of the detector as shown in figure 3.1(a) and (b) [5]. Figure 3.1(c) shows the geometrical configuration for the back irradiation, where the neutron source was placed behind the detector. The parameters relevant to neutron source like the energy, number of particles and direction was specified using General Particle Source class.

Mono energetic thermal neutrons impinge on the detector (see figure 3(b)) and interacts at random depth in the boron converter region and these depths were determined by random numbers generated by Ranceu Engine of toolkit [4]. The magnitudes of neutron cross section values for ((n, α)-see equation (1)) interaction were taken from built-in library of G4ENDL (Evaluated Nuclear Data Library B/VII) [4]. The charged particles generated upon neutron interaction with B^{10} (equation (1)) are tracked by G4Track class whereas their energies deposited in different regions are traced by G4GetEnergyDeposit function. The Low Level Discriminator (LLD), which is a threshold parameter for discriminating against background gamma radiation was set at a value of 300 keV in the simulation by employing G4Stepping class of GEANT4 [4,6]. The variable ‘t’ of 100% enriched elemental B^{10} CM was varied from 0.25μm to 40μm in the simulation. A typical time for simulation for one ‘t’ of CM in the present work was ~95 hours using Intel Pentium Core 5 processor. A representative snapshot of GEANT4 simulation is shown in figure 3.2.

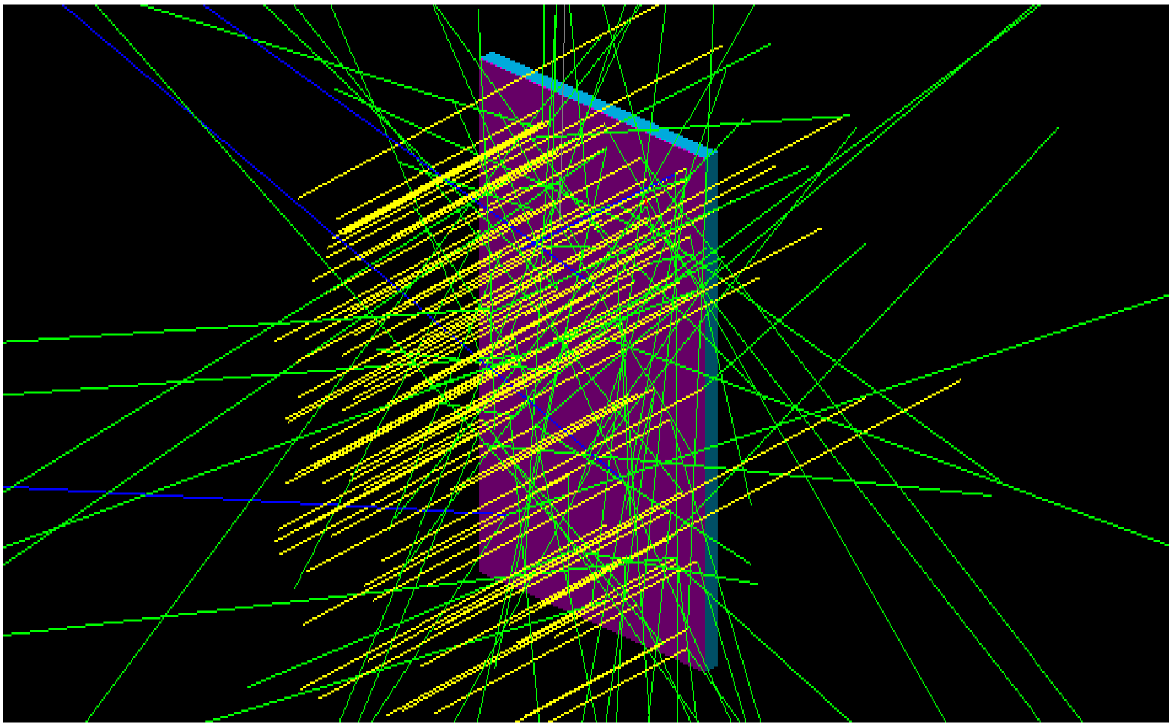

Figure 3.2. Snapshot of GEANT4 simulation for boron (pink color) coated on Si (cyan) for planar configuration geometry. The yellow, green and blue lines represent incident neutrons, emerging gamma rays and charged particles (alpha, Li), respectively.

3.1.1.3 Simulation Result – Comparison of probability of neutron interaction

In order to validate the neutron cross section values of G4ENDL [4], the simulated probability of neutron interaction ‘$P_s(t)$’ was obtained from GEANT4 and compared with the analytical result of the probability of neutron interaction ‘$P_a(t)$’ (equation (2)). The number of neutron interactions (i.e., (n, α) – equation (1)) was recorded for different ‘t’ of CM from the output file of the simulation for estimating ‘$P_s(t)$’.

The equation (1) for (n,α) interaction with B^{10} is given below.

$$ {}^{10}_{5}\mathbf{B} + {}^{1}_{0}\mathbf{n} \rightarrow \begin{cases} {}^{7}_{3}\mathbf{Li}\ (\mathbf{0.839\ MeV}) + {}^{4}_{2}\boldsymbol{\alpha}(\mathbf{1.47\ MeV}) - \mathbf{94}\ \% \\ \ {}^{7}_{3}\mathbf{Li}(\mathbf{1.015\ MeV}) + {}^{4}_{2}\boldsymbol{\alpha}(\mathbf{1.78\ MeV}) - \mathbf{6\%} \end{cases} \qquad (1) $$

The analytical expression for the probability of neutron interaction '$P_a(t)$' is given by,

$$ \mathbf{P_a}(\boldsymbol{t}) = \mathbf{1} - \boldsymbol{e}^{(-\boldsymbol{\Sigma}\mathbf{t})} \qquad (2) $$

where Σ is the macroscopic cross section for elemental B^{10} and 't' is the thickness of CM [7].

The macroscopic cross section 'Σ' was calculated using,

$$ \boldsymbol{\Sigma} = \frac{\boldsymbol{\rho N_A}\ (\boldsymbol{n_i \sigma_i})}{\boldsymbol{M}} \qquad (3) $$

where, ρ is the density of the material, N_A is the Avogadro number, while n_i is the number of atoms, σ_i is the microscopic cross sections of element '*i*' at the given neutron energy, and M is the molecular weight. The Σ computed from equation (3) was found to be ~535 cm^{-1}, by substituting the values (M = 10.1 g/mol , N_A=6.022 x 10^{23} atoms/mole, ρ=2.34 g/cm^3, n = 1, σ = 3840 at thermal energy of 25 meV) for 100% enriched elemental B^{10}.

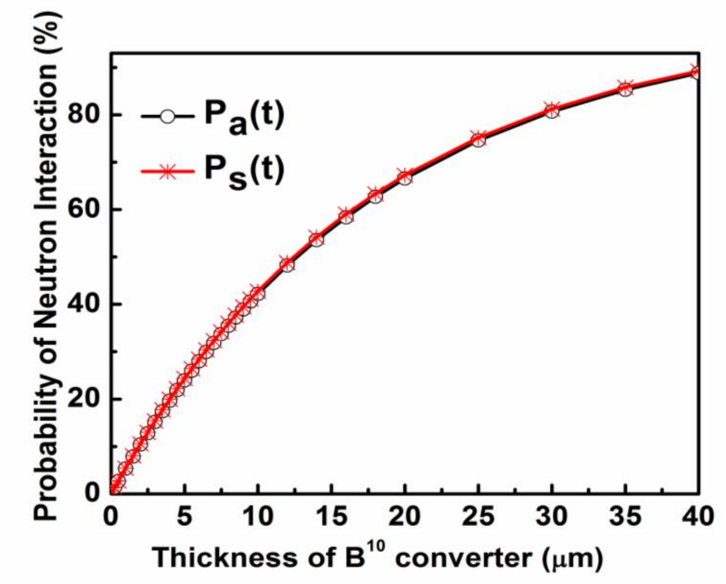

Figure 3.3.Variation of probability of neutron interaction (for both analytical calculated '$P_a(t)$' and simulated by GEANT4 '$P_s(t)$') with thickness of ^{10}B converter.

Using computed 'Σ', '$P_a(t)$' was computed analytically for 't' varying from 0.25 µm to 40 µm and compared with the simulated $P_s(t)$ obtained from GEANT4 which are shown in figure 3.3. Figure 3.3 clearly shows a one to one correspondence between the '$P_s(t)$' and '$P_a(t)$'. It is seen from the figure that both '$P_s(t)$' and '$P_a(t)$' increases with increasing 't' which is attributed to the exponential decay as dictated by second term of equation (2). This also validates neutron interaction cross section value of G4ENDL library for (n, α) interaction in CM.

3.1.1.4 Simulation Result – Efficiency (η) validation with literature

The neutron detection efficiency (η) is defined as the ratio of

$$\frac{\textbf{The total number of charge particles (}Li^{7}\textbf{-0.839 MeV or }\alpha\textbf{-1.47 MeV) depositing energy greater than the set LLD value (300 keV) in Si detector region}}{\textbf{The total number of neutrons incident on the detector}}$$

The η evaluated from the output files generated in GEANT4 for front and back irradiations are shown in figure 3.4 (a) along with the results reported by D.S.McGregor et al. [8] for identical material and geometrical configurations as shown in figure 3.4 (b).

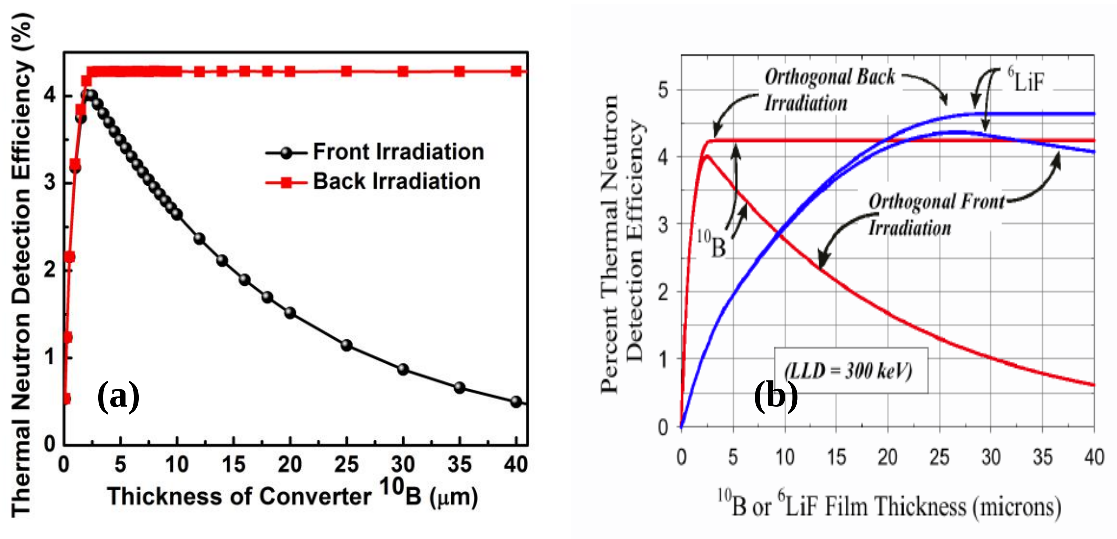

Figure 3.4. Variation in efficiency (η) of thermal neutron detection with the thickness of enriched elemental B^{10} as converter for front and back neutron irradiation (a) GEANT4 simulation (b) Literature Ref. [8].

All the simulation parameters such as LLD, energy of the incident neutron, converter and detector material, thickness of converter and detector were kept identical to the simulations as described in ref. 8. The objective of the simulation was to estimate η with the variation in thickness 't' of CM.

It is clearly seen from the figures 3.4 (a) and (b) that the 'η' variation with 't' of CM obtained from literature [8], matches well with the present GEANT4 simulation result. For the front irradiation, the variation of 'η' with 't' of converter B^{10} shows an initial increase, reaching a maximum at a particular thickness and thereafter a monotonic decrease. The thickness corresponding to maximum efficiency is defined as critical thickness 't_c', as it gives an estimate to optimize the conflicting requirements of thickness. In other words, for thicknesses lower than 't_c', fewer charged particles are generated in the CM region leading to low 'η'. For thicknesses larger than 't_c', inevitable self absorption of charged particles takes place in the CM itself, thereby leading to decrease in 'η' value.

In case of back irradiation, 'η' saturates, which is in contrast to the case of front irradiation [8]. The reason for the saturation in 'η' is that the neutron interaction remains constant close to the Si/CM interface and therefore the charged particles generated always contribute to the 'η'. The disadvantage of the back irradiation is that it warrants the thickness of Si layer to be very thin so that significant numbers of neutrons reach the CM region.

The maximum efficiency (η_{max}) for the front irradiation case obtained from the GEANT4 simulation was 4.01% at a 't_c' of 2.5 μm which is well in agreement with the values reported in ref. [8]. Similarly, for the back irradiation case, 'η_{max}' of 4.28% for the same 't_c' of 2.5 μm agrees well with values reported in literature [8]. The above efficiency result validates our simulation for the 2D planar geometry detector configuration.

3.1.2 Stack Geometry- Benchmarking

The detector in planar configuration had a very low 'η' as perceived from the previous section and this limitation is marginally overcome by designing a detector in stack configuration [8]. The stack detector configuration consists of individual planar Detector Unit (DU) arranged in the form of stacks i.e., are placed adjacent to each other as shown in figure 3.5. The single planar DU refers to the design of planar detector configuration as depicted in figure 3.1 (a). The stack detector configuration was designed by replicating single DU along the z-axis using G4Replica function of the GEANT4 toolkit [4]. In other words, several such DUs are integrated together to form N-DU stacked configuration, N being the number of DUs. The only difference in the design of single DU in figure 3.5 from figure 3.1 (a) is that the thickness of Si detector region was reduced from 300 µm to 10 µm so as to improve on the background gamma rejection [9]. Thinner the Si detector region better is the gamma rejection [9].

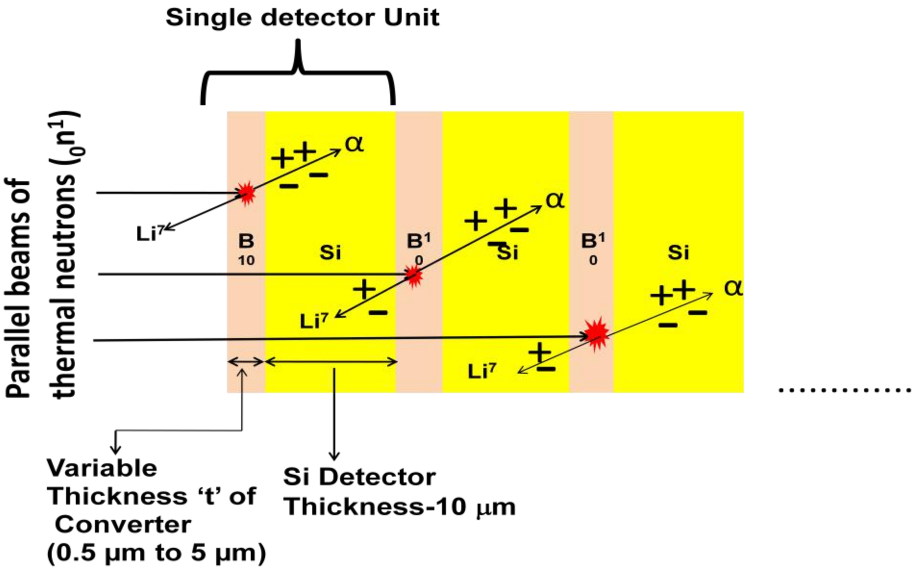

Figure 3.5. Stack detector configuration consisting of enriched B^{10} as CM and Si as detector material arranged in the form of several (Here N=3) DUs. The B^{10} thickness of converter region was a variable parameter 't' in simulation and while for Si detector region thickness was kept constant at 10 µm.

Simulation methodology remains identical to planar configuration geometry as described in section 3.1.1.2. The only difference was that the efficiency of stack detector configuration case was estimated for two parameters:

[1] N varying from 1 to 15.

[2] Variation in thickness 't' of CM from 0.25 μm to 5 μm.

Unlike planar configuration, the methodology adopted for estimating the 'η' for stack detector configuration is slightly different. 'η' in this case is defined as the ratio of

$$\frac{\textbf{Total number of charge particles (}\mathbf{Li^{7}}\textbf{-0.839 MeV and }\boldsymbol{\alpha}\textbf{-1.47 MeV) depositing energy greater than the set LLD value (300 keV) in the sensitive Si detector region divided by a factor of 2}}{\textbf{The total number of neutrons incident on the detector}}$$

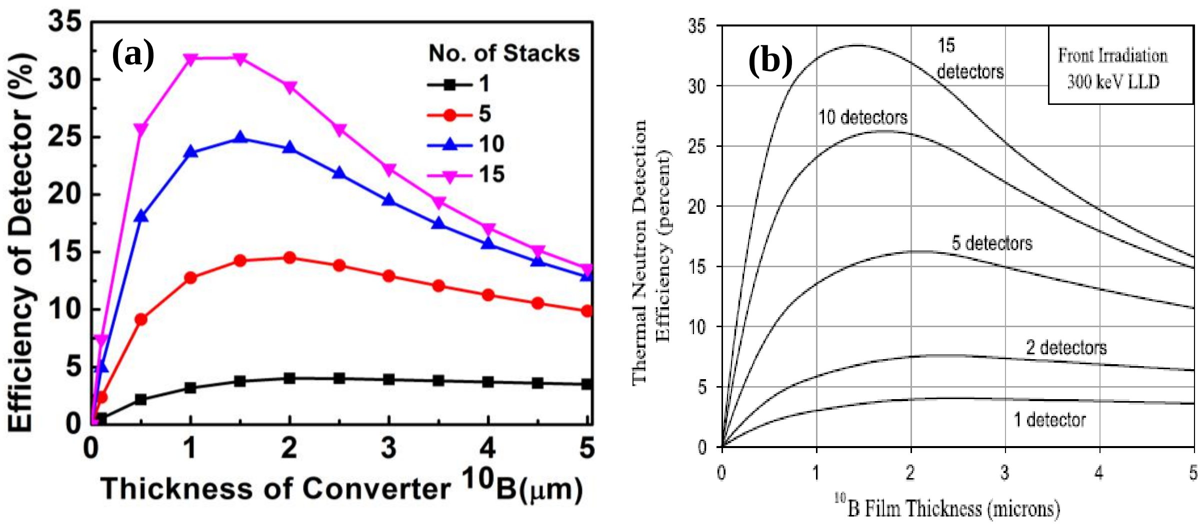

Figure 3.6 Variation in η vs thickness of converter ^{10}B for N=1, 5, 10 and 15 (a) using GEANT4 simulation result and (b) from literature Ref. [8].

Figures 3.6 (a) and (b) present the results of variation in 'η' with 't' along with the number of stacks for stack detector configuration simulated using GEANT4 toolkit and as reported in ref. [8], respectively. It is observed that there is a good agreement between the two, thereby validating the simulations carried out in the present work. Also, the 'η' for stack configuration case has increased considerably in comparison to planar configuration detector which is evident from figures 3.6.

3.2 Boric Acid-Converter material

Having validated the simulations by benchmarking with literature, the simulation was employed for investigation of boric acid as a converter material. The advantage of boric acid is its non toxicity and ease of handling over conventional B^{10} converter as explained in section 1.7 of chapter 1 of this thesis. The simulations were performed for 2D-planar and stack configuration followed by 3D geometry configurations. Only the material parameters were altered in the simulation i.e., instead of converter material B^{10}, boric acid was defined as the converter material. The simulation parameters including LLD value (300 keV), energy of the neutrons (25 meV), number of neutrons (10^8), and detector surface area ($1cm^2$) along X-Y plane were unaltered. The following section compiles the simulation results with boric acid as a converter material.

3.2.1 Two Dimensional (2D) detectors

3.2.1.1 Simulation result for planar configuration

As seen from previous sections, for any planar geometry detector configuration, there exists a critical thickness 't_c' of CM that is dictated mainly by three factors

1) Probability of neutron interaction in CM.
2) Range of the generated charge particles in CM.
3) Probability of charged particles reaching the Si detector.

GEANT4 simulation was performed to optimize the thickness 't_b' of boric acid (H_3BO_3) as a CM in a semiconductor neutron detector for planar configuration, in order to achieve maximum efficiency 'η_{max}' for thermal neutron. The detector design and simulation methodology remains the same as discussed in the previous section 3.1.1.1 and 3.1.1.2, except that the material parameter of the CM was changed. The boric acid (H_3BO_3) compound was defined as a CM with 3, 1 and 3 atoms of $^{1}H_1$, $^{10}B_5$ and $^{16}O_8$, respectively. The other input parameter to the simulation includes the density of boric acid (1.435g/cm^3).

It is well known that natural boron consists of two isotopes viz., B^{10} and B^{11} having compositions of ~ 20% and 80%, respectively and only B^{10} isotope is sensitive to the thermal neutrons [10]. Therefore, in the present simulation, the enrichment of B^{10} content (henceforth referred to as 'B_E') in boric acid was varied from 20% to 100% in steps of 10% for all detector configurations to estimate the simulated 'η'. The thickness of boric acid 't_b' was varied from 0.5 μm to 80 μm in the simulation. Apart from simulation of efficiency estimation, a histogram plot which depicts the energy deposited by the charged particles (Li^7- 0.839 MeV and α-1.47 MeV) in the Si detector region for different 't_b' of CM was also studied using analysis manager of toolkit [4,11].

Fig. 3.7 indicates the variation in the probability of neutron interaction '$P(t_b)$' with thickness of boric acid 't_b', for 'B_E' levels varying from 20% to 100% in steps of 10%. There are two inferences that can be drawn from the above figure. First, '$P(t_b)$' increases with increasing 't_b' for a particular enrichment and second, '$P(t_b)$' increases with increasing enrichment for a particular 't_b'. As mentioned previously, the increase of $P(t_b)$ with 't_b' is due to the exponential decay as dictated by equation (2) while the increase due to enrichment is attributed to the increase in Σ of boric acid (see figure 3.8) which increases with percentage of enrichment.

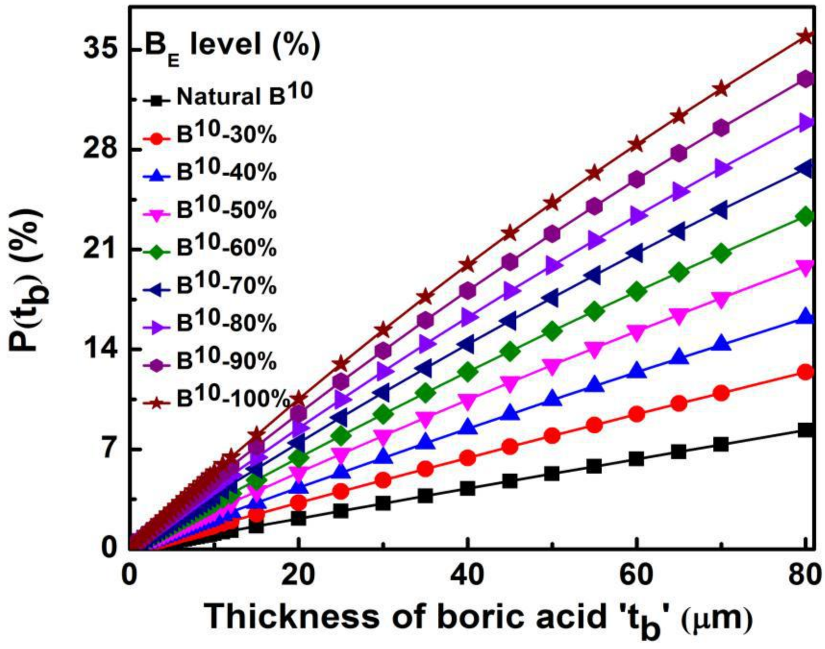

Figure 3.7. Probability of neutron interaction $P(t_b)$ with thickness of converter material boric acid and its dependence on the enrichment of B^{10} level.

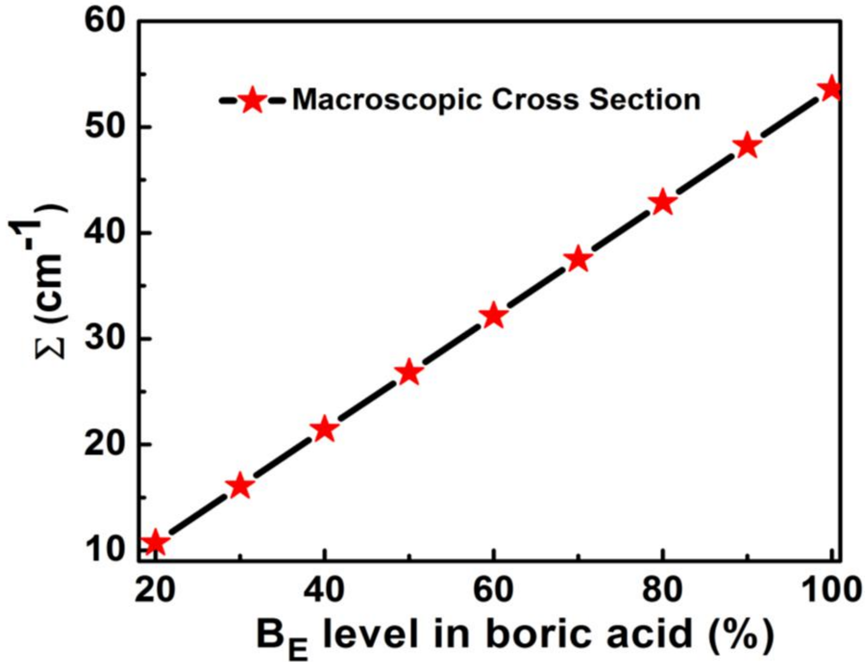

Figure 3.8.Variation in macroscopic cross section 'Σ' with the B^{10} enrichment 'B_E' level in the boric acid.

Figure 3.9 depicts the variation of 'η' with 't_b' of boric acid at various level of B^{10} enrichment content in boric acid. It clearly shows the conflicting thickness requirement and imperative optimization of critical thickness that is required for fabrication of neutron detectors with η_{max} in planar configuration geometry. The variation of ‘η’ with ‘t_b’ for varying content of ‘B_E’ shows an initial increase, reaching a maximum at a particular critical thickness ‘t_{bc}’ and thereafter shows a monotonic decrease. The ‘t_{bc}’ as computed from the simulation was found to be ~5μm, yielding a ‘η_{max}’ of 0.73% for 100% enriched B^{10} (see figure 3.9). Further, critical thickness validation was performed by estimating range of ions Li^7 and α in boric acid by TRIM code which is found to be 3.12 μm and 6.16 μm, respectively [12], as indicated in the figure 3.10. This agrees well with the results generated by GEANT4 simulations and has a decisive role on the ‘t_{bc}’ of the detector.

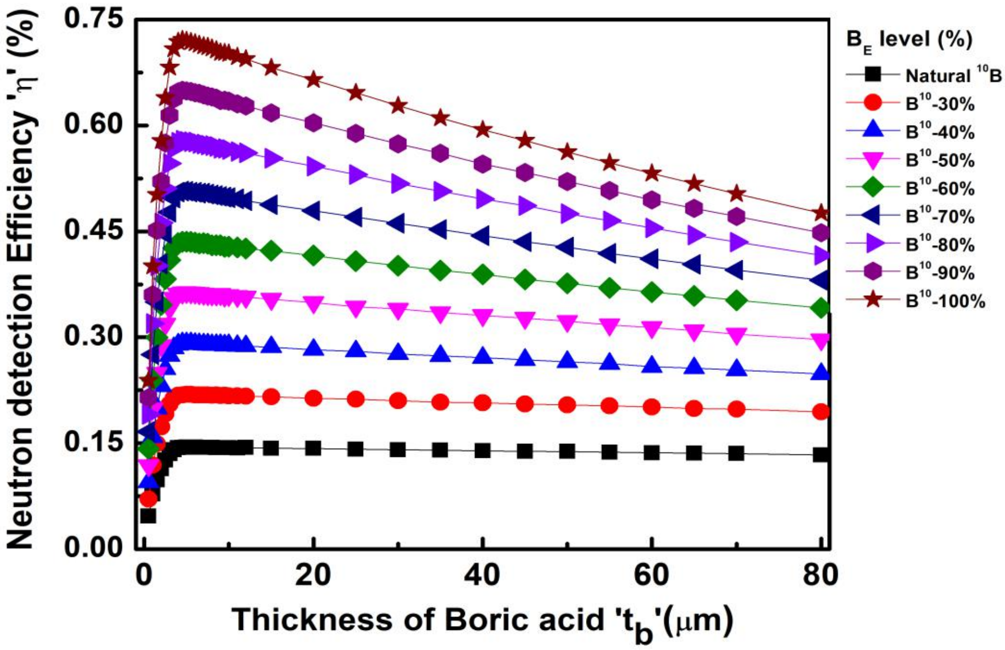

Figure 3.9. Variation in the neutron detector efficiency ‘η’ of a planar configuration detector with thickness of boric acid ‘t_b’, for varying enrichment of B^{10} level ‘B_E’.

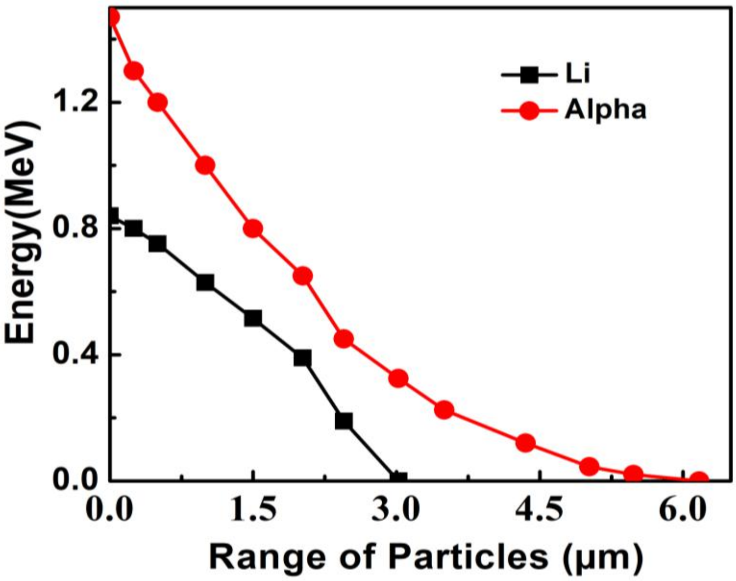

Figure 3.10. The range of charged particles (Li^7 and α) in boric acid having 100% enriched B^{10} was estimated using TRIM code.

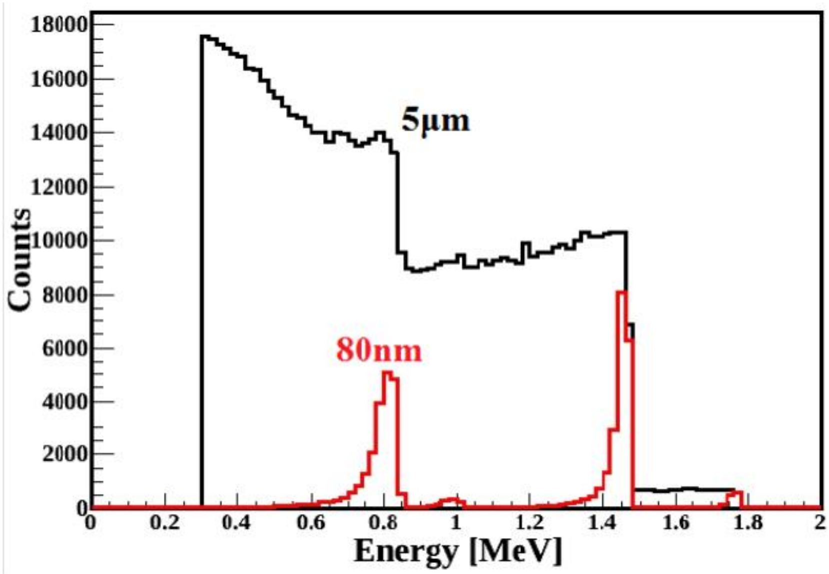

Figure 3.11. Histogram plot of energy deposited by Li^7 and α particles in Si detector for 80nm (red color) and 5μm (black color) thickness of converter layer.

Histogram plots of energy deposited by both Li^7 and α particle in Si detector region for two representative thicknesses of boric acid namely, 80 nm (lower) and 5 μm (higher) are shown in Figure 3.11. Two peaks corresponding to energies of the two charged particles (Li^7- 0.839 MeV) and (α-1.47 MeV) generated in (n,α) reaction are clearly discernible for 80 nm thick boric acid film. For higher thickness, the peaks evolve to step like features and the poor energy resolution for higher 't_b' is attributed to the long paths the charge particles travel before being detected. A point to note is that the counts for 80 nm thick converter layer is low as compared to 5µm thickness, thereby resulting in lower detector efficiency of the former.

3.2.1.2 Simulation results for stack configuration

Figure 3.12 shows the design of two dimensional planar stack configuration which consists of boric acid as a CM on Si detector together to form one single DU. As explained in previous section 3.1.2, i.e., DUs are replicated along Z-axis and integrated together to form N-DU stacked detector configuration. In the present design, N was varied from 5 to 30 and thickness 't_s' varied from 0.25 µm to 10 µm. The other parameters of simulation remained the same. Also methodology adopted for estimating the simulated 'η' remains the same as described in section 3.1.2. A snapshot of the simulation is presented in figure 3.13 and the colour coding in the snapshots is the same as in figure 3.2 except that the pink colour now represent boric acid.

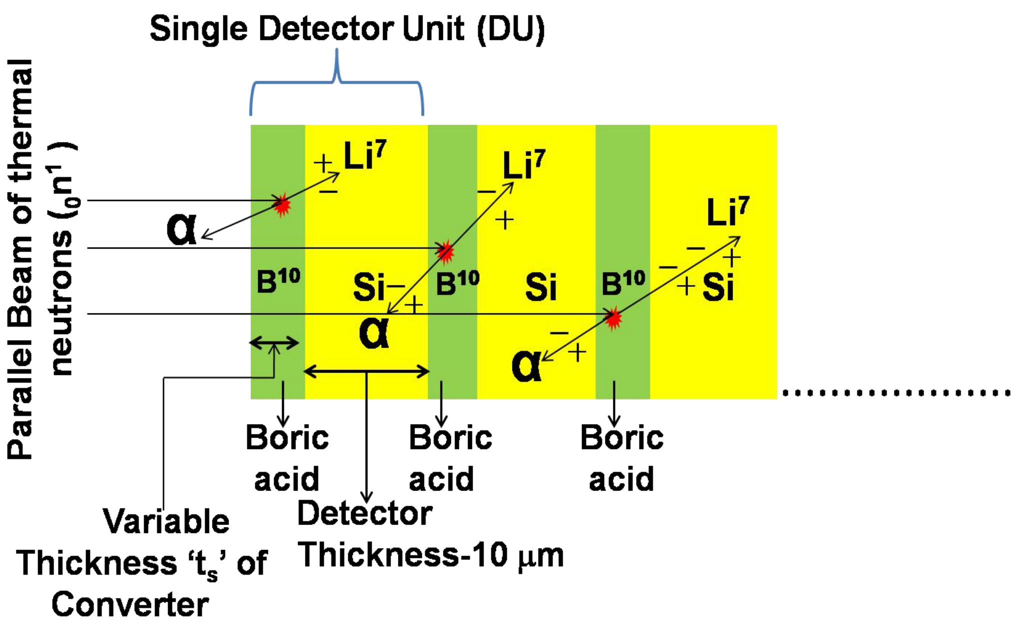

Figure 3.12. Stack detector configuration consisting of boric acid as converter material and Si as detector material arranged in the form of N (Here N=3) Detector Units (DUs). The boric acid thickness 't_s' of converter region was a variable parameter in simulation and whereas for Si detector region thickness was kept constant at 10 µm.

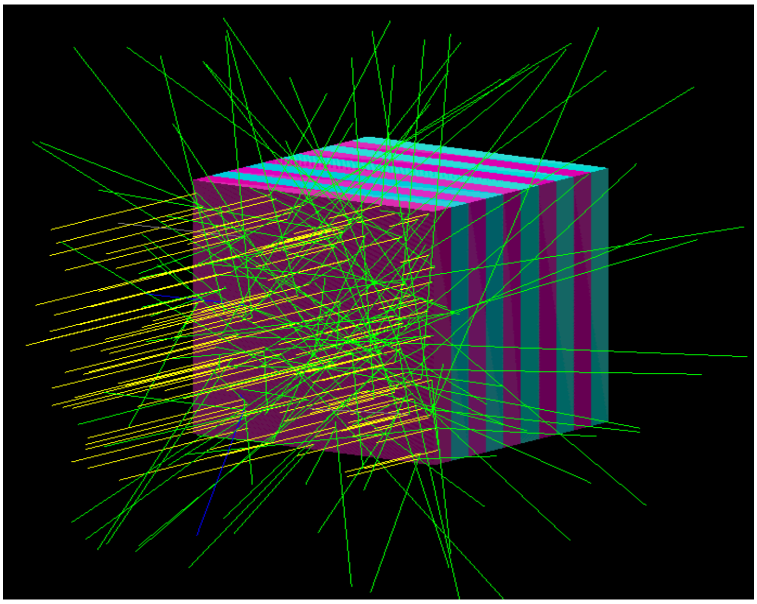

Figure 3.13. Snapshot of GEANT4 simulation for stack detector configurations.

Figures 3.14 (a) and (b) shows the variation of the estimated 'η' with t_S for various number of DUs (B_E constant at 100%) and enrichment content (constant N = 30), respectively.

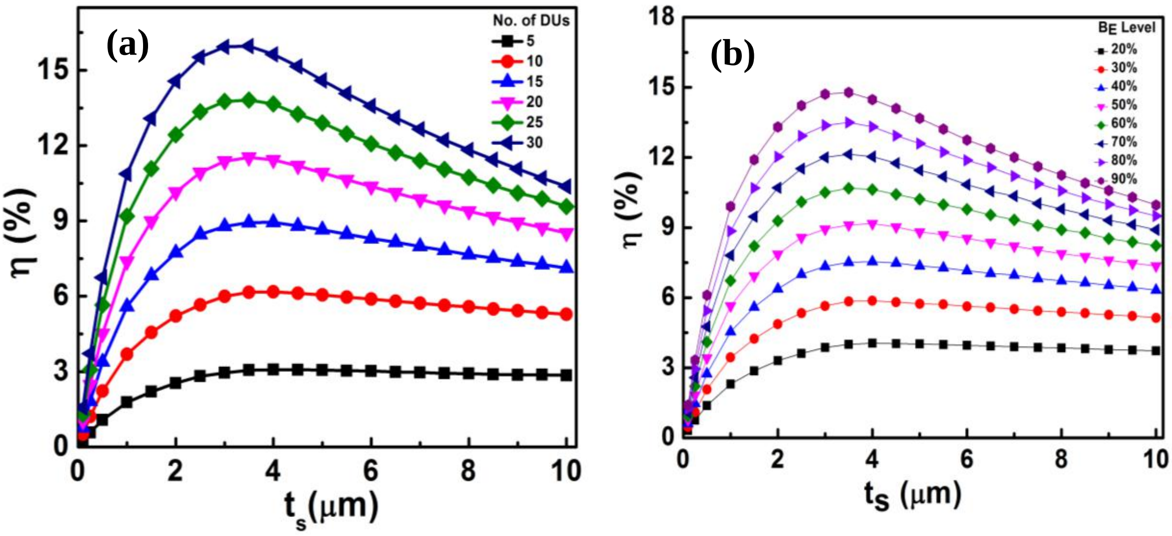

Figure 3.14. Variation of 'η' with 't_s' for planar stack configuration (a) Variable N at fixed B_E=100% (b) Variable B_E with N fixed at 30.

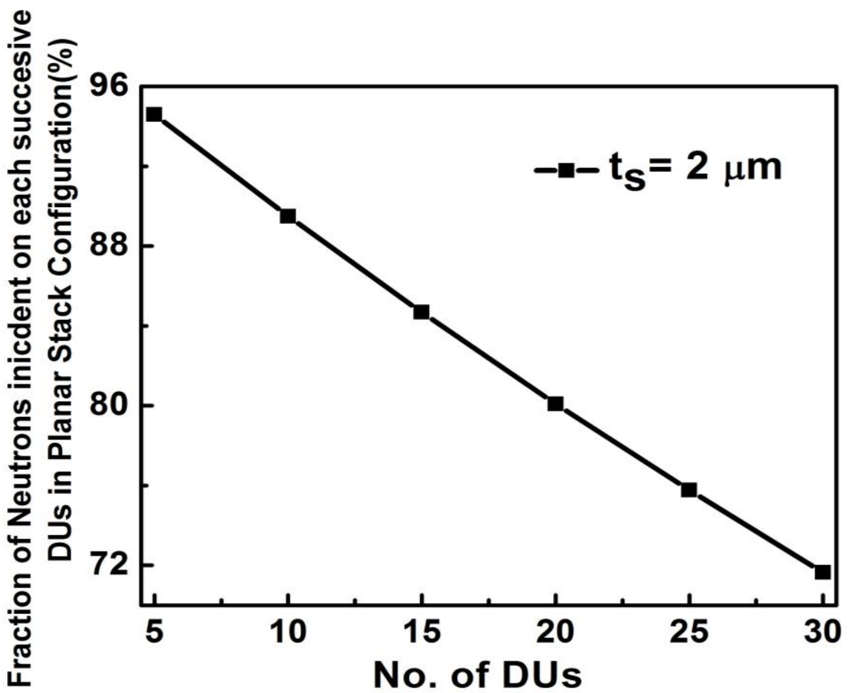

Figure 3.15. Variation in the fraction of incident neutrons seen by each successive DU_s in the planar stack configuration with the number N of DUs at constant thickness of 't_s'=2μm boric acid.

From these figures four striking observations can be made. Firstly, with increasing 't_s' , 'η' increases, reaches maximum at the critical thickness (t_{sc}) and then decreases for any given number of DUs. Secondly, with increase in the number of DUs, 't_{sc}' shifts towards a lower value. This is due to the fact that as DUs increase, most of the incident neutrons are attenuated in the first few stacks (see figure 3.15)

Thirdly, 'η' increases with increase in the number DUs at any given 't_s' and is attributed to the increase in the probability of neutron interaction. This is more evident from figure 3.16 which shows the variation in 'η' with number of DUs at typical constant 't_s' of 3 μm and 'B_E' =100%. It is clear from this figure that the η sharply raises from 2.94% to 15.96% when numbers of DUs are varied from 5 to 30.

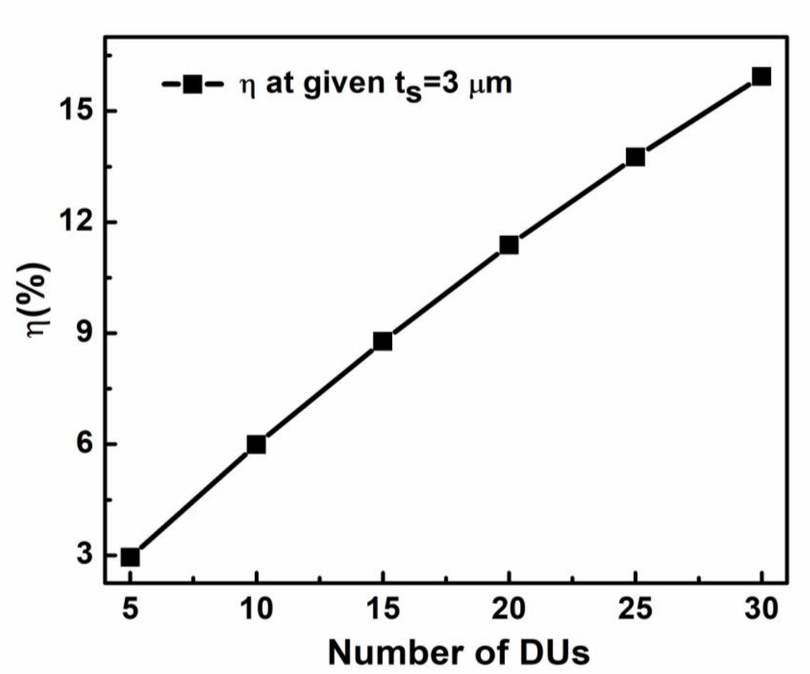

Figure 3.16. Variation in η with number of DUs at a given constant thickness 't_s'=3 μm.

Fourthly, with increase in 'B_E', 'η' increases and is again due to the increase in 'Σ' of boric acid with increasing 'B_E' as seen in figure 3.8.

Simulation studies carried out for similar 2D planar stacked configuration by McGregor et al. [8] for elemental boron with 100% enrichment B^{10} as a converter material, showed 'η' of 32% for 'N'= 15 and 't_s' ~ 1.5 μm . However, in the present case, for the same number of DUs, thickness and 'B_E' level in boric acid, 'η' is found to be 6.821%. This difference is attributed to smaller mass fraction of B^{10} in boric acid and difference in the densities between elemental B^{10} and boric acid. Concurrently, experimental efforts have also been attempted for the planar stack configuration by X.Gao et al. [13] with LiF as a converter material. Their studies have shown an improvement in the thermal neutron detection efficiency for planar stack configuration compared to single DU.

The simulation studies so far discussed above focused on 2D detector configuration i.e. on planar and stack configuration. With the advancement in the micro fabrication technique, it is indeed possible to create perforation structures in Si detector and subsequently backfilling the perforation structures with CM. Such classes of detector are known as the three dimensional (3D) neutron detectors [14]. The following section presents the detector design and simulation results for 3D neutron detectors, namely spherical, cylindrical perforation and cuboidal trench structures. The simulation methodology remains identical to 2D detector configurations except that the number of neutron flux was set at 10^7, in order to compensate for the truncated surface area of $1mm^2$ along the X-Y plane of all the 3D detector configurations. It is also important to note that efficiency (η) estimation methodology in 3D detector configurations remains same as stack detector configuration.

3.2.2 Three Dimensional (3D) detectors

3.2.2.1 Embedded Spherical configuration detector design

The advancements in direct silicon - silicon wafer bonding [15] technology makes it possible to conceive fabrication of boric acid sphere embedded in silicon as shown in figure 3.18. The fabrication involves scooping of hemispherical structures in silicon wafers followed by filling the scooped regions with boric acid (see figure 3.17 (a)). Two such silicon wafers are then bonded by wafer bonding technology resulting in embedded boric acid sphere in silicon (as depicted in figure 3.17 (b)). Such hemispherical trenches on Si wafer have been designed by L. Monteiro et al. for different applications [16].

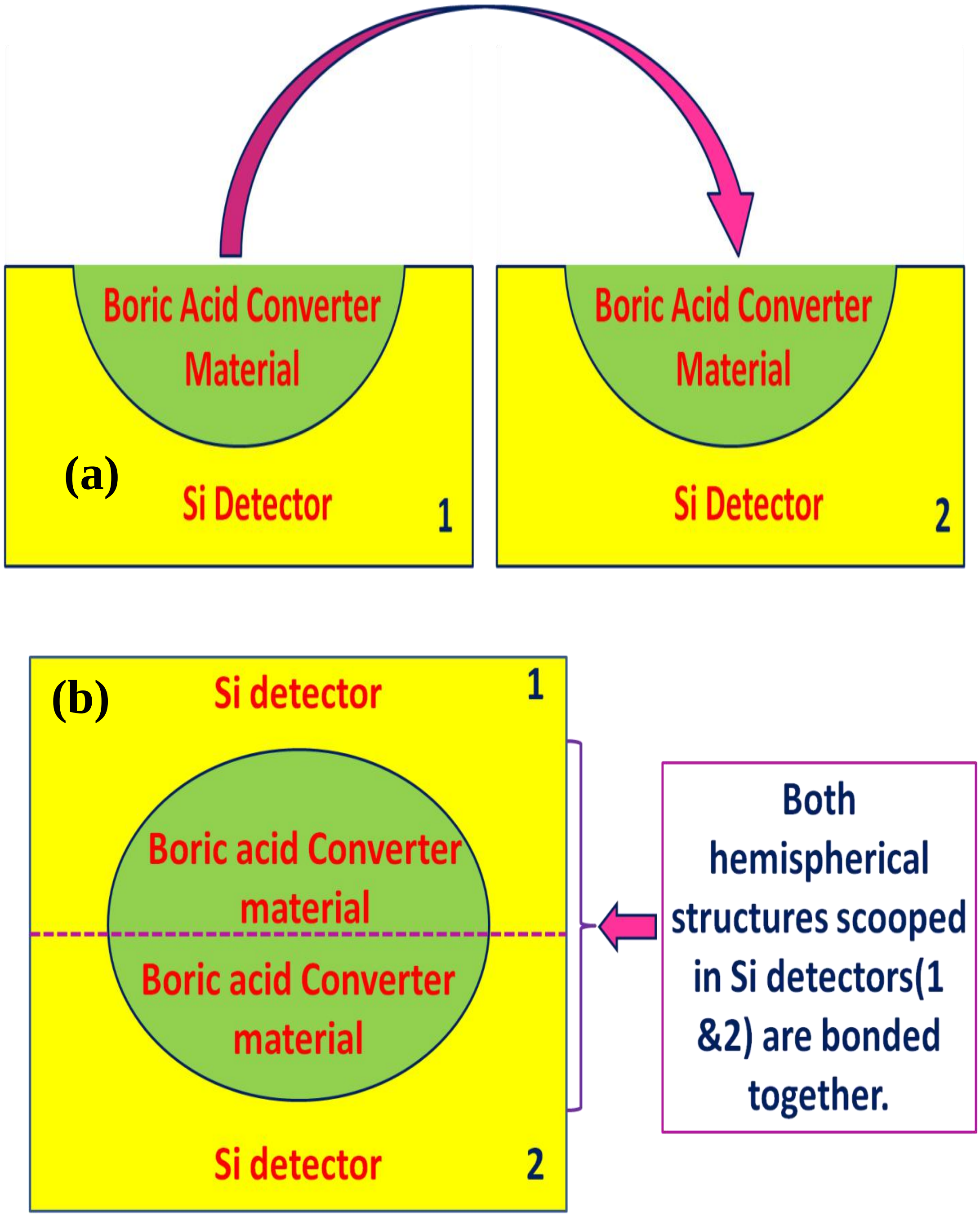

Figure 3.17. Schematic representation of (a) two hemispherical structures consisting of boric acid scooped in two Si detectors (1 and 2) individually. (b) wafer bonding of both the hemispherical structure of (a).

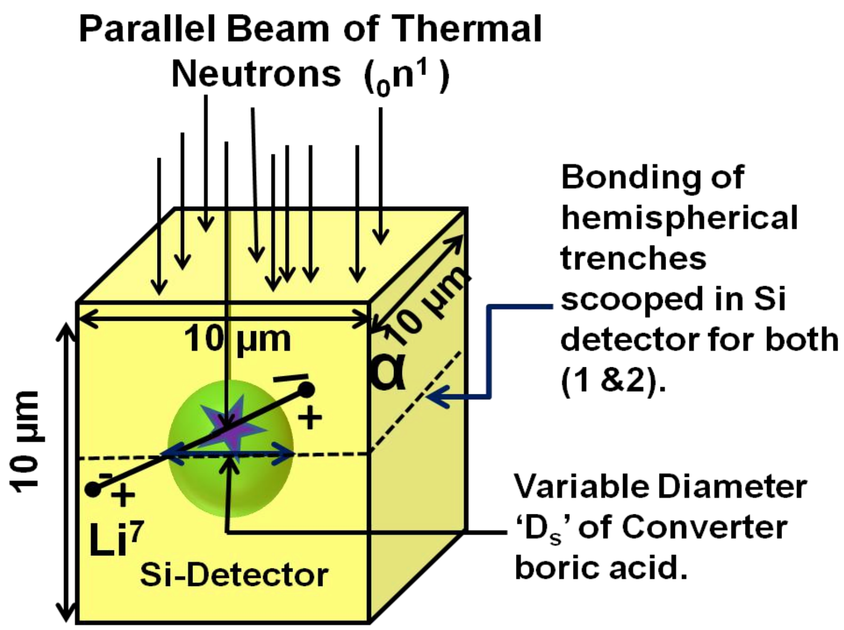

Figure 3.18. Unit cell representation of embedded spherical detector configuration in which the sphere consists of boric acid inscribed inside at the centre of cubical Si detector. The diameter 'D_s' of sphere was the variable parameter in the simulation. The dimension of unit cell was 10 µm x 10 µm x 10 µm.

The embedded spherical detector was conceived using unit cell (see figure 3.18) concept in the geometry class of toolkit. The dimension of the unit cell was 10 µm x 10 µm x10 µm. The entire detector was constructed by duplicating this unit cell 100 times along the X-Y plane direction using G4Replica function of toolkit [4] which results in a matrix form of detector and is designated as single layer embedded spherical detector (see figure 3.19 (a)). When this single layer detector of embedded spheres is replicated in the Z-direction again, it results in stacked embedded spherical detector configuration as shown in figure 3.19 (b). In both configurations (single layer and stacked) the top and bottom surface areas are $1mm^2$ with length and breadth kept 1mm each. The diameter 'D_s' was a variable parameter in the simulation and was varied from 0.5 µm to 9.5 µm with step size of 0.5 µm for both configurations (single layer and stacked). A snapshot of simulation for single layer and stacked embedded spherical detector are shown in figure 3.19 (a) and (b), respectively. The colour coding remains identical to figures 3.2 and 3.13.

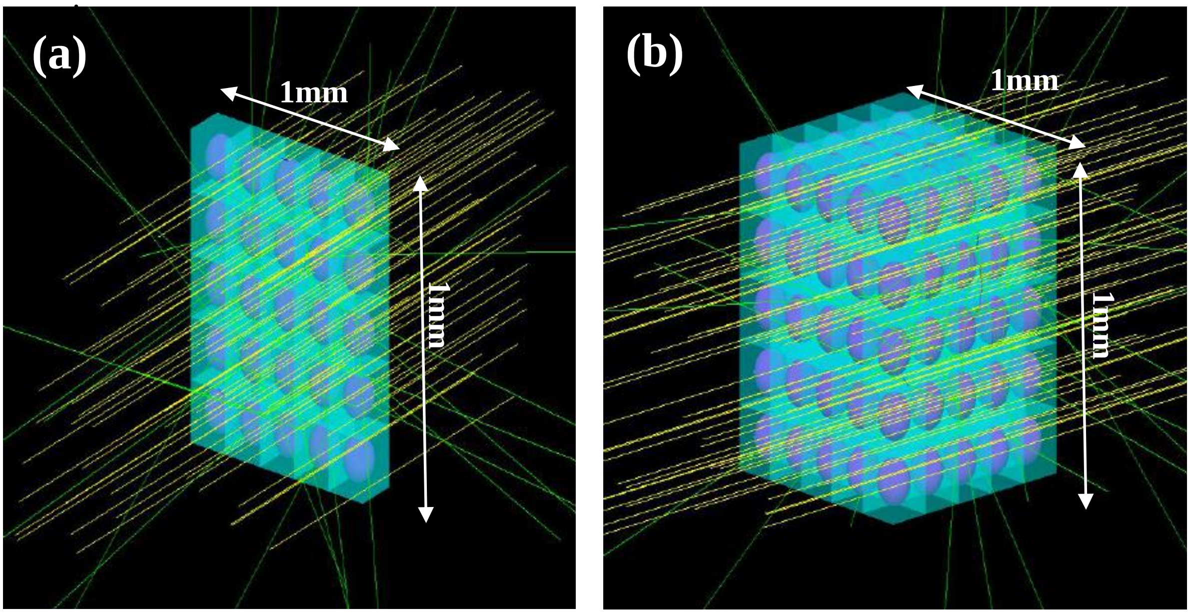

Figure 3.19. Snapshot of GEANT4 simulation for embedded spherical detector configurations (a) Single layer (b) Stack configuration

3.2.2.2 Embedded spherical detector- simulation result

Figure 3.20 represents variation in 'η' with increasing 'D_s' for a single layer embedded spherical detector (see figure 3.19 (a)) for different 'B_E' levels in boric acid.

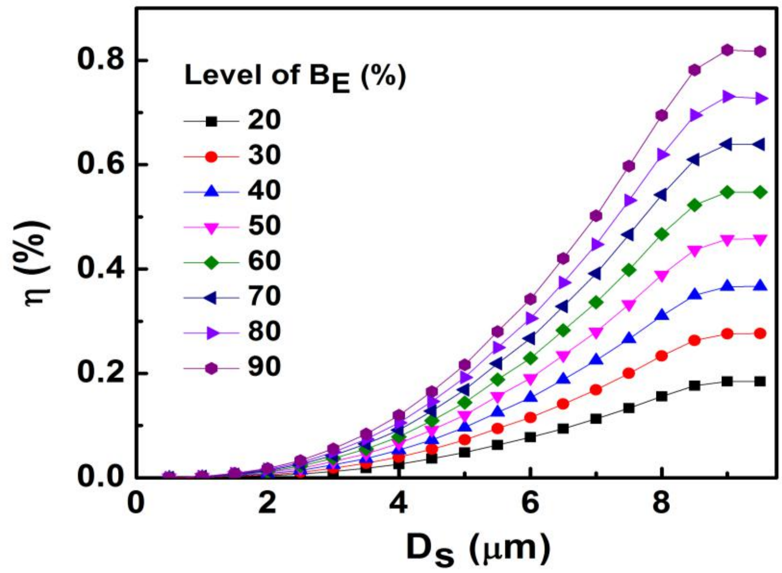

Figure 3.20. The variation in the efficiency 'η' of neutron detection with varying diameter 'D_s' for the single layer embedded spherical detector at different B_E level content in the boric acid.

From this figure it is clear that 'η' increases with both increase in 'D_s' and 'B_E' content. The increase in 'η' with 'D_s' due to the increase in the surface area of converter region leading to an increased probability of neutron interaction (P_{int} (D_s)) as shown in figure 3.21. At 'D_s' = 9 µm, 'η_{max}' = 0.91 % which is higher than the value obtained in 2D planar configuration detectors. Increase in efficiency with increasing 'B_E' is also expected as Σ increases with the 'B_E' content in boric acid (see figure 3.8).

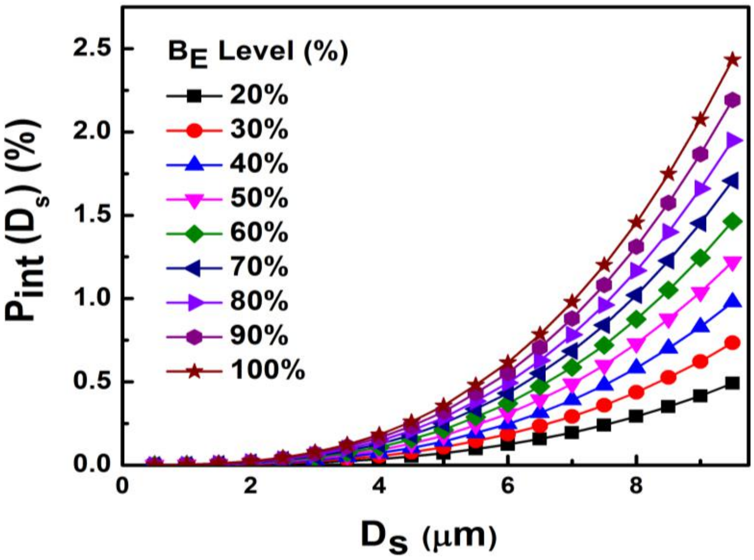

Figure 3.21 The variation in the probability of neutron interaction 'P_{int} (D_s)' with varying diameter 'D_s' for the single layer embedded spherical detector at different B_E level content in the boric acid.

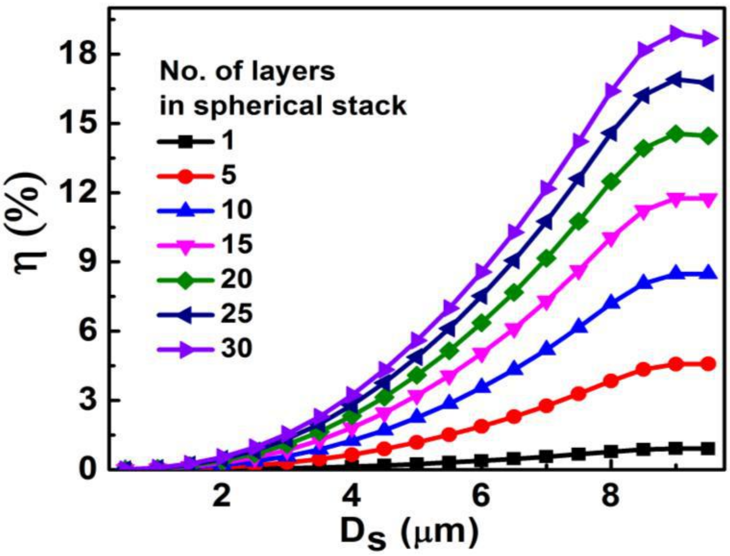

Figure 3.22. The variation in the efficiency 'η' of neutron detection with varying diameter 'D_s' for the stacked embedded spherical layer detector having B_E=100% content in the boric acid. Number of layers varied from 1 to 30.

Efficiency of these detectors can be further enhanced by stacking these detectors in z-direction (see figure 3.19 (b)) as shown in figure 3.22. It is evident from this figure that η_{max} rises from 0.91% to 18.89 % for 30 layers of stacked spherical detectors. This value is also slightly higher than the value obtained in planar stack configuration for the same 30 DUs (see figure 3.14 (a)).

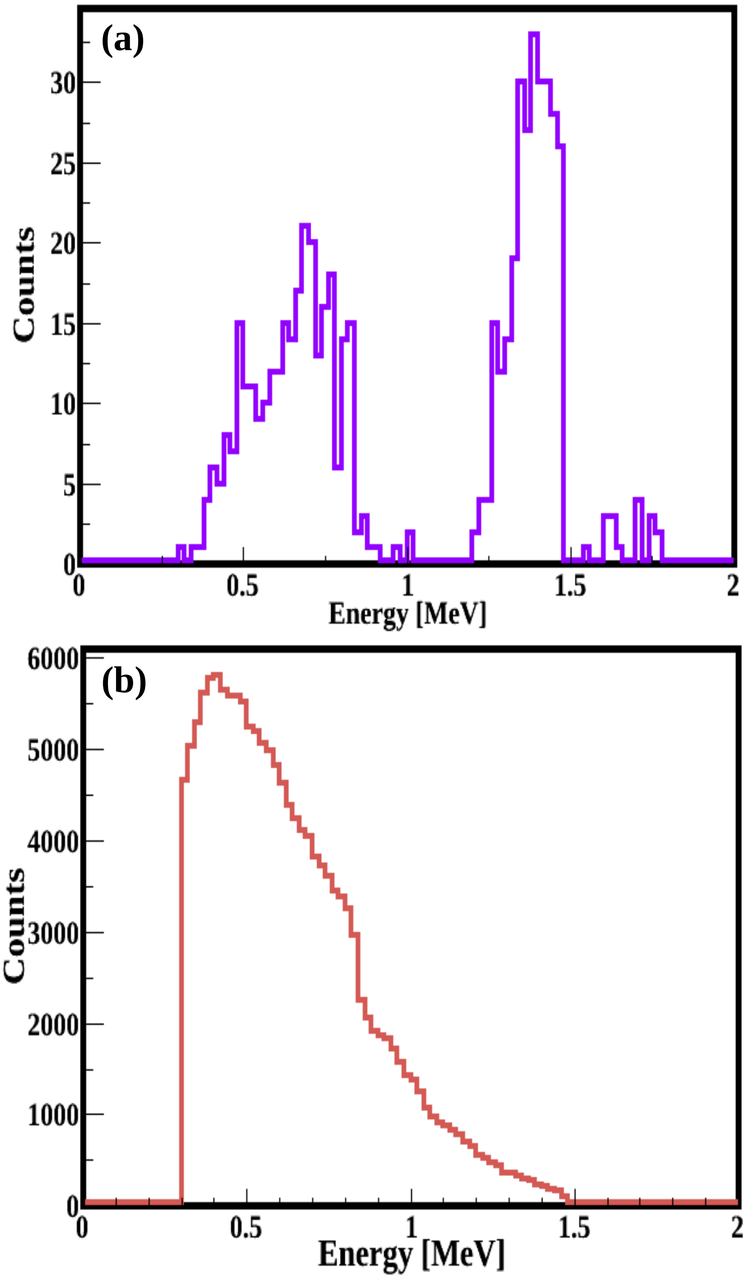

Figure 3.23. Histogram plot depicting the energy deposited by charged particles (Li^7 and α) in Si for single layer embedded sphere detector at (a) D_S-1µm and (b)D_s -8 µm.

The histogram plots generated for single layer embedded spherical detector at two typical diameters i.e. for 'D_s'=1 μm (lower) and 'D_s'=8 μm (higher) are shown in figures 3.23 (a) and (b) respectively. For these simulations, 'B_E' was set at 100%. Similar to planar configuration detectors, the energy peaks corresponding to Li^7 and α charge particle are clearly distinguishable at lower 'D_s', where as it is imperceptible at higher 'D_s'. Also, counts are significantly higher in the later case, leading to an enhanced 'η'. However, at higher 'Ds', it is interesting to note that the higher energy counts are substantially reduced, which is in contrast to the planar detectors. This is attributed to the diminishing volume of the Si region in embedded spherical design, which limits the charge particle energy deposition.

From the foregoing discussions it is clear that the 'η' of planar stack (2D) and embedded spherical (3D) detectors can be enhanced by increasing the number of DUs and stacking the layers, respectively in z-direction. However, fabrication of such configurations imposes certain practical difficulties such as achieving the conformal coating of converter material and complex electrode design for contacts. Also, in these detectors gamma discrimination efficiency will be poor due to the increase in effective thickness of Si [9] and requires high power for operation [8]. Some of these shortcomings can be overcome by designing cylindrical perforation and cuboidal trench configurations and will be discussed now.

3.2.2.3 Cylindrical perforation and Cuboidal trenches configuration detector design

Similar to single layer embedded spherical detector, cylindrical perforation and cuboidal trenches shown in figures 3.24 (a) and (b), respectively were designed based on unit cell concept, except for the difference in the dimensions of unit cell. The unit cell for both cylindrical perforation and cuboidal trench was taken as 10 μm x 10 μm x 300 μm.

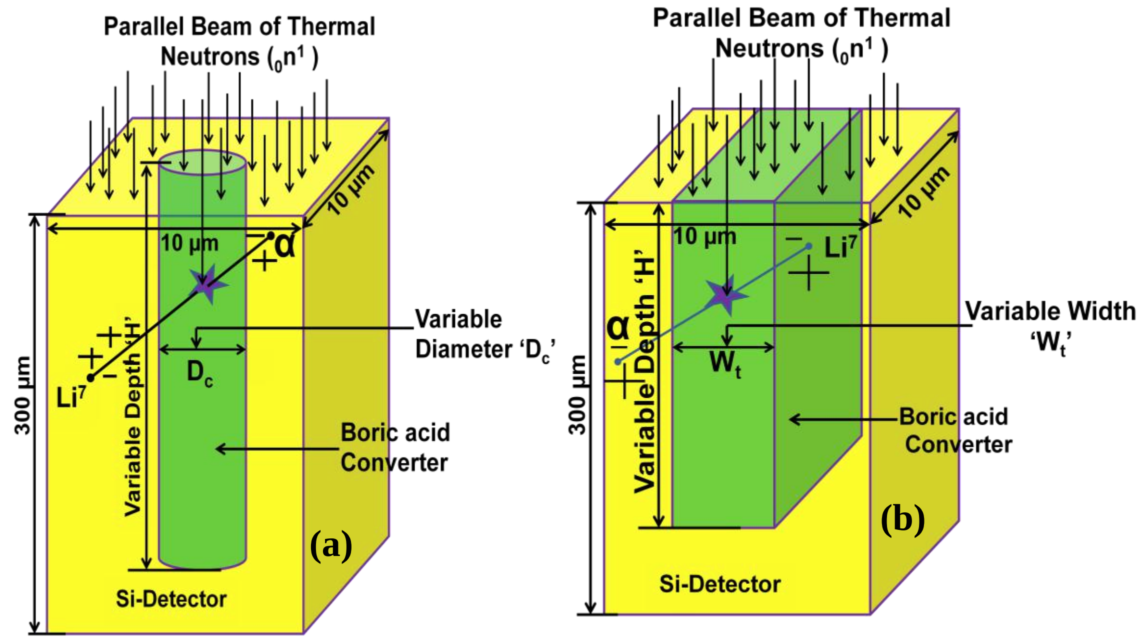

Figure 3.24 Unit cell representation of (a) Cylindrical perforation geometry with variable diameter 'D_c' and depth 'H' (b) Cuboidal trench geometry with variable width 'W_t' and depth 'H'. The dimension of unit cell in both geometries is 10 µm x 10 µm x 300 µm.

The unit cell was replicated 100 times along the X-Y plane for entire construction of detector for both the configuration. The depth (H) in both cylindrical perforation and cuboidal trench detector configuration was taken as variable parameter in the simulation i.e., it varied from 25 µm to 275 µm in steps of 25 µm. The other variable parameters were diameter (D_c) and width (W_t) in the cylindrical perforation and cuboidal trench detector configuration, respectively. Both 'D_c' and 'W_t' were varied from 0.5 µm to 9.5 µm in steps of 0.5 µm in the simulation. The snapshot for the simulation for both the configuration is shown in figures 3.25 (a) and (b). Again the colour coding for the figures remains same as described in figures 3.2 and 3.13.

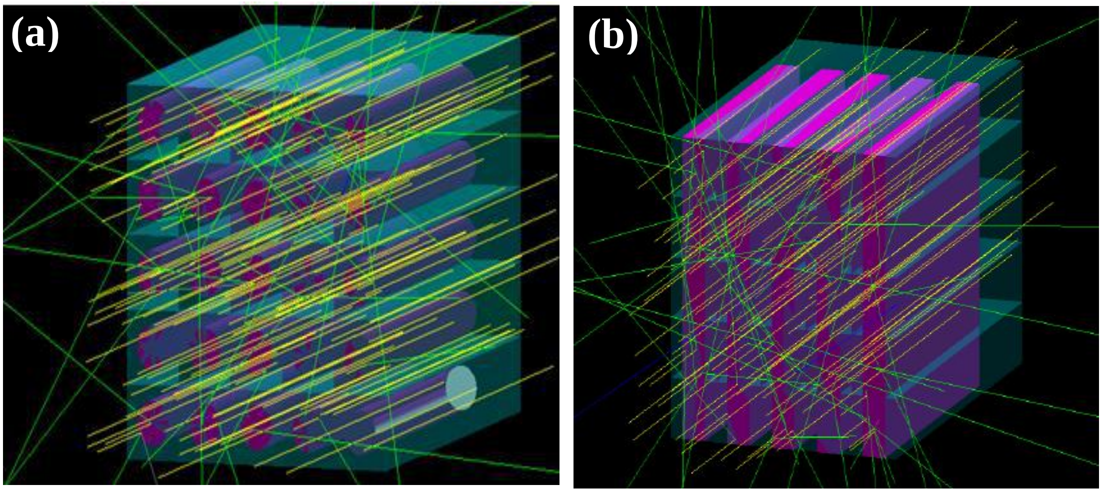

Figure 3.25. Snapshot of GEANT4 simulation for (a) Cylindrical perforation (b) Cuboidal structures.

3.2.2.4 Cylindrical perforation and cuboidal trench detector-simulation result

Figures 3.26 (a) and (b) represents variations in ‘η’ with diameter ‘D_c’ and ‘W_t’ at various depths ‘H’ for cylindrical perforation and cuboidal trench, respectively at B_E =20%. It is clear from figure 3.26 (a), that the ‘η’ increases with increasing ‘D_c’, reaches a maximum at a critical ‘D_c’ of 8 μm and there after it reduces. In contrast to this, cuboidal trench configuration shows a plateau like behaviour till ‘W_t’ = 8μm and there after it falls drastically. This is attributed to the higher probability of neutron interaction and larger interfacial surface area between the boric acid layer and Si region which facilitates the transport of charges particles into Si, in this configuration. Decrease in ‘η’ after 8 μm in both the configurations is due to the following two reasons. First, though probability of neutron interaction increases with D_c (W_t) (see figure 3.27 (a) and (b)), there is an unavoidable self absorption of charged particles in boric acid layer itself. Second, increase in D_c (W_t) beyond 8 μm decreases the detector volume, which limits the charged particles to deposit their energy above LLD.

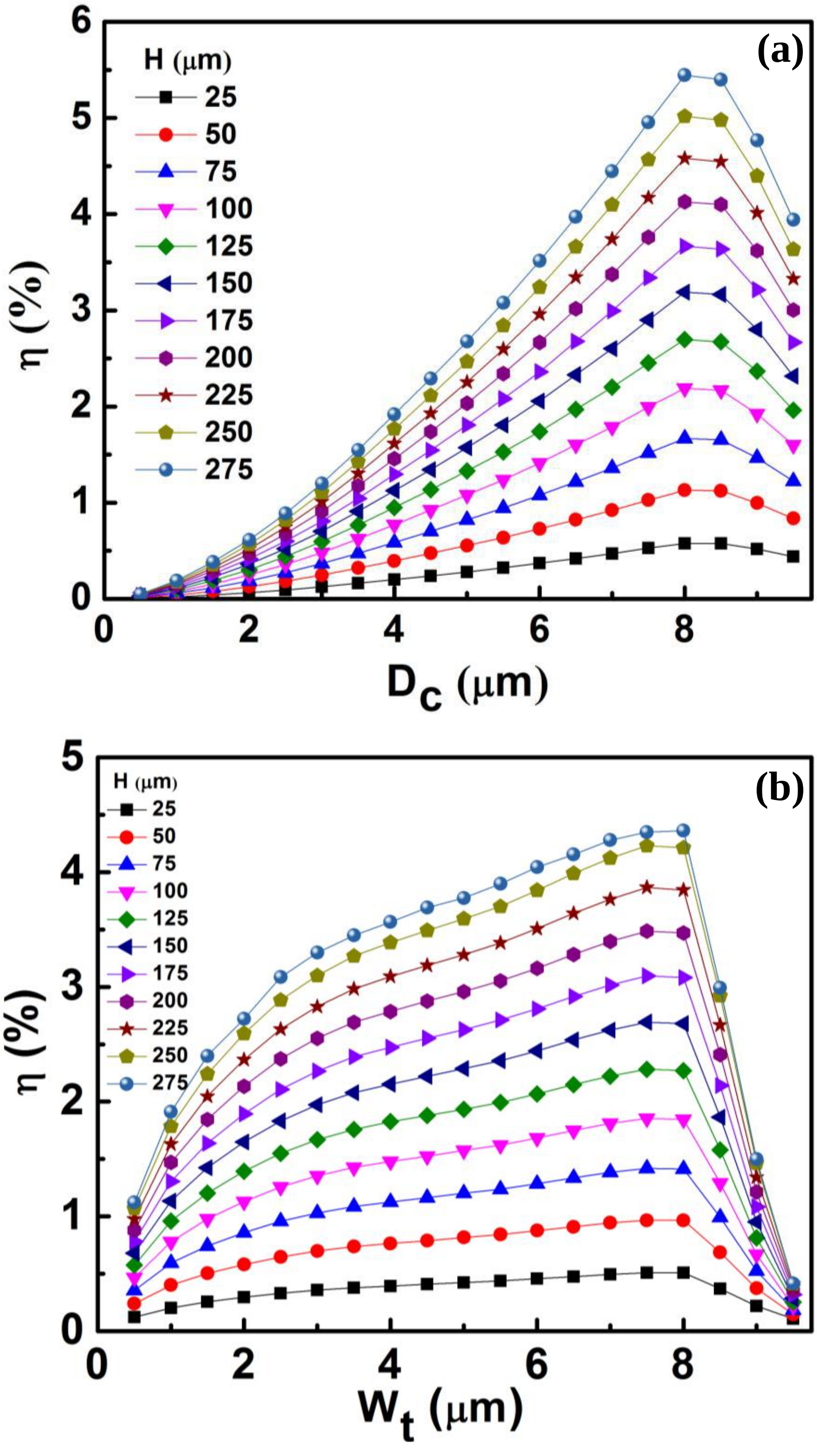

Figure 3.26 The variation in the efficiency 'η' of neutron detection for B_E=20% content in boric in (a) Cylindrical perforation and (b) Cuboidal trench, detector configuration at varying geometrical parameters like diameter 'D_c', width 'W_t' and depth 'H'.

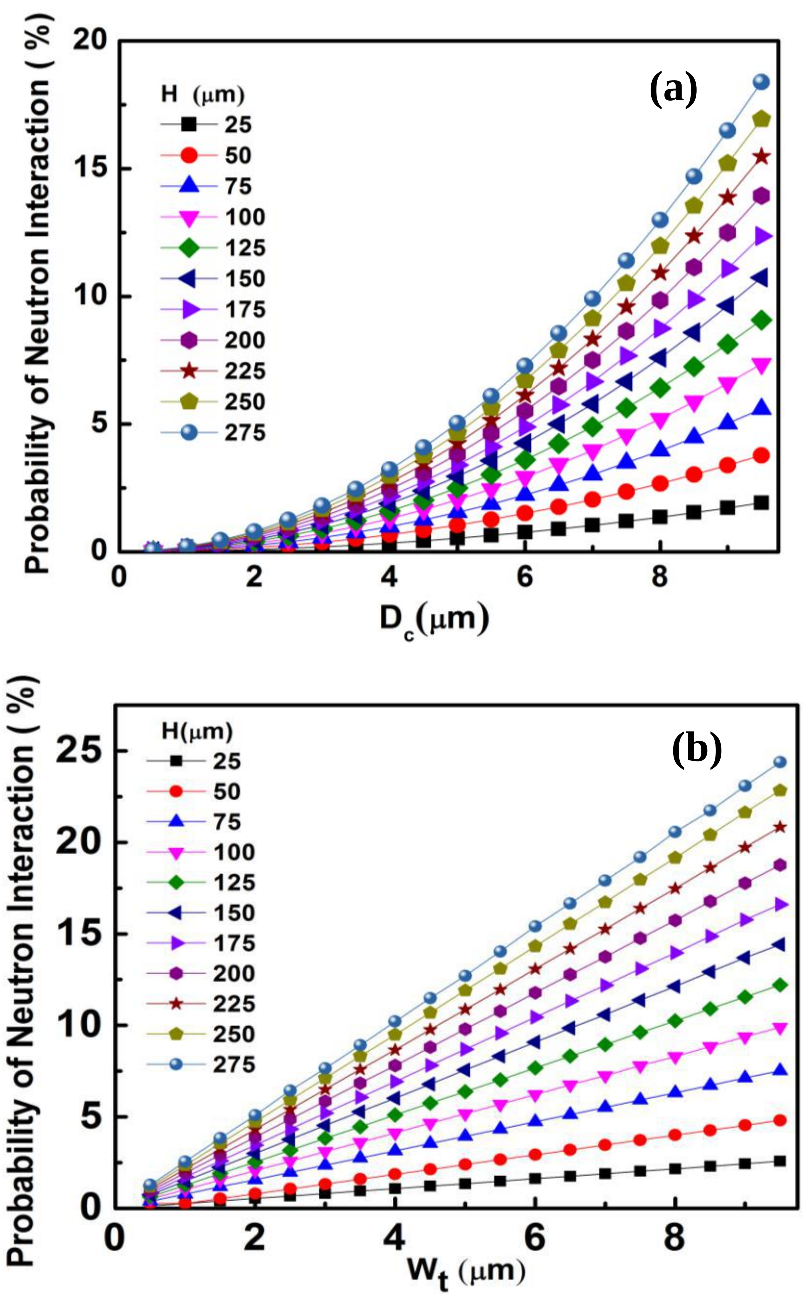

Figure 3.27. Variation of probability of neutron interaction for B_E=20% content in the boric acid at varying diameter 'D_c' and width 'W_t' in (a) cylindrical perforation and (b) Cuboidal trench structure geometries detector configuration, respectively along with their varying depth 'H'.

At a given D_c (W_t), 'η' also increases with increasing depth 'H' in both the configurations, which is due to the increase in the converter material volume, which in turn increases the probability of neutron interaction as shown in figures 3.27 (a) and (b). The η_{max} for cylindrical perforation at 'D_c' =8 μm and 'H'=275 μm was found to be

5.44%, whereas at same dimension of 'W_t' and 'H' the η_{max} in case of cuboidal trench was found to be 4.36%.

The variation in 'η' was also studied and estimated for different 'B_E' levels (30% to 100%) for both configurations and the results are shown in figures 3.28 (a) and (b) at a given typical 'H' of 275μm. The same explanation as in 2D planar stack configuration holds good for the increase in 'η' with enrichment, i.e., the Σ increases with the 'B_E' content in boric acid (as shown in figure 3.8)

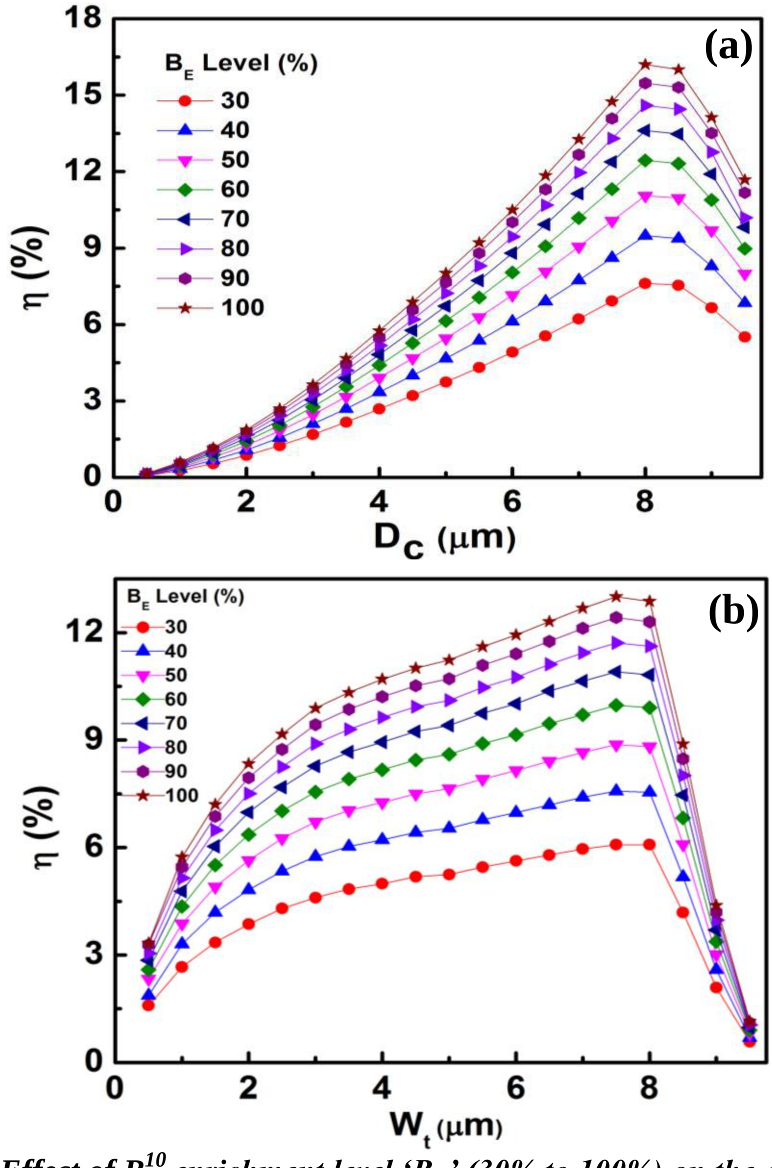

Figure 3.28. Effect of B^{10} enrichment level 'B_E' (30% to 100%) on the efficiency 'η' of neutron detector at varying diameter 'Dc' and width 'Wt' in (a) cylindrical perforation and (b) Cuboidal trench structure geometries detector configuration, respectively for the typical depth 'H' of 275μm.

Similar trends in simulated efficiencies were reported by Shultis et al. [17] while studying the 3D neutron detectors with elemental B^{10} as converter layer. However, achievable peak efficiency is lower in our case and is attributed to lower Σ of boric acid with respect to elemental B^{10}. For comparison, Shultis et al. have reported 'η' of 16.31% for cylindrical perforation configuration for a typical D_c = 7 μm , H = 40 μm with a unit cell width of 10 μm. However, in the present studies to reach same η value with same unit cell width dimension and 'B_E' level, 'D_c' and 'H' has to be around 8 μm and 275 μm, respectively. Though 'η' is low in boric acid than the elemental B^{10} it can still be considered as an alternate converter material due to its overwhelming advantages like its ease of handling as it is non-toxic nature.

The histogram plots were obtained from the analysis manager for both the configurations in order to study the pulse height spectra. A typical histogram plots for the cylindrical perforation is shown in figures 3.29 (a) and (b) for the 'D_c' =0.5 μm and 8 μm, respectively for 100% B_E content in boric acid and 'H'=275 μm.

Again the trends are similar to the embedded single layer spherical detector i.e. at lower D_c of 0.5 μm, the peaks corresponding to individual charge particles (Li^7 and α) are discernible, while for higher D_c of 8 μm, the peaks are indiscernible. The observed trend in behaviour has the same explanation as in single spherical detector.

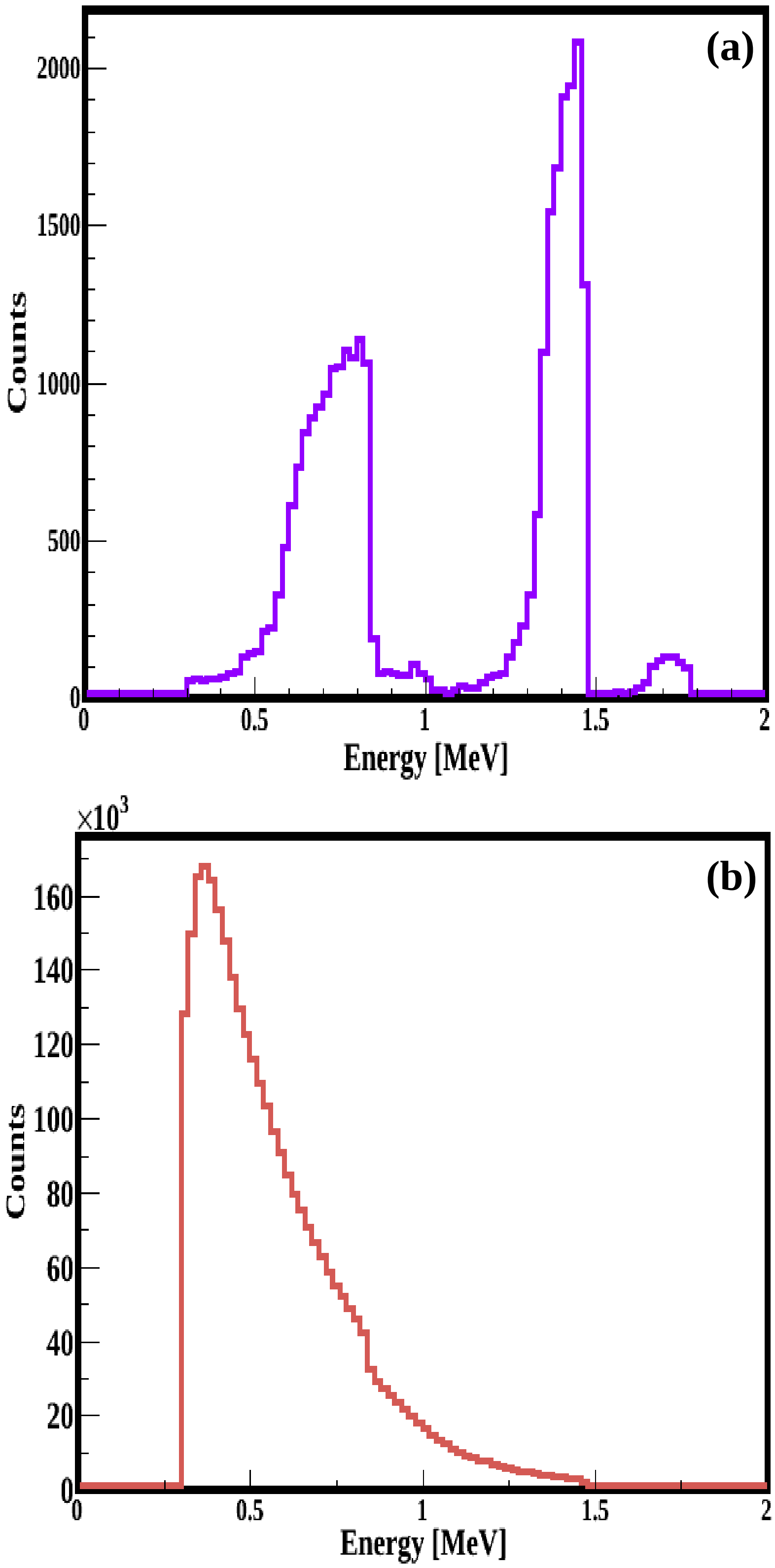

Figure 3.29. Histoplot depicting the energy deposited by charged particles (Li^7 and α) in Si detector region for cylindrical perforation detector at (a) D_c=0.5µm and (b) D_c= 8µm for constant depth 'H'=275 µm for 100% B_E level in boric acid.

3.3 Summary of maximum neutron detection efficiency (η) for all configurations

A summary of maximum neutron detection for all the configurations along with the critical geometrical parameters at B_E =100% are tabulated in table 3.1

Table 3.1. The maximum simulated efficiency for different detector configuration along with the critical geometry.

Sl.No	**Detector Configuration**	**Maximum Efficiency (η_{max}) in (%) for 100% B_E level in boric acid.**	**Critical geometry parameter**
1.	Planar (Single DU)	0.73% for DU=1	Thickness 't_s'~5 μm
2.	Planar Stack	15.96% for DU=30	Thickness 't_s'~3.5 μm
3.	Single layer Embedded Spherical detector	0.91%	Diamter 'D_s' ~9 μm
4.	Stacked layer Embedded spherical detector	18.89% for 30 layers	Diamter 'D_s' ~9 μm
5.	Cylindrical perforation	16.20% at 275 μm depth (H)	Diamter 'D_c' ~ 8μm
6.	Cuboidal trench	13.02% at 275 μm depth (H)	Width 'W_t' ~ 8μm

Though the stacked embedded spherical detector has the highest efficiency it has certain practical limitation as discussed in section 3.2.2.2 which limits its usage. Hence, it can be seen from the table 3.1 the next best configuration for maximum efficiency is cylindrical perforation which can be deployed for thermal neutron detection.

3.4 Conclusions

The present chapter focused on two aspects, the first being benchmarking simulation to validate the GEANT4 simulation with literature. The benchmarking simulation was performed for two test cases i.e., planar and stack configuration using enriched B^{10} as a converter material. The efficiency results of GEANT4 simulation matches well with the literature. The next focus was to estimate the efficiency of thermal neutron detection with boric acid as a CM for 2D (planar and stack) and 3D (embedded sphere, cylindrical perforation and cuboidal trench structure) geometry configurations. In case of 2D planar configuration, it was found that 'η_{max}' reaches a value of 0.73% at a critical thickness of 5 µm for 100% enriched B^{10} content in boric acid. For planar stack detector configuration, the 'η' can be enhanced by increasing the number of DUs. For instance, 30 DUs in planar stack configuration leads to 'η_{max}' of 15.96% at a critical thickness of 3.5µm having 100% B_E content in boric acid. For 3D embedded spherical detector consisting of single layer, 'η_{max}' is 0.91% at a critical diameter of ~ 9 µm for 100% 'B_E' content in boric acid as deduced from the simulation. However, 'η_{max}' increases considerably to 18.89 % for 30 numbers of layers in stacked embedded spherical design. In case of cylindrical perforation and cuboidal trench 3D detector configuration, the optimum critical diameter and width was found to ~8 µm. It was also found that in both the configurations, 'η' increased with increasing depth of perforation and trench. For a typical diameter/width of 8µm and depth of 275 µm, the 'η_{max}' were 16.20% and 13.02 % for cylindrical perforation and cuboidal trench detector, respectively for 100% 'B_E' content in boric acid. This is much higher than the 2D planar configuration detector.

In summary, boric acid is a natural choice of converter material for detection of thermal neutrons owing to its non- toxic nature, ease of handling and amenability to fabrication in different configurations. To achieve higher efficiency, cylindrical perforation and cuboidal trench are the preferred geometrical configurations.

The simulations on boric acid with different geometries presented in this chapter were carried out with LLD set at 300keV due to the low Q-value of neutron interaction. This makes it rather unsuitable for field applications with high energy background radiation, such as in a nuclear reactor. Therefore, alternative converter materials with higher Q-value need to be explored and this is the subject of the next chapter.

References

[1] R. G. Sargent, “Verification and validation of simulation models,” in Proceedings of the 2009 Winter Simulation Conference (WSC), 2009, pp. 162–176.

[2] S. Agostinelli et al.,Geant4—a simulation toolkit, Nuclear Instruments and Methods in Physics Research Section A: Accelerators, Spectrometers, Detectors and Associated Equipment. 506 (2003) 250–303. doi:10.1016/S0168-9002(03)01368-8

[3] J. Allison et al., Geant4 developments and applications, IEEE Transactions on Nuclear Science. 53 (2006) 270–278. doi:10.1109/TNS.2006.869826.

[4] Geant4 User’s Guide for Application Developers, (n.d.). http://geant4.web.cern.ch/geant4/UserDocumentation/UsersGuides/ForApplicationDeveloper/html/index.html (accessed October 31, 2016).

[5] D.S. McGregor, J. Kenneth Shultis, Reporting detection efficiency for semiconductor neutron detectors: A need for a standard, Nuclear Instruments and Methods in Physics Research Section A: Accelerators, Spectrometers, Detectors and Associated Equipment. 632 (2011) 167–174. doi:10.1016/j.nima.2010.12.084.

[6] S.L.Bellinger, Advanced Microstructured Semiconductor Neutron detectors: Design, fabrication and performance, A Doctoral thesis submitted to Kansas State University (2011).

[7] P. Rinard, Neutron Interaction with Matter-Chapter-12, Passive Nondestructive Assay of Nuclear materials, US Nuclear Regulatory Commission Washington DC, Los Alamos National Lab,March 1991.

[8] D.S. McGregor, M.D. Hammig, Y.-H. Yang, H.K. Gersch, R.T. Klann, Design considerations for thin film coated semiconductor thermal neutron detectors—I: basics regarding alpha particle emitting neutron reactive films, Nuclear Instruments and Methods in Physics Research Section A: Accelerators, Spectrometers, Detectors and Associated Equipment. 500 (2003) 272–308. doi:10.1016/S0168-9002(02)02078-8.

[9] J.W. Murphy, G.R. Kunnen, I. Mejia, M.A. Quevedo-Lopez, D. Allee, B. Gnade, Optimizing diode thickness for thin-film solid state thermal neutron detectors, Appl. Phys. Lett. 101 (2012) 143506. doi:10.1063/1.4757292.

[10] D.S.McGregor,R.T.Klann,H.K. Gersch, J.D.Sanders, Designs for thin-film-coated semiconductor thermal neutron detectors,in:2001 IEEE Nuclear Science Symposium Conference Record (cat.No. 01CH37310),2001:pp.2454-2458. doi: 10.1109/NSSMIC 2001.1009315.

[11] ROOT: Data Analysis Framework [*https://root.cern.ch/drupal/*].

[12] TRIM website- http://www.srim.org/

[13] X. Gao, F. Li, M. Lu, Y. Jiang, C. Li, Characteristics of Si-PIN nuclear radiation detectors stacked in series and parallel, Science China Technological Sciences. 58 (2015) 1091–1095. doi:10.1007/s11431-015-5802-7.

[14] R.J. Nikolic,Chin Li Chung, C.E.Reinhardt ,T.F.Wang, Roadmap for High Efficiency Solid-State Neutron Detectors, Proceedings of SPIE , (2005)6013.

[15] M. Shimbo, K. Furukawa, K. Fukuda, K. Tanzawa, Silicon-to-silicon direct bonding method, Journal of Applied Physics. 60 (1986) 2987–2989. doi:10.1063/1.337750.

[16] de L. Monteiro, D. W, F.P. Honorato, R.F. de O. Costa, L.P. Salles, Surface Texturing with Hemispherical Cavities to Improve Efficiency in Silicon Solar Cells, International Journal of Photoenergy. (2012). doi:10.1155/2012/743608.

[17] J.K. Shultis, D.S. McGregor, Design and performance considerations for perforated semiconductor thermal-neutron detectors, Nuclear Instruments and Methods in Physics Research Section A: Accelerators, Spectrometers, Detectors and Associated Equipment. 606 (2009) 608–636. doi:10.1016/j.nima.2009.02.033.

Chapter-4

GEANT4 Simulation on Depleted UO_2

Previous chapter dealt with benchmarking and simulation of boric acid as a converter material in 2D and 3D geometry such as planar, stack, sphere, cylindrical perforation and cuboidal trenches to achieve maximum neutron detection efficiency for thermal neutrons. This chapter explores yet another alternative converter material which can be used for detection of both fast and thermal neutrons using GEANT4 simulation. The aim of the GEANT4 simulations is primarily to estimate neutron detection efficiency.

4.1 Introduction

In the pursuit of designing neutron detectors, the merits of depleted Uranium Oxide (DUO_2) as a neutron sensitive converter material as discussed in chapter 1 needs to be considered and it is worthwhile to examine its theoretical efficiency, for three basic designs, namely, planar, cylindrical perforations and trench structures. For the planar structure, both direct and indirect configuration detectors have been considered. The perforated and trenched configurations are inherently indirect as they are constructed by scooping out cylindrical and cuboidal holes in silicon and backfilling them with DUO_2 converter material. In the present chapter, a detailed discussion on the GEANT4 systematic simulation studies to estimate the efficiency of solid state semiconductor neutron detection with different thickness in planar configuration, perforation diameters/depths in cylindrical perforation, and trench widths/depths in cuboidal structures of DUO_2 converter material, for both thermal (0.025 eV) and fast neutron (1 to 10 MeV) energies are presented. The objective of simulation was to optimize critical parameters such as thickness, perforation diameter and trench width, in planar, cylindrical and trench configurations, respectively, for the maximum neutron detection efficiency (η_{max}). The LLD parameter for all the configurations was kept constant at 20

MeV. Histogram plots were also studied for the energy distribution of fission products in all the three detector configurations. The next section discusses briefly on the design aspects of the various configurations of detector in terms of its size, area and thicknesses.

4.2 Detector Configuration and Design

4.2.1 Planar detector design

The principle of operation of direct and indirect configuration neutron detectors is delineated briefly in the present section along with its design. In planar direct configuration, the neutron sensitive converter material itself serves as the detector material and is coated on a thin metal film such as gold ‘Au’ to form a Schottky barrier diode [1]. The planar direct configuration detector is inherently advantageous owing to the fact that the neutron conversion and detection takes place in the same material. Therefore, it has the potential to achieve high efficiency, as the entire energy of fission products in the detector medium is available for generating the current pulse signal. Although direct detectors are attractive in terms of efficiency, there are practical difficulties in their realization due to challenges in fabrication and processing of materials [1].

Unlike the planar direct configuration, the planar indirect configuration consists of two distinct regions - one for the neutron conversion, comprising of DUO_2 and another region for detection of fission products, which is a semiconductor. The principle of neutron detection in the planar indirect configuration is that, the neutron upon interaction in the conversion region leads to ejection of two energetic fission products in opposite directions. Any one of these fission products reaching the adjoining semiconductor detector region would create electron-hole pairs, which provides a detectable small current signal pulse as an output. However, the inevitable self absorption of fission products inside the converter region limits the efficiency of planar indirect configuration. This limitation of efficiency is overcome by fabricating 3D geometry design viz., cylindrical perforations and trench structure in the semiconductor detector medium and then backfilling them with the DUO_2 converter materials [2]. The principle of neutron detection in 3D geometries remains similar to planar indirect detector except that now both the fission products contribute to the detection of neutrons. It may be noted that, the 3D detector configurations are inherently indirect in nature, as the detector consists of converter regions embedded inside the silicon detector in the form of cylindrical rods and cuboidal trenches.

The planar direct detector in the form a Schottky diode, as shown in figure 4.1 (a) was constructed by appending a Au layer of 50 nm (metal layer) on the bottom surface of the DUO_2 layer (semiconductor region). It is to be pointed out that in the planar direct detector configuration, DUO_2 itself acts as a active sensitive region for charge collection, as it is a semiconductor medium. The sensitive region was specified using the G4VSensitive Detector class of toolkit [3].

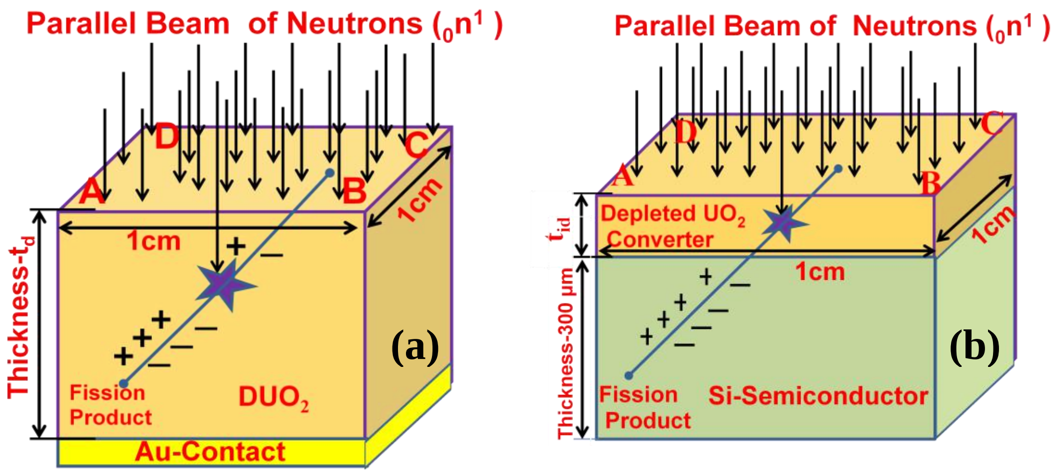

Figure 4.1. Schematic representation of DUO_2 based semiconductor neutron detector in (a) planar Direct and (b) planar Indirect detector configuration mode.

For the construction of indirect detector in planar configuration, the Au layer of direct configuration (in figure 4.1 (a)) was replaced with Si layer which is 300 µm thick, as shown in (figure 4.1(b)). It is to be noted that the Si is the active sensitive layer for charge collection for this configuration. However, unlike in the direct configuration case, DUO_2 is a passive layer in the indirect configuration mode and does not record the fission products generated by neutron interaction.

In the present thesis work, GEANT4 simulations based on Monte-Carlo technique are performed for estimating the efficiency of DUO_2 in planar direct and indirect configurations as shown in figures 4.1(a) and (b), respectively. Planar detectors are constructed in the form of cuboids using Geometry category of the toolkit with top and bottom surface cross sectional area of 1 cm^2 having fixed length and breadth of 1 cm each. The thickness of the detector is varied and denoted by 't_d' and 't_{id}' for direct and indirect planar configurations, respectively.

4.2.2 3D detector design

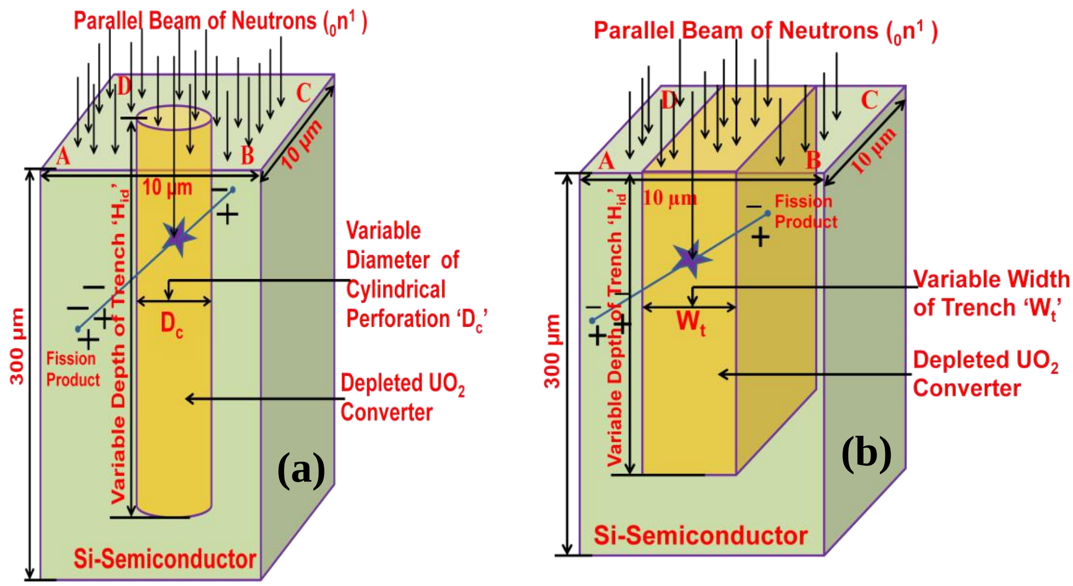

Figure 4.2. Schematic representation of (a) 3D indirect cylindrical perforation designed detector configuration shown with a representative unit cell and (b) 3D indirect trench structure designed detector configuration shown with a representative unit cell.

The '3D' detectors consists of two different geometries namely, cylindrical perforation and trenched structures were designed by employing unit cell concept in Geometry category of GEANT4 toolkit. Initially, a single unit cell of 10 µm x 10 µm x

300 μm was designed consisting of cylinder perforations and trench geometry that were circumscribed inside the Si detector cubical volume at the top face centre as shown in figures 4.2 (a) and (b), respectively.

The diameter 'D_c' (width 'W_t') and depth 'H_{id}' of the cylindrical perforations (trench structure) were the variable parameters in the simulation. The entire detector (both cylindrical perforation and trench structure) was constructed by replicating a unit cell 100 times in the X-Y plane in the form of a matrix using G4Replica function [3]. The top and bottom surface area for both the cylindrical perforated and trench structure detector geometries are 1mm^2 with length and breadth of 1mm each.

It may be noted that, the dimensions of the 3D detector in the cylindrical perforated and trench structures were limited to 1mm^2 in contrast to planar detectors in order to reduce the computation time. The entire construction of detectors (both planar and 3D) was performed inside the mother volume having dimension of 1000 cm^3.

In the present simulation, the isotope constituents of DUO_2 were 0.3% of U^{235} and 99.7% of U^{238}. The densities of DUO_2, Si and Au were given as 10.97 g/cm^3, 2.33 g/cm^3 and 19.32 g/cm^3, respectively.

4.3 Simulation Methodology

The simulation methodology remains the same as discussed 3.1.1.2 section of chapter 3, except for the change in energy of incident neutrons and the setting of LLD values. The energies were varied from 1 MeV to 10 MeV for fast neutron case and fixed at 25 meV for thermal neutron case. The LLD value was changed from 300 keV to 20 MeV. All other parameters like number of neutrons, direction of particles, distance between source and detector were unaltered.

In each run of the simulation, a plane parallel beam of mono-energetic neutrons (thermal or fast, as the case may be) emanating from a planar neutron source was incident uniformly and normally on the top surface (ABCD as indicated in ((planar figures 4.1.(a) & (b)) and (3D figures 4.2. (a) & (b))) of the schematic detector for all the configurations [4].Neutrons upon impingement on DUO_2, interacted at random depths which were determined by random numbers generated by Ranceu Engine of toolkit [3]. The fission cross section (Σ_f) values were taken from built-in library of G4ENDL (Evaluated Nuclear Data Library) in GEANT4 [3]. Further, neutrons generate highly energetic fission products on interaction with DUO_2. The liberated fission products range and their energies were tracked in GEANT4 program using G4Track class and Get Energy Deposit function, respectively. It is to be noted that those fission products which deposits energy > set LLD value (20 MeV) in DUO_2 region for planar direct configuration are considered as counts for estimating the efficiency, whereas in case of planar indirect and 3D configurations, the energy deposited in silicon region are considered. The simulations for both the planar configurations were performed for thicknesses ('t_d' for direct configuration and 't_{id}' for indirect configuration) of the DUO_2, ranging from 0.25 μm to 1000 μm. In case of 3D detectors, efficiency simulations were carried out by varying 'D_c' and 'H_{id}' of cylindrical perforations, whereas 'W_t' and 'H_{id}' were varied for cuboidal trench structures. The D_c (W_t in case of trench design) and H_{id} for both geometries was varied from 1 μm to 9 μm in steps of 0.5 μm and 50 μm to 275 μm in steps of 25 μm, respectively.

The objective of DUO_2 as an alternative material for neutron detectors is primarily driven by the possibility of setting high LLD values. It is known that, in typical reactor or field conditions, fission reactions yield alpha and gamma rays which are in the energy range of 5–10 MeV [5]. DUO_2, as a material therefore, facilitates the setting up of LLD at values ~ 20 MeV, so as to achieve the intended background gamma discrimination. In the GEANT4 simulation toolkit, an LLD value of 20 MeV was incorporated using stepping action class.

The mechanism of neutron detection differs in the direct and indirect configuration and this warrants appropriate definitions and explanations of method of computing its efficiency (η). In the case of planar direct configuration detector, the neutron detection efficiency (η_d), is defined as ratio of

$$\frac{\textbf{Number of fission products depositing energy greater than set LLD (20 MeV) value in the } \mathbf{DUO_2} \textbf{ sensitive detecting medium divided by factor of 2}}{\textbf{Total number of neutrons incident on the detector}}$$

For the planar indirect configuration detector case, a different methodology is used to estimate the efficiency of detection (η_{id}). Here, the fission products are tracked till they enter the sensitive detector volume i.e., the silicon region. It is defined as the ratio of the

$$\frac{\textbf{Number of fission products that deposit energy greater than set LLD (20 MeV) value in the Si sensitive detecting medium}}{\textbf{Total number of neutrons incident on the detector}}$$

For the 3D configuration detectors efficiency (η_{3d}), the methodology adopted for direct planar configuration detector was applied. Only the sensitive detector region in 3D detector case was Si instead of DUO_2.

While η gives the efficiency of neutron detection via the count of fission products, the energy deposited by the fission products is estimated by studying the simulated pulse height spectra, which is obtained from the Analysis manager category of GEANT4 toolkit [3,6].

A snapshot of typical simulation is shown in figures 4.3(a), 4.3(b), and 4.3(c), 4.3(d) for the planar direct, indirect configuration detectors and 3D configuration detectors for cylindrical, trench geometries, respectively. The colour coding for the snapshots shown in the figures is as follows. The light blue and orange colour blocks represent DUO_2 and Si, respectively. The yellow, green, blue and grey lines depict the incoming neutron, gamma rays, alpha particles and fission products, respectively.

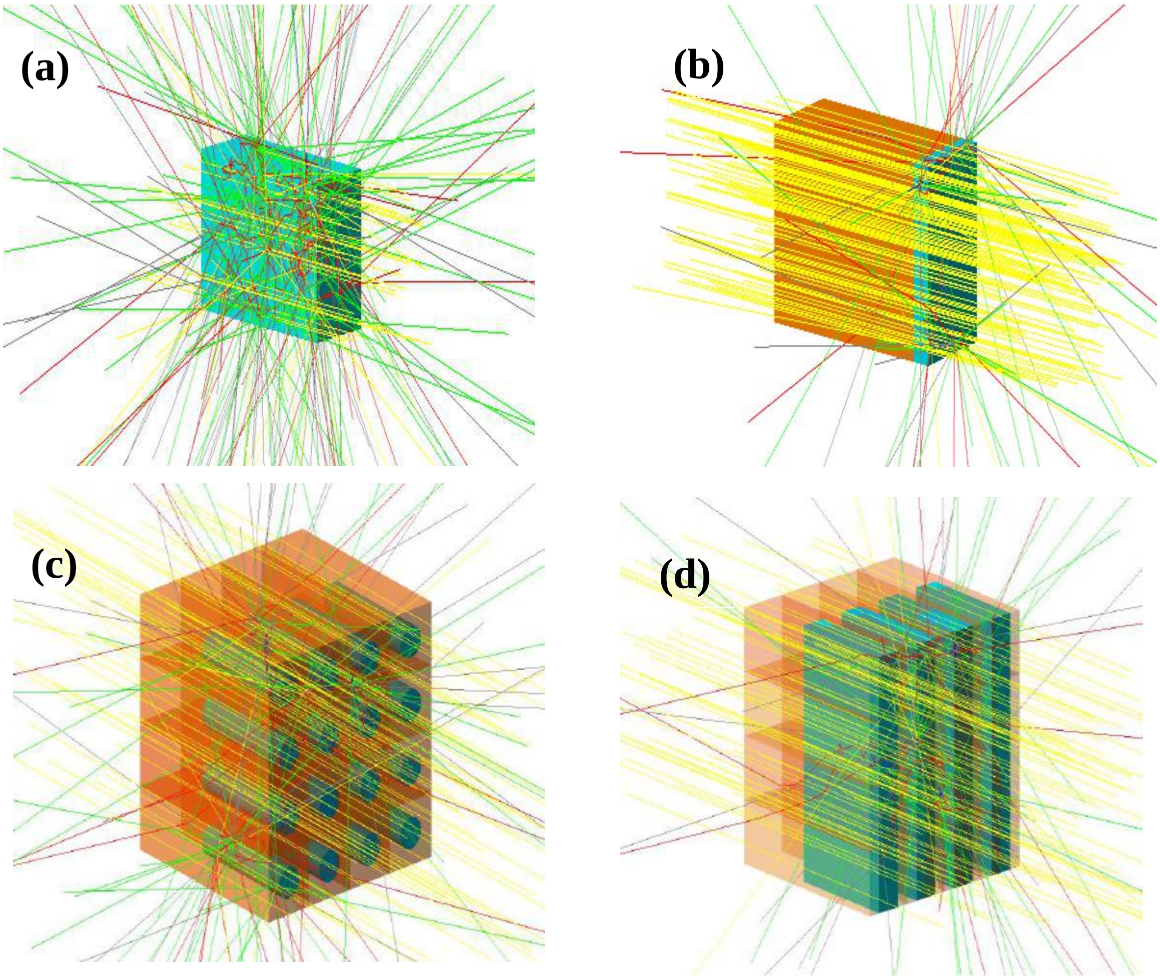

Figure 4.3. Snapshot of GEANT4 Simulation for DUO_2 (blue colour) as neutron reactive material in (a) planar Direct, (b) planar Indirect detector configuration mode with Si (orange colour) as sensitive detector and (c) 3D Cylindrical perforation indirect detector configuration, (d) 3D Trench structure indirect detector configuration.

4.4 Results and Discussions

4.4.1 Planar direct configuration detector

It is to be noted that the detector efficiency (η) is limited by the fission probability 'P(t)' and this criterion is often used to validate simulations [7]. In this regard, figure 4.4 (a) shows the simulated η_d, analytically computed fission probability '$P_a(t_d)$' and GEANT4 simulated fission probability '$P_s(t_d)$' for thermal neutrons incident on DUO_2 at lower thickness. The analytical computation was performed using the following relation [8]

$$P_a(t_d) = 1 - exp(-\Sigma t_d) \tag{1}$$

where t_d is the thickness of DUO_2 and Σ is its macroscopic fission cross section at incident neutron energy of 'E_{inc}' [8]. The figure shows a good agreement between $P_a(t_d)$ and $P_s(t_d)$ and η_d does not exceed $P_s(t_d)$, thereby validating the simulations. Moreover, $P_s(t_d)$ at thermal energy compares well with that reported by Kruschwitz et al. [9], as shown in table 4.1. Figure 4.4(a) further shows that η_d does not exceed $P_s(t_d)$ and is slightly lesser than it. This is owing to the fact that there is always a finite probability of few fission products escaping the sensitive detector volume, without registering their energy larger than the LLD.

Table. 4.1 Comparison of fission probability of the direct conversion detector in the present work and the values reported by Kruschwitz et al. [9]. Thickness of DUO_2 in both the cases is kept at 2μm.

S.No.	**Neutron energy (MeV)**	**$P_s(t_d)$** **Kruschwitz et al. [9] using MCNP**	**$P_s(t_d)$** **Present work using GEANT4**
1.	2.5×10^{-4}	8.6×10^{-4}	5.84×10^{-4}
2.	1	8.3×10^{-6}	3×10^{-6}
3.	10	4.9×10^{-4}	3.8×10^{-4}

As for the fast neutrons, the results of the simulations pertaining to the detector efficiency η_d for various thicknesses of DUO_2, at different neutron energies 'E_{inc}' are shown in figure 4.4(b). For comparison purpose, the η_d for thermal neutrons is also shown. Four observations emerge from this figure. Firstly, η_d for thermal neutron detection is highest as compared to that obtained for fast neutrons. It is well known that the fission cross section for U^{235} for thermal neutrons is very high as compared to U^{238} [see table 4.2] [10]. Therefore, even though the percentage composition of U^{235} in DUO_2 is 0.3%, contribution from U^{235} to efficiency is still overwhelmingly high. In contrast to the thermal neutrons, the contribution from U^{238} present in DUO_2 is dominant for the fast neutron case. Secondly, for any fixed value of neutron energy, η_d increases with the increase in thickness. This is attributed to the increase in the fission probability 'P(t)' with increase in thickness as dictated by equation (1). Thirdly, for a specified thickness t_d of DUO_2, η_d increases with the increase in neutron energy for fast neutrons. This is attributed to the increase in microscopic and macroscopic fission cross section of U^{238} with neutron energy as seen from table 4.2 and from figure 4.4(c), respectively. Fourthly, the slope or the rate at which η_d increases with thickness is different for different neutron energies. The slope as a function of incident neutron energy is shown in figure 4.4(c) and is attributed to respective behavior of macroscopic fission cross section 'Σ' at these neutron energies. It is to be pointed out that in figure 4.4(b), the η_d values of 2 and 5 Mev, 8 and 10 MeV are approximately the same.

This is indeed a manifestation of similar magnitudes of the macroscopic cross sections, as shown in figure 4.4(c). The macroscopic cross section 'Σ' was calculated using the microscopic fission cross section values from table 4.2 and equation (2) as given below.

$$\boldsymbol{\Sigma = \frac{\rho N_A\,(n_i \sigma_i)}{M}} \qquad (2)$$

where, M is the molecular weight, N_A is the Avogadro number, ρ is the density of the compound and n_i , σ_i are the number of atoms and the microscopic cross section of the element 'i', respectively, at the given neutron energy. In the above expression, the fission macroscopic cross section for typical thermal neutron energy, was estimated by substituting these values (M = 270, N_A = 6.022 x 10^{23} atoms/mole, ρ = 10:97 g/cm^3, n = 0.003 for U^{235} and 0.997 for U^{238},σ = 584 barns for U^{235} and σ = 0:00002 for U^{238}) for DUO_2 at E_{inc} of 0.025 eV.

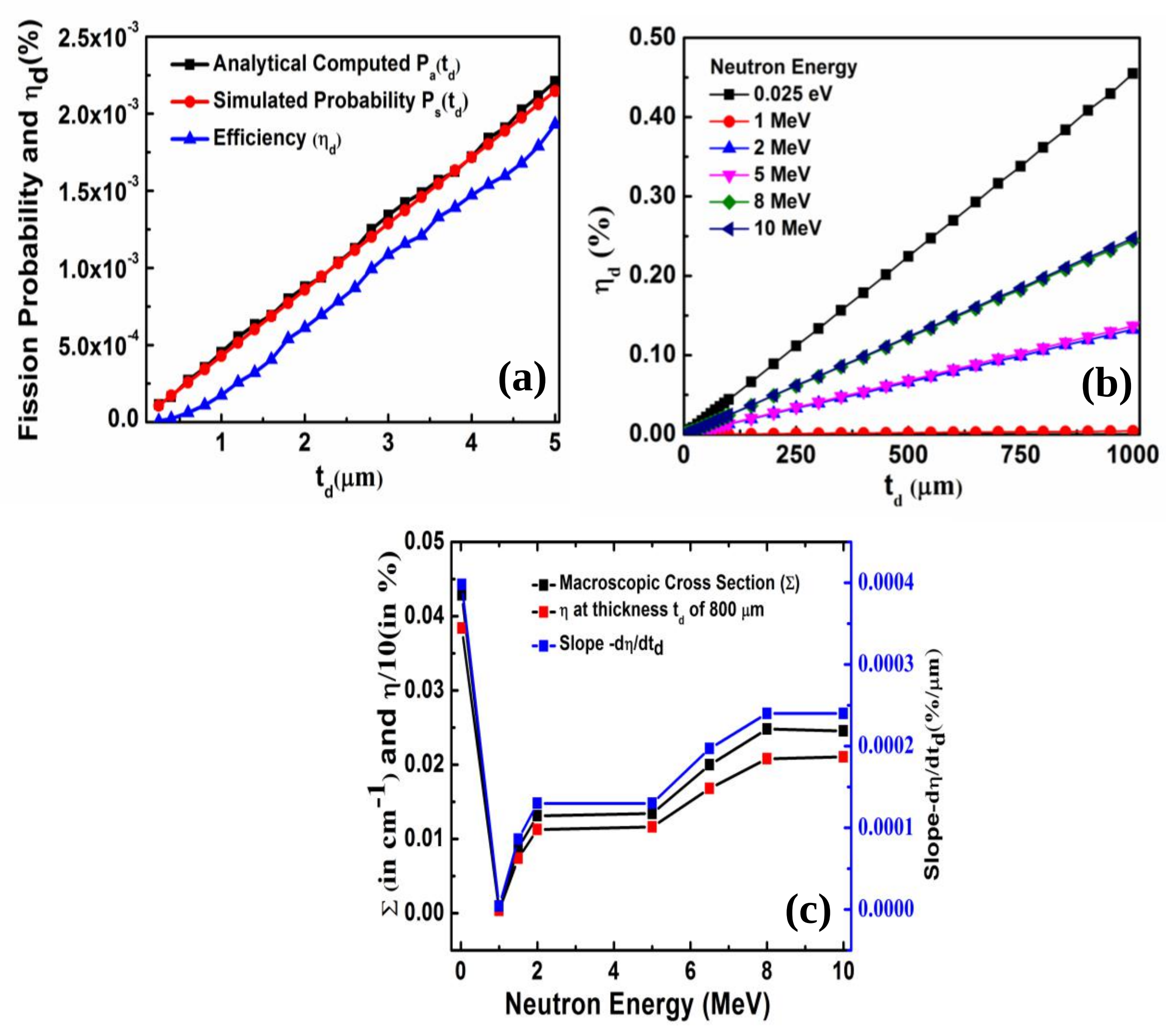

Figure 4.4. (a)Comparison of fission probability (both analytical ($P_a(t_d)$) and simulated ($P_s(t_d)$)) and detector efficiency (η_d) with the thickness of $DUO_2(t_d)$ when exposed to thermal neutrons in planar direct configuration mode. (b) Variation of η_d with t_d in planar direct configuration for various incident neutron energies. (c) Variation in macroscopic fission cross section (Σ), efficiency (η/10) and slope of efficiency with Neutron Energy for planar direct configuration mode.

For the direct configuration detector, thermal neutron energy experimental detection efficiency of 3 x 10^{-3} % was reported for B_4C of 0.232 μm thickness by Day et al. [11] whereas at same thickness the simulated detection efficiency for DUO_2 is in the range of 10^{-6} %. This efficiency is three orders lesser. However, DUO_2 has unprecedented advantage of gamma discrimination over B_4C.

Table 4.2 Microscopic Fission cross section for Uranium Isotope U^{235} and U^{238} at different neutron energies.

Neutron Energy (MeV)	**Microscopic Fission Cross Section (barns)**	
	U^{238}	**U^{235}**
0.025 eV	2.00×10^{-5}	584 .44
1	0.013	1.19
1.5	0.36	1.23
2	0.53	1.28
5	0.55	1.07
6.5	0.82	1.33
8	1.01	1.78
10	1.001	1.76

In order to understand the pulse height spectra of fission fragments in the detector medium, the histogram plots were studied for typical fast neutron energy case. Figures 4.5(a) and 4.5(b) show the histogram plots of the energy deposited by the fission products in the detector volume, for typical 10 MeV neutrons incident on two representative thicknesses of DUO_2, namely, 0.25 μm (low thickness) and 500 μm (high thickness), respectively. The LLD was set at 20 MeV in these simulations. Two inferences can be drawn from the apparent relationship displayed between the counts and the notion of peaks. A point to note at this step is that, the counts correspond to the number of fission products depositing energies larger than LLD in DUO_2. As seen from figures 4.5(a) and 4.5 (b), the magnitude of counts is less in the case of 0.25 μm thickness of DUO_2 as compared to the 500 μm thickness.

From the simulation, it was found that a sizable fraction of fission products escape from the very thin DUO_2. The low statistics of counts forbids the formation of a discernable peak for the 0.25 μm thick specimen. In stark contrast to the 0.25 μm thick specimens, the entire energy of fission products is deposited in 500 μm thick DUO_2

specimen and peaks are centered around 70 and 100 MeV. Similar observation was made by Kruschwitz et al. [9], while simulating the energy deposited by the fission products in 1, 2 and 100 μm thick DUO_2 specimens using GEANT4. They found broad spectra for 1 and 2 μm thick specimen, whereas a well defined peak around 165 MeV was reported for 100 μm thick specimen. Also, counts are very less in case of 0.25 μm thick detector compared to those for 500 μm thick detector at the neutron energy 10 MeV, which is consistent with efficiency simulations.

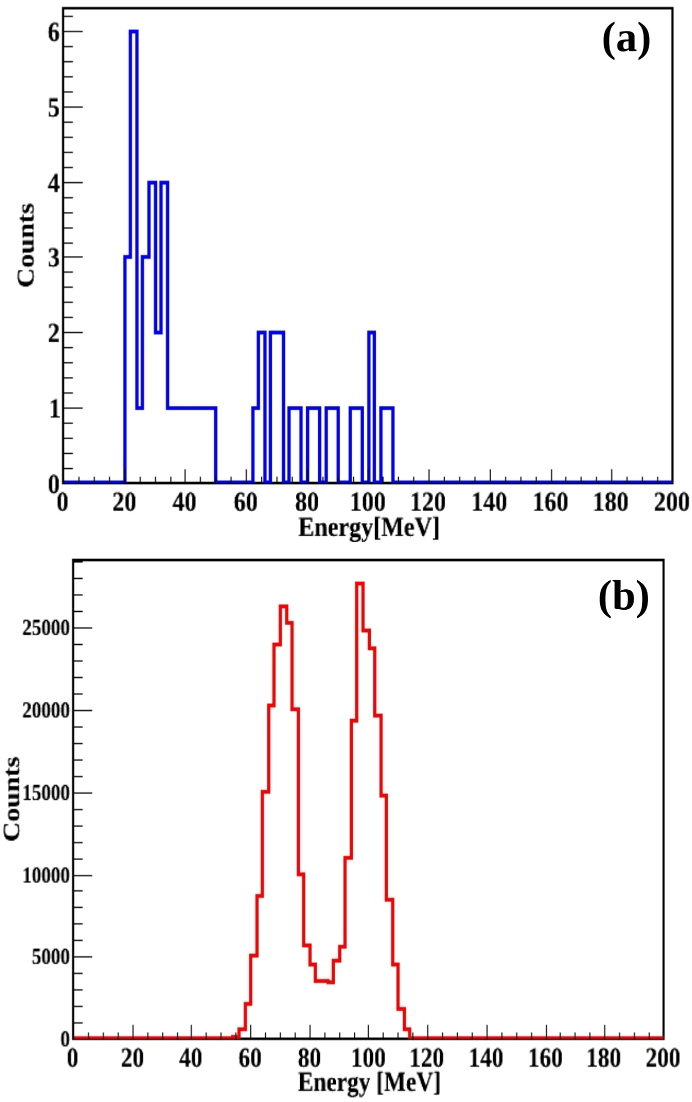

Figure 4.5. Histogram of energy deposited by fission products in (a) 0.25 μm and (b)500 μm thick DUO_2 for planar direct configuration detector mode when exposed to 10 MeV neutrons.

From the above simulations, it is clear that efficiency of the planar direct conversion detectors can be enhanced to higher values, with good gamma discrimination, by suitably increasing the thickness of DUO_2. However, electrical transport of charge carriers and junction capacitance of UO_2 do not scale with thickness, thereby limiting the maximum efficiency achievable [1]. Fabrication of DUO_2 crystals with desired semiconducting properties strongly depends on its stoichiometry, which is important for practical realization of these detectors [12]. These difficulties are overcome in planar indirect detector configuration, where DUO_2 acts only as a passive converter layer.

4.4.2 Planar indirect configuration detector

Figure 4.6 (a) shows the simulated η_{id} of the planar indirect configuration detector for various thicknesses 't_{id}' of DUO_2, when exposed to different neutron energies. It is evident from the figure that, η_{id} is maximum for the thermal energies (25 meV), as compared to fast neutron energies (MeV). As far as thermal neutrons is concerned, the large η_{id} observed is attributed to the high fission cross section of U^{235} (see table 4.2) in DUO_2. Moreover, the efficiency η_{id} initially increases till ~3 μm and thereafter it saturates for both thermal and fast neutron case.

The saturation behavior observed in DUO_2 is in contrast to the conventional B^{10} based thermal neutron planar detectors for the range of thicknesses considered in the present simulation [13,14]. The initial increase in η_{id} till ~3 μm is attributed to the increase in fission probability $P(t_{id})$ with increasing t_{id}, as is evident from the plot in figure 4.6(b). However, above 3 μm, which is the critical thickness dictated by the range of fission products in DUO_2, η_{id} is expected to decrease. The saturation in η_{id} beyond a thickness of ~3 μm implies that, although the number of fission products generated increases with increase in t_{id} as shown in figure 4.6(b), the fraction of fission products reaching Si detector remains constant and is therefore independent of t_{id}. The independence to thickness can be understood from an estimation of the mean free path 'λ' of neutrons, as they traverse the DUO_2. Although in principle, λ can be estimated for both thermal and fast neutron case, the present discussion is limited to thermal neutrons only.The λ of thermal neutrons in DUO_2 calculated from the inverse of equation (2) was found to be ~23.33 cm. However, figure 4.6 (a) shows the behavior of η_{id} till 0.1 cm, which is much smaller as compared to the mean free path of thermal neutrons (23.33 cm). In order to facilitate a comparison of η_{id} of DUO_2 with ^{10}B and to examine if the saturation behavior in DUO_2 extends to larger thicknesses as well, the simulation was performed for higher thicknesses (typically, till 5 cm) and higher enrichment of UO_2 (90%). It is to be noted that the mean free path of thermal neutrons in 90% enriched UO_2 is ~700 μm. The results of simulations upto 5 cm and 0.1 cm thickness for DUO_2 and 90% enriched UO_2 are shown in figures 4.6(c) and 4.6(d), respectively. Figures 4.6(c) and 4.6(d) indicate that the efficiency η_{id} begins to decrease at t_{id} of ~2000 μm and 3 μm, respectively which is similar to the behavior as observed in the case of B^{10}.

Unlike DUO_2, in enriched UO_2, the efficiency decreases beyond ~ 3 µm as evident from figure 4.6 (d). This decrease is due to the reduction in the number of neutron interactions near the Si region, as neutron has lower λ in enriched UO_2.In fact, for thermal neutrons incident on enriched UO_2 detector in the indirect configuration, decrease in η_{id} with increasing thickness was also verified experimentally by P.G. Litovchenko et al.[15].Incidentally, Steve Kahn et al. [16] studied the energy spectra of fission products escaping from the enriched UO_2 films of various thicknesses using a surface barrier detector, when exposed to thermal neutrons. They concluded that the efficiency of energy deposition decreases with increasing UO_2 thickness and attributed the same to the fission products being stopped in thicker films. They also reported that the fraction of fission products that escape, starts reducing after 2.53 µm, which is comparable to the value as estimated in this simulation. The above simulation results for higher thickness and enrichment of UO_2, indeed proved that the saturation in the efficiency was due to the higher mean free path of neutron and limited range of fission products in DUO_2.

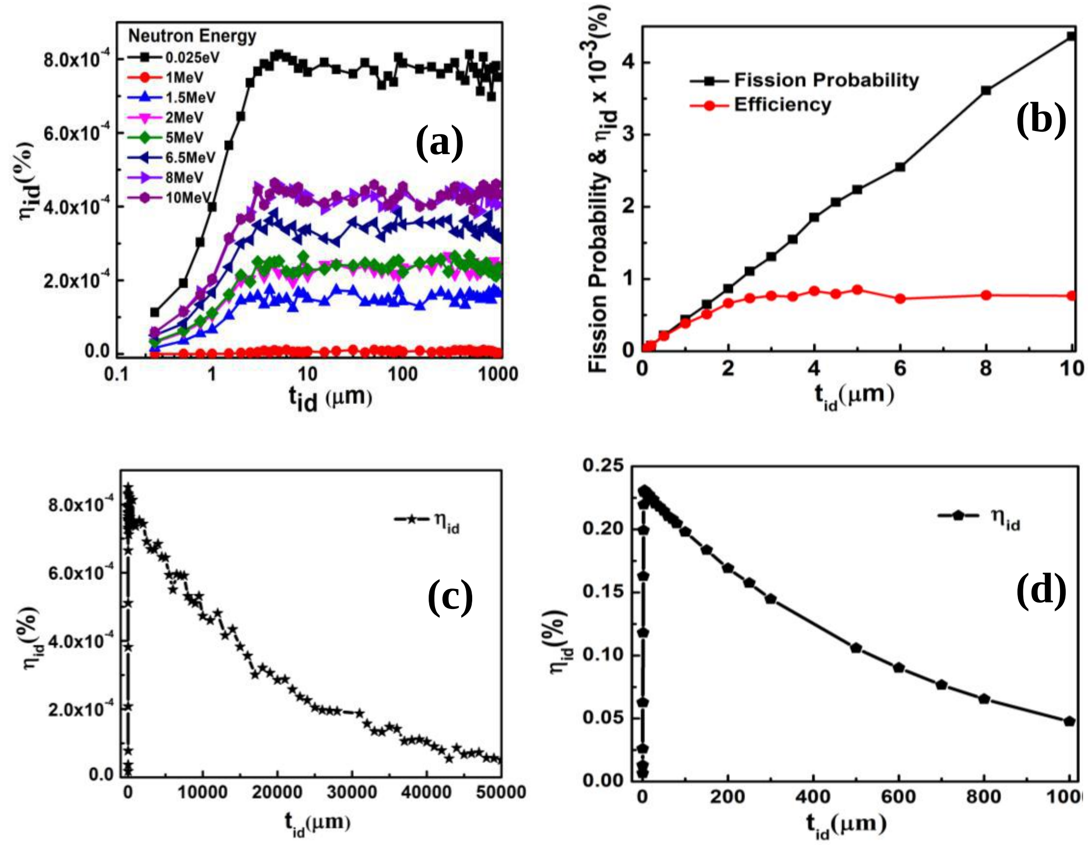

Figure 4.6.(a) Variation of efficiency (η_{id}) of neutron detectors in planar indirect configuration detector mode with thickness (t_{id}) of DUO_2 for various incident neutron energies. (b) Fission probability ($P(t_{id})$) and η_{id} with t_{id} whenexposed to thermal neutrons. Variation in η_{id} with t_{id} for (c) Higher thicknesses of DUO_2 and (d) 90% enriched UO_2 when exposed to thermal neutrons.

The above discussion based on mean free path is focused on thermal neutrons. However, the same argument goes through for fast neutrons also. The role of thickness 't_{id}' on the energy deposited by fission products can be seen from figures 4.7(a) and 4.7(b), which show the histogram plots for two representative thicknesses, namely, 0.25 μm (low) and 500 μm (high) for the typical 10 MeV neutrons energy.

The fission products depositing energies larger than 20 MeV (set LLD) are shown in the figures 4.7 (a) and 4.7 (b). It is observed that for lower thickness of 0.25

μm, two peaks corresponding to energy deposited by fission products are clearly discernible; while for higher thicknesses, a single broad band is seen. This is in contrast to that observed in planar direct configurations detectors, in which the peaks are clearly discernible for higher thicknesses as compared to the lower ones.

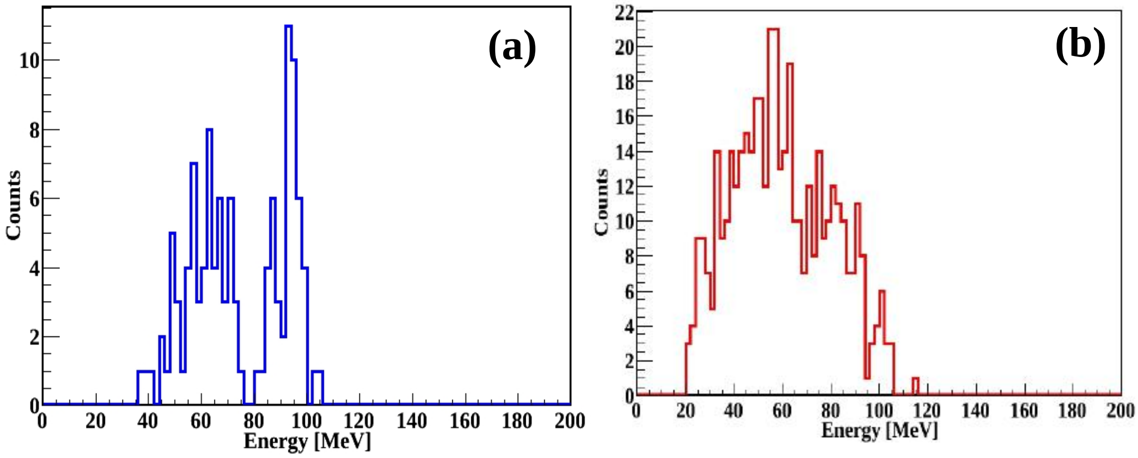

Figure 4.7. Histogram of energy deposited by fission fragments in planar indirect configuration detectors when exposed to 10 MeV neutrons for (a) 0.25 μm and (b)500 μm thickness of DUO_2.

In case of planar indirect detector configuration, even though the fission probability P(t) is less for lower thicknesses, the fission products generated will deposit most of the energy in the Si region and thus the peaks are resolved. With increasing thickness, fission products lose significant part of their energy in DUO_2 itself, before entering the Si region. Moreover, unlike the planar direct detector configuration, number of counts is lower even at higher thicknesses, thereby leading to lower η_{id}. This is because of the fact that the large fraction of fission products generated in DUO_2 will be completely self absorbed in itself above a thickness of 3 μm, and thus, is not expected to reach the Si detector.

4.4.3 3D Indirect configuration detectors

Figures 4.8 (a) and (b) (4.9(a) and (b)) show the efficiency 'η_{3d}' of thermal (representative fast neutron of 10 MeV energy) neutron detection in 3D cylindrical perforation and trench structures configurations, respectively. The diameter ‘D_c’/width ‘W_t’ of cylindrical perforation/trench structures were varied from 1 μm to 9 μm, while their depth ‘H_{id}’ were varied from 50 μm to 275 μm.

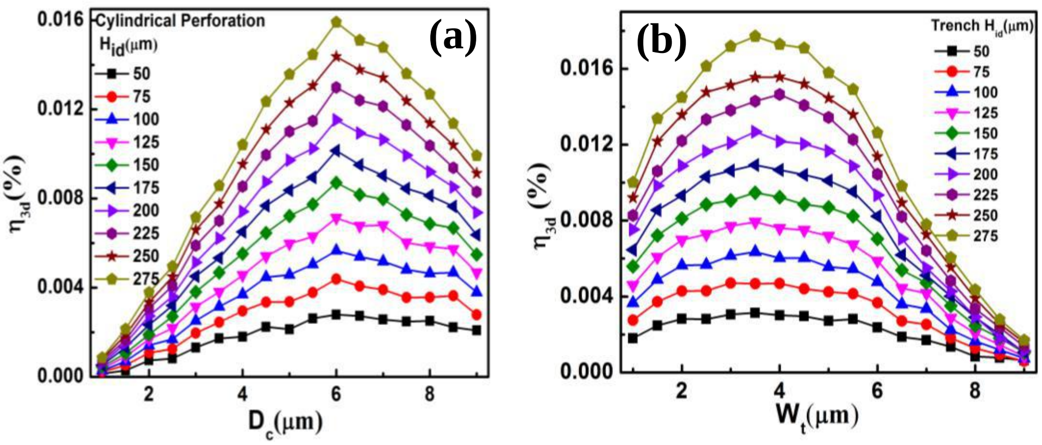

Figure 4.8. Variation of efficiency ‘η_{3d}’for 3D indirect detector configuration at varying diameter ‘D_c’ and width ‘W_t’ in (a) cylindrical perforation and (b) trench structure geometries, respectively along with their varying depth ‘H_{id}’ for thermal incident neutron energy.

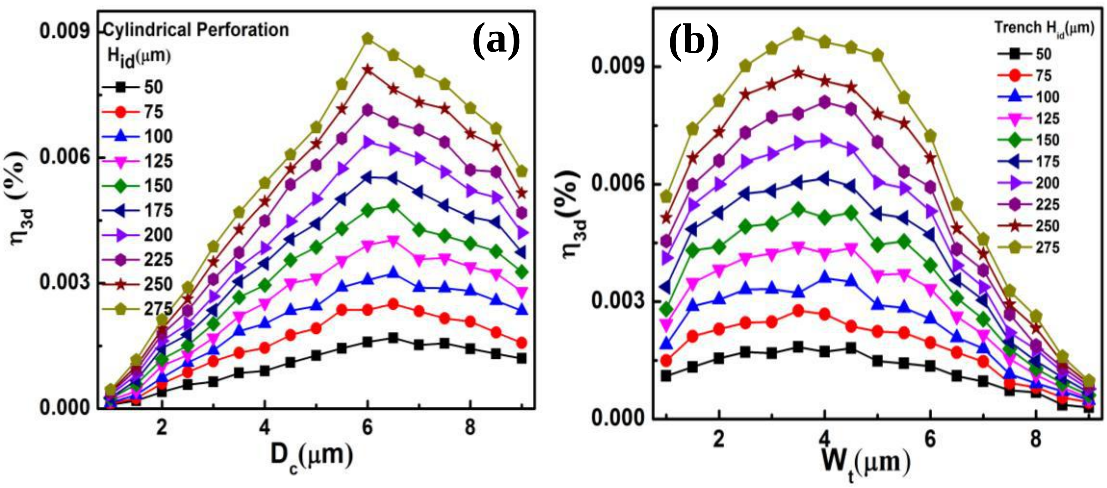

Figure 4.9. Variation of efficiency ‘η_{3d}’for 3D indirect detector configuration at varying diameter ‘D_c’ and width ‘W_t’in (a) cylindrical perforation and (b) trench structure geometries, respectively along with their varying depth ‘H_{id}’ for representative fast incident neutron energy of 10 MeV.

From these figures, three important observations can be made. For the cylindrical perforations, at a given depth of perforation, η_{3d} for detection of thermal and fast neutrons starts increasing with increasing D_c and reaches a maximum at a critical diameter ~6 μm and thereafter starts decreasing. While for the trench structure configuration, the η_{3d} is relatively higher than cylindrical perforations even for a lower trench W_t of 1 μm. Moreover, unlike the peaking of efficiency in cylindrical perforations case, a plateau like behaviour is observed till ~6 μm trench width and thereafter efficiency falls drastically. The plateau like behaviour is attributed to the larger interfacial area between the converter and Si sensitive layers of the trench structure configuration.

One more important observation from figures 4.8 and 4.9 is that decrease in η_{3d} above 6 μm in both configurations is attributed to two reasons. Firstly, though the fission probability increases with D_c of cylindrical perforation/W_t of trench (see figures 4.10 (a) and (b)), there is an inevitable self absorption of fission fragments in DUO_2 converter region itself.

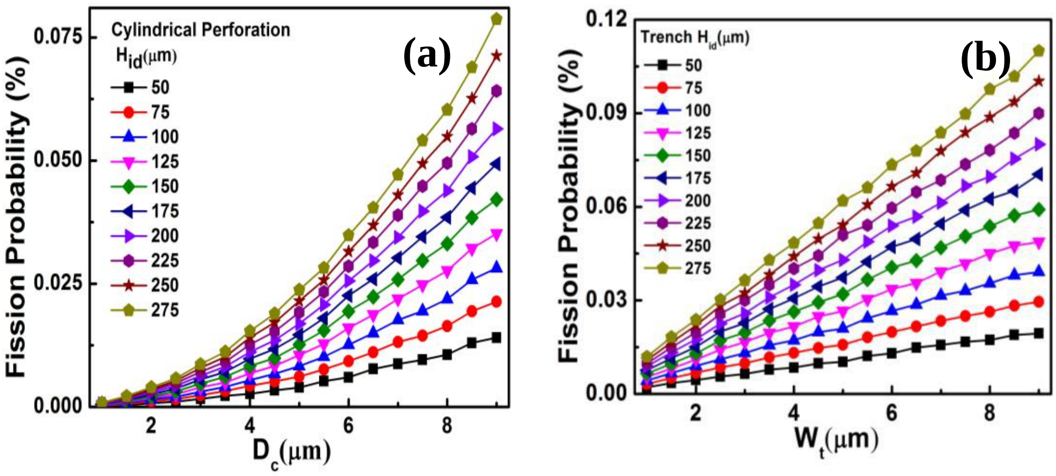

Figure 4.10. Variation of fission probability for 3D indirect detector configuration at varying diameter 'D_c' and width 'W_t'in (a) cylindrical perforation and (b) trench structure geometries, respectively along with their varying depth 'H_{id}' for thermal incident neutron energy.

Secondly, increase in D_c/W_t beyond 6 μm, decreases the sensitive semiconductor detector volume, thereby restricting the deposition of energy greater than LLD value of 20 MeV, by fission products. For a given D_c/W_t of the configurations, efficiency in general, increases with increasing H_{id} which is attributed to the increase in the converter material volume which in turn increases the fission probability (see figures 4.10 (a) and (b)).

The maximum efficiency (η_{max}) of detection of thermal and fast neutrons (10MeV) for cylindrical geometry achieved for a H_{id} = 275 μm, D_c = 6 μm was 0.0159% and 0.0088%, respectively. For the trench counterpart, for the same H_{id} and a W_t of 3.5 μm, the η_{max} were 0.0177% and 0.0098% for the thermal and fast neutron cases, respectively. The magnitudes of efficiencies are two (one) orders higher than the planar indirect detectors for thermal (fast-10 MeV) neutrons. The increase in efficiency in both the cases of 3D geometrical structures is primarily attributed to the possibility of both the fission fragments contributing to the detector efficiency compared to former one. Amongst the cylindrical and trench geometrical configurations, the efficiency for the trench geometry is 11.32% (11.19%) higher compared to that of cylindrical perforation for thermal (fast) neutrons. This is due to the increase in DUO_2/Si volume ratio in the trench structure design.

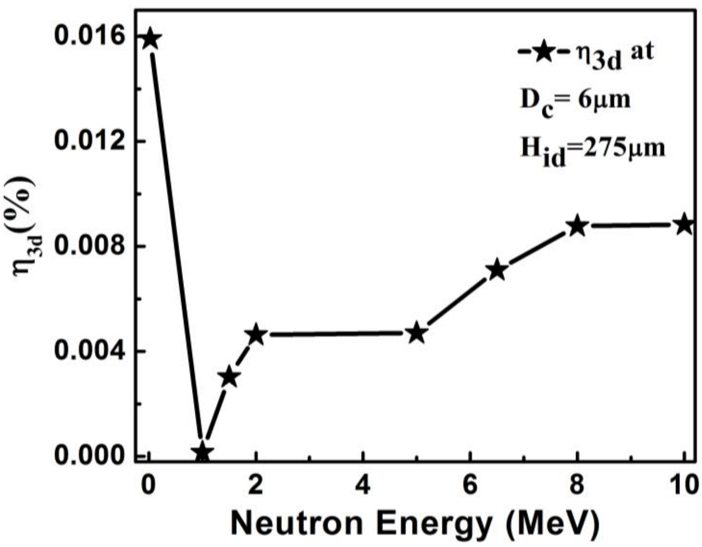

Figure 4.11. Variation of efficiency 'η_{3d}' for 3D indirect cylindrical perforation detector with various neutron energies at fixed diameter 'D_c=6μm' and depth 'H_{id}'=275μm.

Figure 4.11 shows the variation of detector η_{3d} with neutron energy at fixed D_c and H_{id} of 6 μm and 275 μm, respectively. From this figure, it is clear that the detector efficiency is maximum for thermal neutrons and is minimum for 1MeV neutrons. However, η_{3d} increases with increase in fast neutron energy. Also, the trend seen in this figure is similar to the one shown in figure 4.4 (c) for planar direct detector configuration. The reason for this behaviour is again attributed to their respective fission cross section which varies with neutron energies [10].

The role of D_c of cylindrical perforation on the fission fragment depositing energy in the sensitive region of the Si detector can be understood from figures 4.12(a) and (b) which show the histogram plot of two representative diameters, namely D_c = 2 μm (lower) and D_c = 8 μm (higher), for typical H_{id} = 275 μm and 10MeV neutron energy. From these figures, it is clear that the counts are larger for the 8 μm diameter and the peak shifts from 40 MeV to 20 MeV compared to 2 μm diameter perforation. This is because, with increasing diameter, most of the energy is deposited by fission fragments in DUO_2 itself before reaching the sensitive Si detector region.

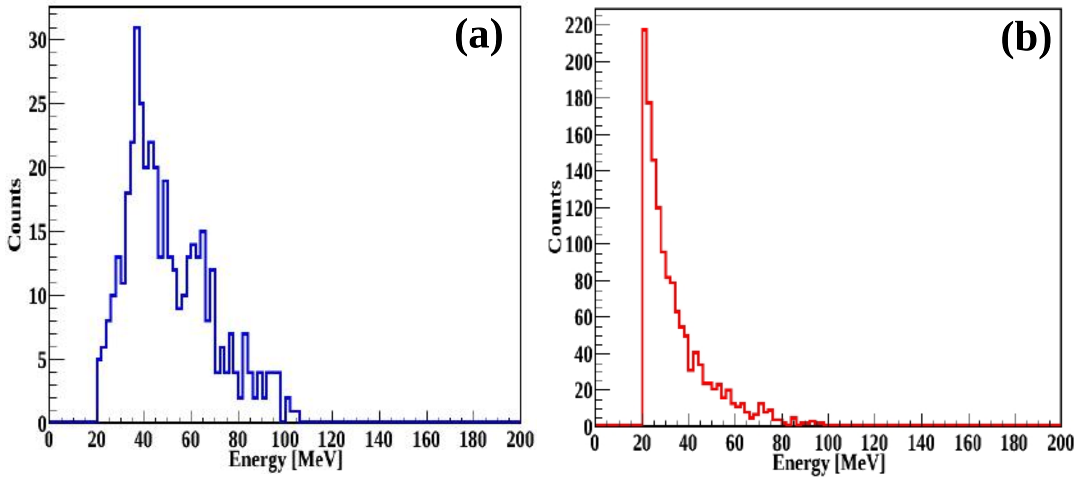

Figure 4.12. Histogram plot of energy deposited by fission fragments in 3D indirect cylindrical perforation detectors when exposed to 10 MeV neutrons for diameter (a) D_c= 2 µm (lower) and (b)D_c=8 µm(higher) at fixed depth 'H_{id}'=275µm.

Efficiency calculations at different neutron energies and histogram plots at different trench widths were also studied and the trends were found to be similar to the cylindrical perforations design.

From these simulations, it is evident that the efficiency achievable in indirect configuration detector is lower than that of direct detector ones. However, as mentioned previously, in case of indirect configuration, DUO_2 acts only as a passive converter layer, and therefore is relatively easy to fabricate. In comparison to other conventional converter materials like B^{10} and Li^7, DUO_2 has an added advantage of a better gamma discrimination, as evidenced from the histogram plots. It is worthwhile to note that, DUO_2 based detectors proposed in the present work can be used in future fusion reactors and related facilities, where the detection of neutrons emitted from plasma presents an extreme challenge due to expected mixing of large gamma radiation fields [17].

4.5 Conclusions

In summary, it is found that DUO_2 based semiconductor neutron detectors can be used for detecting dual neutron energies of thermal and fast neutrons, with good gamma discrimination, which is a distinct and indispensable advantage over other conventional converter materials. Efficient background discrimination is an inherent feature of this converter material, as the energy possessed by the generated fission products are significantly above the background radiation. Efficiencies of the DUO_2 based converter material detectors in both planar (direct and indirect) and 3D (cylindrical perforations and trench structures) configurations were studied. The studies revealed that, for a typical thickness of ~1000 μm, efficiency for thermal neutron (0.025 eV) and fast neutron (typically 10 MeV) detection for planar direct (indirect) configurations are 0.45% and 0.24% (0.0008% and 0.0004%), respectively.

Even though the efficiency of DUO_2 in planar direct configuration mode is significantly larger than the indirect configuration, synthesis and fabrication of controlled stoichiometry UO_2 is still a formidable task and a major challenge. It is shown that efficiency of planar indirect configuration detectors can be further enhanced by creating

3D structures in Si detector. The simulations of 3D configurations of both cylindrical perforation and trench structure showed an enhancement in efficiency over planar indirect configurations by two (one) orders for thermal (fast) neutrons. Therefore, as inferred from the simulations, for applications in high background environments which require good background discrimination, it is prudent to use DUO_2 in the 3D indirect configuration mode as a better choice of converter material.

The last two chapter's discussion are solely focused on GEANT4 simulation for Boric acid and depleted UO_2 converter materials to obtain critical geometrical parameters for maximum neutron detection efficiency. Along with the GEANT4 simulation in the present thesis experimental attempts were made to detect thermal neutrons, and are discussed in chapter 5. In the subsequent chapter effect of neutron irradiation on the electrical characteristics of Si PIN diode is discussed.

References

[1] A.N. Caruso, The physics of solid-state neutron detector materials and geometries, J. Phys.: Condens. Matter. 22 (2010) 443201. doi:10.1088/0953-8984/22/44/443201.

[2] R.J. Nikolic,Chin Li Chung, C.E.Reinhardt ,T.F.Wang, Roadmap for High Efficiency Solid-State Neutron Detectors, Proceedings of SPIE , (2005)6013.

[3] Geant4 User's Guide for Application Developers, (developed in CERN). http://geant4.web.cern.ch/geant4/UserDocumentation/UsersGuides /ForApplicationDeveloper/html/index.html (accessed October 31, 2015).

[4] D.S. McGregor, J. Kenneth Shultis, Reporting detection efficiency for semiconductor neutron detectors: A need for a standard, Nuclear Instruments and Methods in Physics Research Section A: Accelerators, Spectrometers, Detectors and Associated Equipment. 632 (2011) 167–174. doi:10.1016/j.nima.2010.12.084.

[5] L. Jarczyk, H. Knoepfel, J. Lang, R. Müller, W. Wölfli, The nuclear reactor as a high intensity source for discrete gamma rays up to 11 MeV, Nuclear Instruments and Methods. 13 (1961) 287–296. doi:10.1016/0029-554X(61)90217-8.

[6] ROOT: Data Analysis Framework [https://root.cern.ch/drupal/].

[7] J.K. Shultis, D.S. McGregor, Efficiencies of coated and perforated semiconductor neutron detectors, in: IEEE Symposium Conference Record Nuclear Science 2004., 2004: pp. 4569-4574 Vol. 7. doi:10.1109/NSSMIC.2004.1466900.

[8] P.Rinard, Neutron Interaction with matter, in Passive Non destructive Assay of Nuclear Materials, US Nuclear Regulatory Commission, March, (1991).

[9] C.A. Kruschwitz, S. Mukhopadhyay, D. Schwellenbach, T. Meek, B. Shaver, T. Cunningham, J.P. Auxier, Semiconductor neutron detectors using depleted uranium oxide, in: International Society for Optics and Photonics, 2014: p. 92130C. doi:10.1117/12.2063501.

[10] Fission Cross section available from: https://wwwnds.iaea.org/exfor/servlet/E4sGetTabSect?SectID=2292099&req=1318&PenSectID=7664758

[11] E. Day, M.J. Diaz, S. Adenwalla, Effect of bias on neutron detection in thin semiconducting boron carbide films, J. Phys. D: Appl. Phys. 39 (2006) 2920. doi:10.1088/0022-3727/39/14/007.

[12] T.Meek,M. Hu, M. J Haire,Semiconductive Properties of Uranium Oxide, in: Waste Management Symposium (2001).

[13] D.S. McGregor, R.T. Klann, H.K. Gersch, J.D. Sanders, Designs for thin-film-coated semiconductor thermal neutron detectors, in: 2001 IEEE Nuclear Science Symposium Conference Record (Cat. No.01CH37310), 2001: pp. 2454–2458. doi:10.1109/NSSMIC.2001.1009315.

[14] C. Guardiola, K. Amgarou, F. García, C. Fleta, D. Quirion, M. Lozano, Geant4 and MCNPX simulations of thermal neutron detection with planar silicon detectors, J. Inst. 6 (2011) T09001. doi:10.1088/1748-0221/6/09/T09001.

[15] P.G. Litovchenko, W. Wahl, D. Bisello, A. Candelori, A.P. Litovchenko, V.F. Lastovetsky, L.I. Barabash, T.I. Kibkalo, L.A. Polivtsev, J. Wyss, Semiconductor detectors for neutron flux measurements, Nuclear Instruments and Methods in Physics Research Section A: Accelerators, Spectrometers, Detectors and Associated Equipment. 518 (2004) 423–425. doi:10.1016/j.nima.2003.11.047.

[16] S. Kahn, R. Harman, V. Forgue, Energy Distributions of Fission Fragments from Uranium Dioxide Films, Nuclear Science and Engineering. 23 (1965) 8–20. doi:10.13182/NSE65-A19254.

[17] M. Angelone, D. Lattanzi, M. Pillon, M. Marinelli, E. Milani, A. Tucciarone, G. Verona-Rinati, S. Popovichev, R.M. Montereali, M.A. Vincenti, A. Murari, Development of single crystal diamond neutron detectors and test at JET tokamak, Nuclear Instruments and Methods in Physics Research Section A: Accelerators, Spectrometers, Detectors and Associated Equipment. 595 (2008) 616–622. doi:10.1016/j.nima.2008.07.107.

Chapter-5

Neutron Detection Experiment[2]

This chapter discusses in brief the testing of a prototype planar semiconductor neutron detector fabricated using a Boron Based Material (BBM) as a converter material and Si PIN diode. The focus is on evaluating the optimum coating thickness of BBM using GEANT4 simulation and coating the same on Si PIN diode to fabricate a planar semiconductor neutron detector. In order to test the sensitivity of Si PIN diode for charged particles, the alpha spectroscopy experiments were carried on these diodes. The experimental results of thermal neutron detection by fabricated planar neutron detector when exposed to a calibrated Am-Be neutron source are briefly outlined in this chapter.

5.1 GEANT4 Simulation- to obtain the critical thickness

A compound based on boron was synthesized (henceforth referred to as Boron Based Material - (BBM)) in IISc and coated on Si PIN diode with an active area of 94.09 mm^2. The optimum coating thickness of the converter material –BBM for a 2D planar configuration was obtained from GEANT4 simulation, after relevant input parameters were fed in the simulation. The details of the simulation methodology and design have already been described in section 3.1.1.2 and 4.3 of chapters 3 and 4 of this thesis, respectively.

5.2 Electrical Characterization (reverse I-V and C-V) of detector

Prior to and after coating BBM on Si PIN diodes with BBM, the reverse I-V and C-V measurements were performed at room temperature, till 100V to ascertain the effect of its coating on Si PIN diode. The results are not shown[2]. From the two measurements,

[2]As a patent application is being filed, only skeletal details (no detailed materials aspects, coating method, spectrum and associated signals) of the fabrication of neutron detector is disclosed in this thesis.

no significant changes were observed upon BBM coating and it is therefore concluded that the BBM coating had not affected the electrical behaviour. It only acts as a passive layer with regard to the electrical characteristics of the diodes.

A typical reverse I-V and C-V measurement carried out on virgin (uncoated) Si-PIN diodes are shown in figure 5.1 (a) and (b), respectively. It is to be noted that measurements were carried out using the Aluminium chamber as shown in figure 2.6 of chapter 2 .

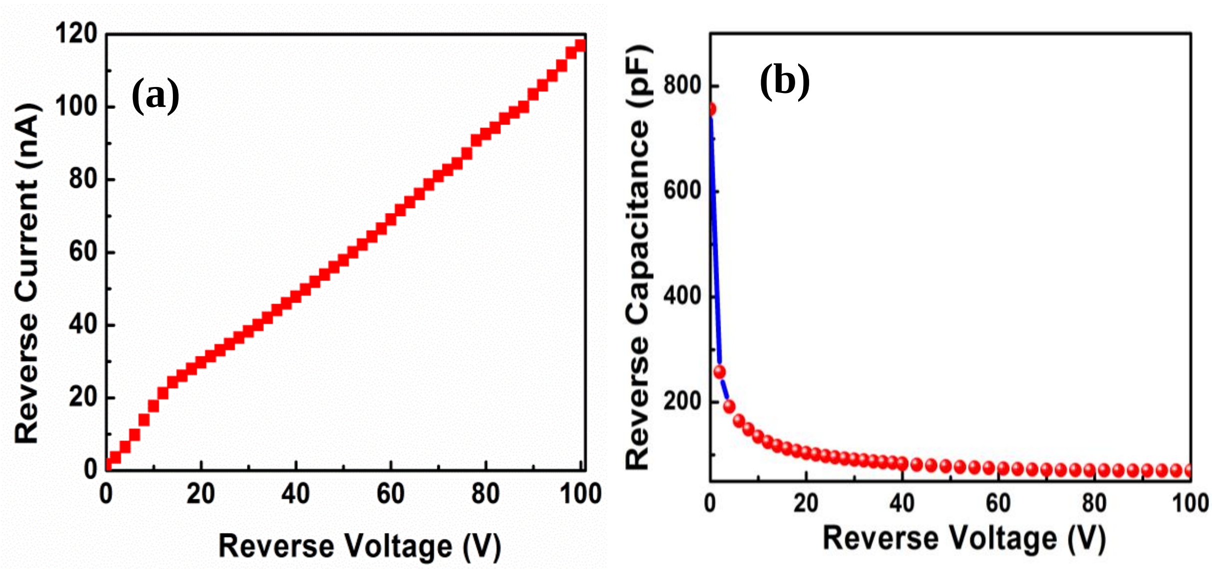

Figure 5.1. Reverse (a) I-V and (b) C-V measurements on virgin Si PIN diode

Like a typical Si PIN diode, the reverse current (I_r) increases with increase in reverse bias voltage (V_r) and is attributed to the increase in the minority concentration of charge carriers in the diode [1]. It reaches a value of 122 nA at V_r of 100 V. As for reverse C-V measurements, the capacitance decreases with the increase in V_r. The reason for this decrease is due to the increase in the depletion width of diode, which increases with the increase in V_r [2]. As capacitance is inversely proportional to the depletion width of diode, capacitance decreases with increase in V_r. As seen from figure 5.1 (b) for a typical V_r of 80 V the capacitance decreases to a value of 70 pf.

5.3 Alpha Spectroscopy on Si PIN diode

The silicon PIN diode is an extremely crucial component in a semiconductor neutron detector for the detection of charged particles (Li^7 and α in case of B^{10} converter material) and it is therefore mandatory to examine its response to charge particles such as alpha radiation as a test case [3] and also to confirm the working of read out nuclear electronics chain. A Si PIN diode firmly appended on a customized PCB and an alpha source (triple energy-Pu^{239}-5.155 MeV, Am^{241} 5.486 MeV and Cm^{244}-5.806 MeV see figure 2.11 of chapter 2) were mounted together in a vacuum chamber (as shown in figure 5.2).

Figure 5.2. Si PIN diode mounted on the PCB board with the aluminum vaccum chamber.

The distance between the alpha source and Si PIN diode was kept at 1 cm. The read out electronics used for the measurement has already been discussed section 2.2.2.1 of chapter 2.The Si PIN diode was reverse biased using a high voltage power supply (model - NHQ105 M) mounted in nuclear bin. The impingement of alpha particles on the diode creates electron hole (e-h) pairs through columbic interaction. The electric field induced in diode due to applied reverse bias voltage sweeps the e-h carriers to opposite electrodes. The movement of these e-h pairs produces a small output current pulse which is coupled to a charge sensitive preamplifier (model- CSP-11) through appropriate connectors and customized cables for amplification. The charge sensitive preamplifier (CSP) integrates the current pulse and generates a voltage output pulse. A typical output pulse as seen on Digital Storage Oscilloscope (DSO) is shown in figure 5.3 for an applied reverse biased voltage of 80 V. From this figure, it is clear that the pulse has a peak amplitude of 27 mV and rise time of 100 nsec.

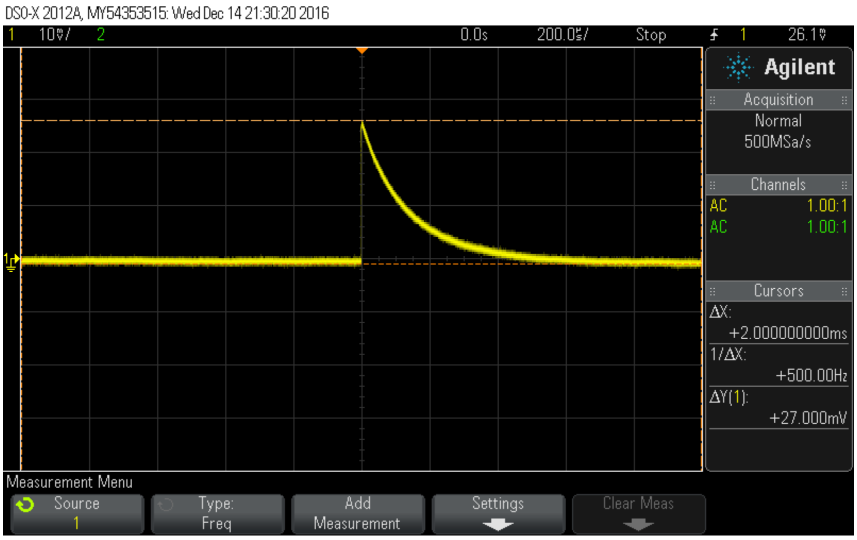

Figure 5.3. A typical preamplifier output pulse for the alpha radiation.

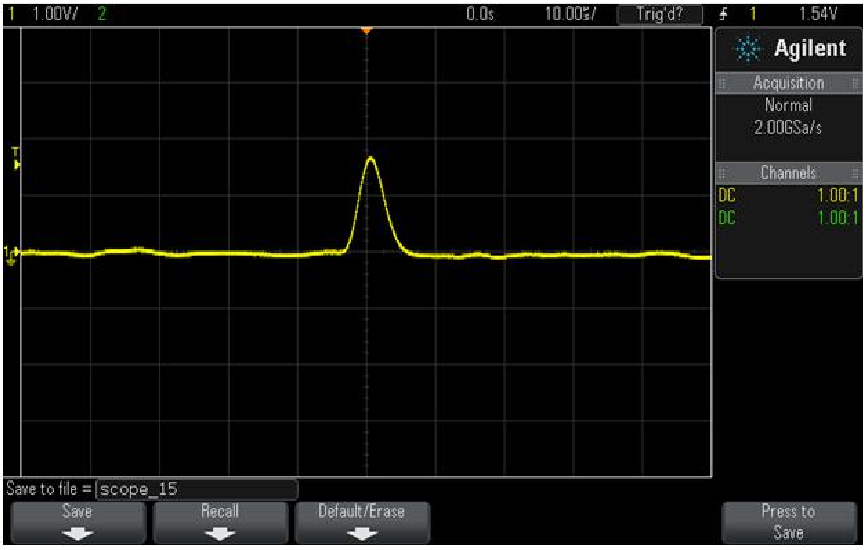

Figure 5.4. A typical output Gaussian pulse of the spectroscopy amplifier.

The CSP output pulse was further amplified by a spectroscopy amplifier (also known as shaping amplifier model-Ortec 673) to improve the signal to noise ratio [4,5]. The gain and shaping time parameters in spectroscopy amplifier was kept at 100 and 2μsec, respectively. A typical gaussian output pulse of the spectroscopy amplifier as seen on DSO is shown in figure 5.4. The rise and fall time of the gaussian pulse are dictated by the integrator and the differentiator time constant of spectroscopy amplifier, respectively. The generated gaussian output pulse which is an analog one is subsequently digitized as counts vs channel number using a MCA (Multi Channel Analyzer- Model MCA-3 Fast Comtec).

Figure 5.5 (a) shows the recorded alpha spectrum as counts vs. channel number, which is the response of Si PIN diode to the alpha source. From the figure, three peaks corresponding to the triple energies (Pu^{239}-5.155 MeV, Am^{241}- 5.486 MeV and Cm^{244}-5.806 MeV) were observed with a resolution of 30 keV. After performing the calibration using the inbuilt features of the MCA software, the channel number was converted into energy scale and the corresponding counts vs. energy is shown in figure 5.5 (b). The spectrum in figure 5.5 (b) confirms the proper functionality of the read out nuclear electronics chain and sensitive of Si PIN diode to charged particles.

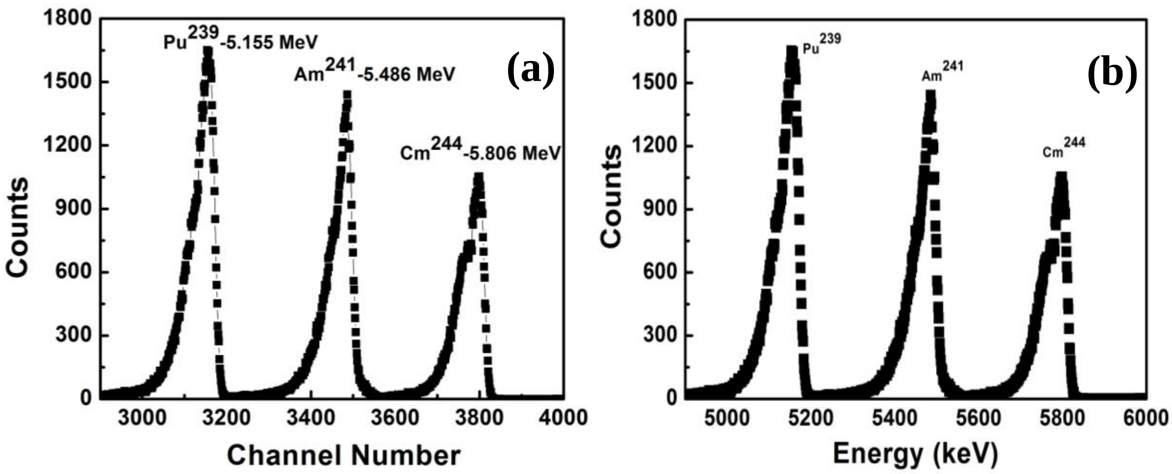

Figure 5.5. Alpha spectrum for Si PIN diode in terms of (a) channel number and (b) energy

5.4 Neutron detection on BBM coated Si PIN diode

The BBM coated Si PIN diodes (herein after referred to as detector) were tested for thermal neutron detection using the nuclear electronics chain setup discussed in the previous section, except that the alpha source was now replaced with a calibrated thermal neutron source as explained in section 2.2.2.2 of chapter 2. The detector was exposed to thermal neutron source by encasing it inside an Aluminum vacuum chamber in order to minimize the effect of the noise. The output pulse obtained from CSP (not shown here[3]) as observed on the DSO compared well with literature [6,7]. Additionally, the detector was operated at low reverse bias voltage of 5V to improve on the gamma discrimination [8]. Although the pulse height was low, it was substantially above the background and discernible as a signal arising out of either α (1.47 MeV) or Li^7(840 keV) charged particles, that deposit their energy in Si PIN diode which are generated upon interaction of thermal neutrons with BBM. In order to improve the signal to noise ratio, the output pulse of CSP was fed to the spectroscopy amplifier with appropriately adjusted gain and shaping time parameters. The obtained gaussian pulse from spectroscopy amplifier, was then fed as input to an MCA to facilitate data storage. The neutron data were recorded till the counts reached around 10,000.

It is important to note that the experiment was also performed on virgin (uncoated) Si PIN diode under identical conditions and this served to estimate the contribution due to background radiation. The experimental results for the uncoated and BBM coated diode in terms of counts vs channel number are (not shown[3]) in this thesis. The calibration of channel number in terms of energy was carried out by acquiring alpha spectrum on uncoated Si PIN diode with the same settings of detector bias, gain and shaping time of

[3]As a patent application is being filed, only skeletal details (no detailed materials aspects, coating method, spectrum and associated signals) are disclosed in this thesis.

neutron experiments. Thus after calibration channel number was converted into the energy scale. The experimental result[2] on BBM coated Si PIN diode revealed a distinct typical plateau like behaviour spanning the energy range from ~700 keV to 1.5 MeV. A comparison between the counts obtained from BBM coated and uncoated Si PIN diodes confirmed that the plateau like feature indeed corresponds to the charged particles generated in B^{10} (n,α) Li^7 reactions and hence confirms that BBM coated Si PIN diode are sensitive to thermal neutrons. As stated earlier, the response to thermal neutrons for BBM is not shown in the thesis. However, the expected response is similar to that of figure 5 of ref [7] and figure 6 of ref [8].

5.5 Conclusions

The optimum coating thickness of BBM material was obtained from GEANT4 simulation. The I-V and C-V measurements performed before and after coating BBM confirmed that the coating had not affected the electrical characteristics of diode. The thermal neutron detection was conducted on BBM coated Si PIN diode and was found to be sensitive to the neutrons.

This chapter presented results on BBM coated Si PIN diodes when exposed to thermal neutrons. It is known from several investigations in literature that Si diode undergoes radiation damage when exposed to neutrons [9]. The next chapter discusses radiation damage of virgin Si PIN diode by investigating its electrical characteristics in terms of I-V measurements for both forward and reverse measurement at different neutron irradiation fluence.

References

[1] Y. Murakami, T. Shingyouji, Separation and analysis of diffusion and generation components of pn junction leakage current in various silicon wafers, J. Appl. Phys. 75 (1994) 3548–3552. doi:10.1063/1.356091.

[2] R.L.Boylestad, Electronic Devices and Circuit Theory, 11th edition, Pearson (2014).

[3] A. Pappalardo, M. Barbagallo, L. Cosentino, C. Marchetta, A. Musumarra, C. Scirè, S. Scirè, G. Vecchio, P. Finocchiaro, Characterization of the silicon+6LiF thermal neutron detection technique, Nuclear Instruments and Methods in Physics Research Section A: Accelerators, Spectrometers, Detectors and Associated Equipment. 810 (2016) 6–13. doi:10.1016/j.nima.2015.11.114.

[4] H.Spieler, Semiconductor detector systems, Oxford University Press (2005).

[5] G. F. Knoll, Radiation Detection and Measurement, John Wiley & Sons, (2010).

[6] N. Hong, J. Mullins, K. Foreman, S. Adenwalla, Boron carbide based solid state neutron detectors: the effects of bias and time constant on detection efficiency, Journal of Physics D: Applied Physics. 43 (2010) 275101. doi:10.1088/0022-3727/43/27/275101.

[7] C. Petrillo, F. Sacchetti, O. Toker, and N. J. Rhodes, Solid state neutron detectors,Nuclear Instruments and Methods in Physics Research Section A: Accelerators, Spectrometers, Detectors and Associated Equipment, vol. 378, no. 3, pp. 541–551, Aug. 1996.

[8] A. Singh, A. Topkar, Thin Epitaxial Silicon PIN Detectors for Thermal Neutron Detection with Improved Gamma (γ) Discrimination , AIP Conference Proceedings, vol. 1731, pp. 1-3, May 2016.

[9] M. Hasegawa, S. Mori, T. Ohsugi, H. Kojima, A. Taketani, T. Kondo, M. Noguchi,Radiation damage of silicon junction detectors by neutron irradiation, Nucl. Instrum. Methods Phys. Res. A 277 (1989) 395–400, http://dx.doi.org/10.1016/

Chapter-6

Effect of Neutron irradiation on I-V characteristics of Si PIN diode

In the present chapter, a detailed investigation is presented on the evolution of forward and reverse current-voltage (I-V) characteristics on silicon PIN diodes, irradiated in thermal research nuclear reactor - KAMINI, for neutron fluences varying from $1x10^{14}$ to $1x10^{16}$ n/cm^2. The experimental details have already been elucidated in chapter 2 of this thesis. The remaining sections of this chapter discuss on the results of the experiments for forward and reverse current analysis on both virgin and neutron irradiated Si PIN diodes as a function of neutron fluence.

6.1 Forward Current Analysis

6.1.1 Forward I-V characteristics of virgin Si PIN diode

The forward current of diode is governed by the majority carriers. The forward current increases with the increases in forward voltage till knee voltage and it increases exponentially after the knee voltage [1]. In general, for an ideal PIN diode [1], the forward current voltage (I_f -V_f) relation is given by the equation (1).

$$\mathbf{I_f} = \boldsymbol{I_0} \, \mathbf{exp}(\boldsymbol{\beta V_f}) + \boldsymbol{I_{re}} \mathbf{exp} \, (\boldsymbol{\beta V_f / 2}) \qquad (1)$$

where I_0 and I_{re} are the diffusion and recombination saturation currents, respectively and β =q/η_ikT, where q is the electronic charge, k is the Boltzmann constant, η_i is the ideality factor and T is the temperature. The η_i indicates the deviation of diode from its ideal forward characteristics. In others word it resembles how accurately diode forward current follow the diode current equation.

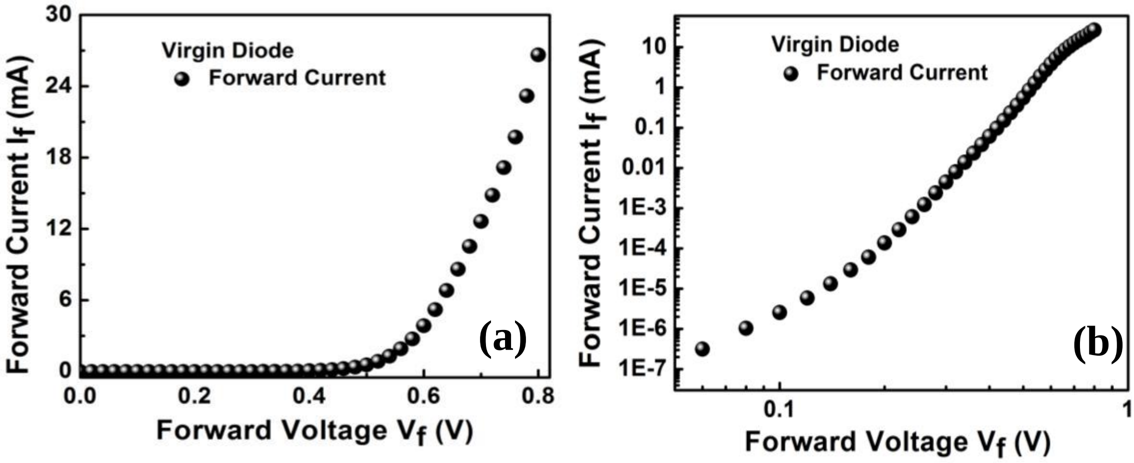

Figure 6.1. Forward I-V Characteristics of virgin Si PIN diode in (a) linear and (b) log-log scale.

Figures 6.1 (a) and (b) show the response of the forward current (I_f) of virgin Si PIN diode as a function of forward voltage (V_f) till 0.8V, in the linear and log-log scale, respectively. The forward I-V characteristics show normal rectification behaviour with a sharp increase in I_f close to a knee voltage (V_{knee}) of ~ 0.5 V.

From a linear fitting of I_f vs V_f to equation (1) for low and high voltage regions on the semilog scale, the saturation current (I_s) and ideality factor (η_i), were evaluated from the intercepts and slopes, respectively. A point to note is that the knee voltage 'V_{knee}' is taken as a voltage, above (below) which the total diode current is driven by diffusion (recombination) mechanism.

Figure 6.2 shows the fitting of equation (1) for virgin Si PIN diode in the recombination and diffusion regions, which yields η_i =2.1 and I_s = 58.3pA for the low voltage range, while for high voltage range, η_i= 2.4 and I_s=185 nA. The ideality factor, in general is ~ 1.2 -1.3 and ~2-3 for silicon and GaAs diodes, respectively [2]. For ideal p-n junctions devoid of any defects, the ideality factor is described by Sah–Noyce–Shockley theory [3], which yields η_i =1 at low voltage range and η_i=2 at high voltage range. Although the experimental ideality factor for the virgin Si PIN diode indicates a small deviation from the theoretical value ~1(2) for low (high) voltage, the diode is still a good rectifier as seen from the measured reverse leakage current (~ 1.69 nA at 100V) in the reverse bias condition as discussed in later sections. The miniscule magnitude of reverse leakage current (I_r) clearly indicates that the rectification property of Si PIN diode is still intact.

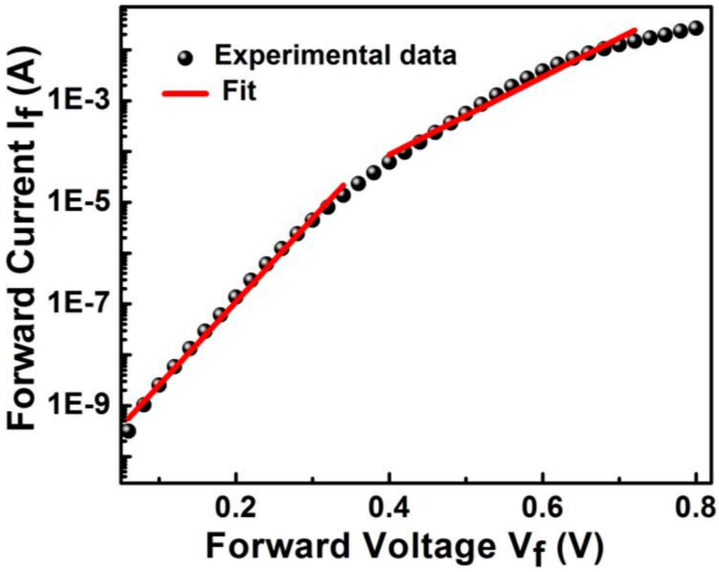

Figure 6.2. Fitting of diode equation (1) for low and high voltage regions for virgin diode, in order to obtain ideality factor (η_i) and saturation current (I_s) in the respective region.

6.1.2 Forward I-V characteristics of neutron irradiated Si PIN diodes

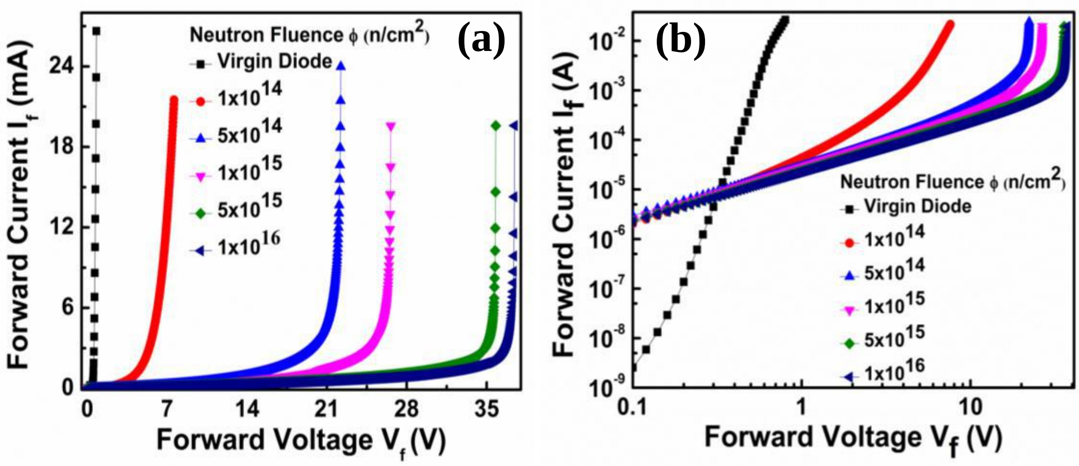

Figure 6.3. Forward I-V Characteristics of neutron irradiated diodes in (a) linear and (b) Log- Log scale.

Figures 6.3 (a) and (b) show the I_f response of the neutron irradiated Si PIN diodes as a function of V_f, for neutron fluences 'ϕ', ranging from $1x10^{14}$ n/cm^2 to $1x10^{16}$

n/cm^2 in the linear scale and log-log scale, respectively. The plot for the virgin Si PIN diode specimen is also shown for comparison.

The forward I-V characteristics in these figures definitely show prominent deviations from exponential behaviour of the virgin Si PIN diode as shown in figures 6.1(a) and (b). In particular, as ϕ increases, the value of V_{knee} at which the diode reaches limiting current also progressively increases. Therefore, the I-V characteristics of the irradiated diodes could be measured for increased forward bias voltages without an electrical breakdown of the diodes. The reason for the shift in V_{knee} is due to the formation of traps caused by neutron damage of the Si PIN diode [4]. Higher the neutron fluence, more the damage the diode undergoes, thereby leading to shifting V_{knee} to higher voltage levels. As for the analysis, the I-V characteristics are fitted to equation (1) for the low and high voltage regions to obtain the ideality factor and saturation currents. A representative fit of the same is shown in figure 6.4.

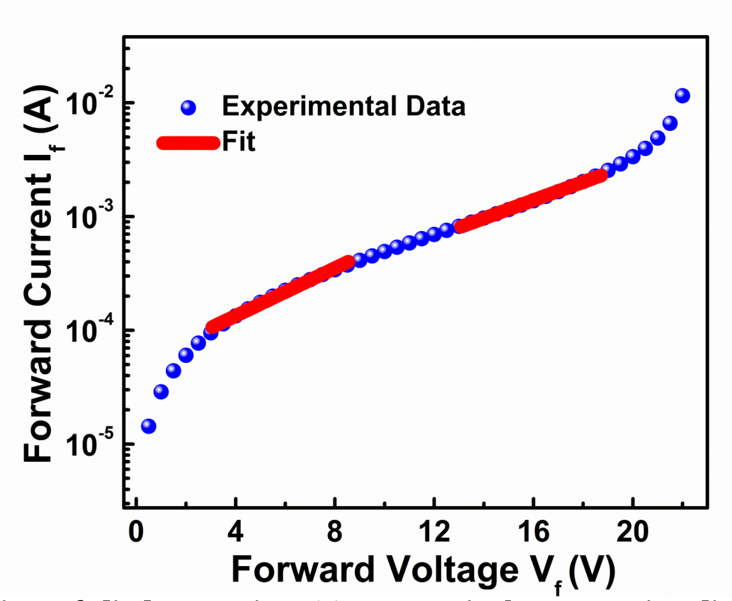

Figure 6.4. Fitting of diode equation (1) to a typical neutron irradiated diode (ϕ=1 x10^{15} n/cm^2) for low and high voltage regions.

The ideality factors and the saturation currents obtained for all the specimens from the fit are shown in figures 6.5 and 6.6, respectively. The ideality factor (η_i) and the saturation currents consisting of both I_o and I_{re}, show distinct increase with increase in ϕ, which indicate considerable deviations from the ideal diode behaviour.

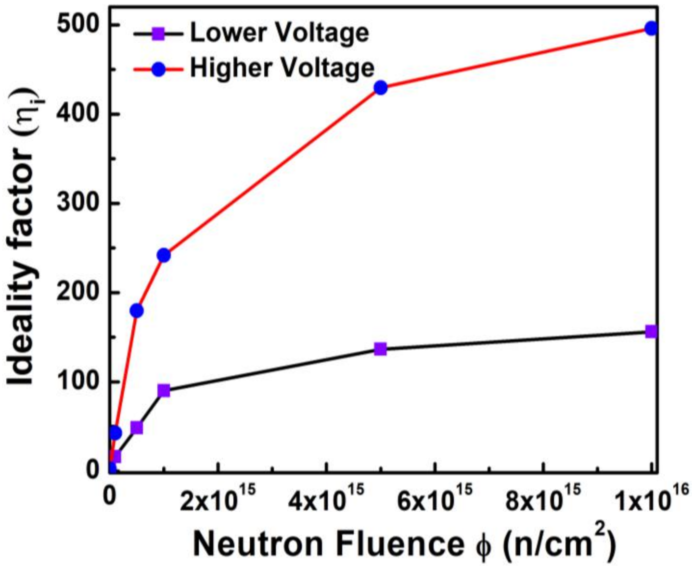

Figure 6.5. Variation of η_i with neutron fluence ϕ (n/cm^2), obtained from fit to equation (1) for low and high voltage ranges.

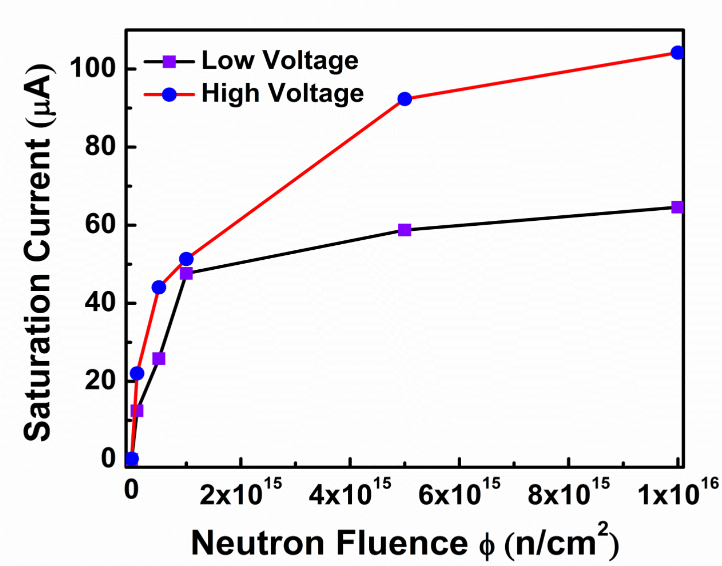

Figure 6.6. Variation of saturation current with neutron fluence ϕ (n/cm^2) obtained from fit to equation (1) for low and high voltage range.

The Shockley-Read-Hall (SRH) recombination theory [5] which assumes recombination via isolated point defect levels has been traditionally used to explain the ideality factor (η_i) in diodes for the diffusion and recombination regions. In the present experiment, η_i typically changes from ~2 for the virgin diode to ~ 496 for the diode with the highest neutron irradiated fluence. Such large ideality factors have been observed in silicon solar cell devices [6], BN/ZnO hetero structured rectifying diodes, phosphorus doped n-Ge/i-Ge/p-Si hetero- structure diodes too [7]. The increase in η_i in the present studies is attributed to the recombination currents being much higher than expected ones [7]. The evolution of increase in η_i and associated saturation currents with fluence are due to the large defects that are created thereby implying more recombination. Other factors such as tunnelling and metal semiconductor junctions also contribute to high η_i [7].

Qualitatively, the forward I-V characteristics of all irradiated diodes become more and more shallow with increase in neutron fluence ϕ (figures 6.3(a) and (b)). Moreover, for voltages below the knee voltage of virgin diode, I_f for all the neutron irradiated diodes increased by three orders of magnitude. The large increase in I_f in this region for the lowest irradiated specimen ($1x10^{14}$n/cm^2) is indicative of the damage that the diode undergoes upon irradiation. This increase is attributed to the increased number of electron-hole pairs generated from the generation-recombination centres during the initial stages of irradiation. For higher fluences, the I_f decreases with increase in fluence as shown in figures 6.3(a) and (b). This decrease is due to the formation of traps which are formed by Frenkel defects [4].The traps lead to increased scattering of carriers, resulting in decreased mobility of carriers. Consequently, the lifetime of the charge carriers [4] decreases thereby leading to increased resistance of the material upon irradiation. It is to be noted that even though the diodes were simultaneously exposed to the inevitable gamma dose rate ~ 3.14 x 10^4 Gy/h, their consequential effect is neglected. In order to corroborate the effect of gamma irradiation, the Si PIN diodes were exposed to gamma radiations from Co^{60} source of strength 12200 curies. Prior to the gamma irradiation, the I-V characteristics were measured. The Si PIN diode was exposed to a gamma dose of 1.38 KGy. In order to nullify the effect of annealing at room temperature after the gamma irradiation, the forward and reverse I-V measurement was carried out immediately. The I-V measurements indicated that the forward and reverse I-V measurement showed little change post gamma irradiation. In particular, the magnitude of reverse current was 5nA (40nA) for pristine (gamma irradiated to 1.38 KGy dose) at reverse voltage of 100V. The change in the reverse current is owing to the Compton scattering [8] of gamma rays on Si PIN diode. Even in literature, J.P Raymond et al. [9] have studied comparison of neutron, proton and gamma ray in semiconductor. In their studies on exposure to Co^{60} gamma source, they found that the gamma ray exposure produces displacement damage through Compton electrons. But they also report that the damage effects are negligible. J.R Sour et al. [8] and J P Raymond et al. [9] have reported the gamma ray damage in silicon is almost three orders of magnitude less than that caused by neutrons.

In order to further understand the quantitative changes and trends in the evolution of I_f on irradiation, the V_f at which I_f is 17.5 mA, is monitored. This magnitude of I_f is chosen for two reasons. Firstly, the slope of I_f vs V_f is very large at I_f =17.5mA and does not change appreciably with further increase in V_f. Secondly, the current was limited by heating effects to avoid damage to the junction of the diode. The V_f corresponding to 17.5 mA is taken as knee voltage and is plotted in figure 6.7 as a function of neutron fluence on a linear scale. It is clear from the graph that, the increase in V_{knee} is maximum in the initial stages of irradiation. The extent of increase in magnitude of V_{knee} with neutron fluence has also been reported in literature by Swartz et al. [10].

With increase in neutron fluence, trap density is known to increase, which leads to the recombination of generated carriers, thereby decreasing the concentration of the intrinsic charge carriers. Consequently, there is a degradation of carrier lifetime and an increased resistivity upon irradiation. Incidentally, as seen from the fit shown in figure 6.7, the V_{knee} rises rapidly for low fluences and nearly saturates at a value 36.3 V for a fluence of $5x10^{15}$ n/cm^2. Such saturation behaviour is not reported in ref. [11], probably due to the fact that the I_f was measured only till ~10-12 volts. The behaviour observed in the present study is almost similar to that reported in Swartz et al. [10] and indicates that there is little change in damage beyond a fluence of $4x10^{15}$ n/cm^2. This ‘flattening off’ is construed to be a consequence of the occupation of displaced atoms and impurities by the Frenkel pairs that have been created by the irradiation, thereby resulting in the material becoming radiation hard or radiation resistant.

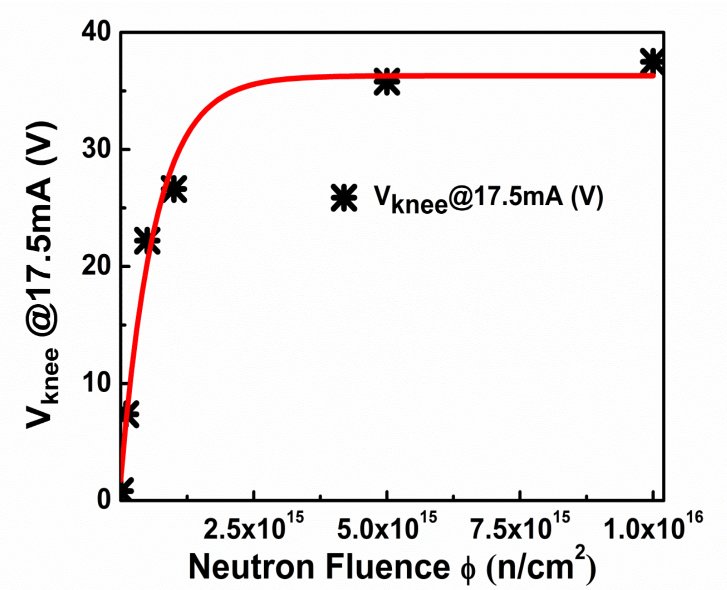

Figure 6.7. Variation of knee voltage (V_{knee}) with neutron fluence at constant forward current of 17.5 mA.

6.2 Reverse Current Analysis

The I-V characteristics in the reverse bias conditions for the virgin diode along with neutron irradiated diodes are shown in figures 6.8 and 6.9 in linear and semilog scale, respectively. The measurements were performed up to a maximum reverse bias voltage ‘V_r’ of 100 V i.e., the limit to which the diodes can be operated in reverse biased condition. Since the interest in the present thesis is on the change in characteristics upon neutron irradiation, the I_r-V_r profile of the virgin diode is taken as reference. The reverse leakage current (I_r) due to minority carriers is typically in the nanoampere (10^{-9}A) range for the virgin diode. The magnitude of I_r is dependent on minority carriers and also on the active volume of the diode, which in turn is determined by the depletion thickness and lateral extension [12].

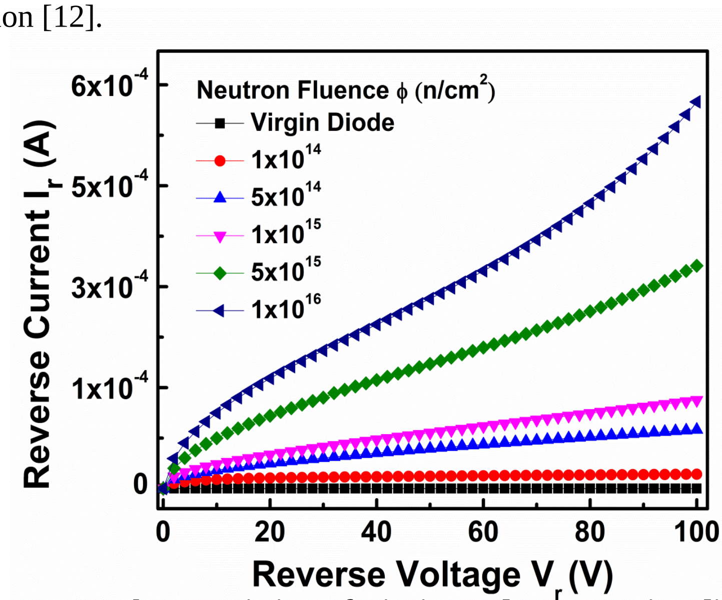

Figure 6.8. Reverse I-V characteristics of virgin and neutron irradiated diodes in linear scale.

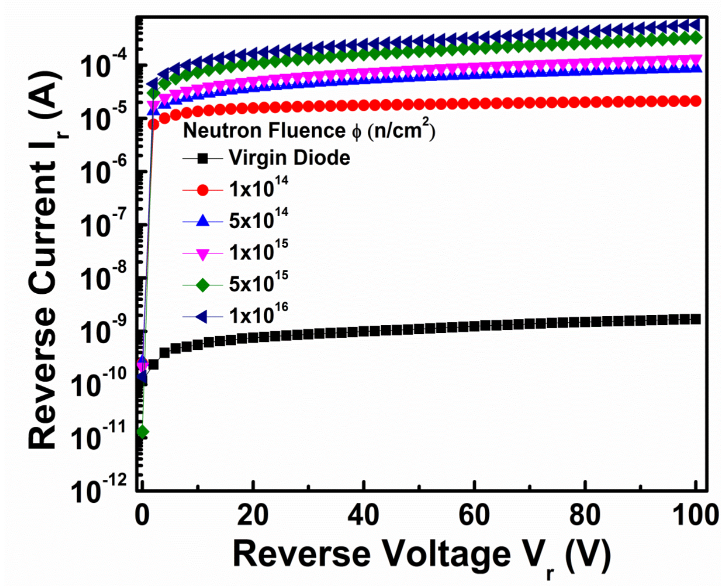

Figure 6.9. Reverse I-V characteristics of virgin and neutron irradiated diodes in semi-log scale.

As for the neutron irradiated diodes, I_r increases by four orders of magnitude for the diode with lowest irradiated fluence of $1x10^{14}$ n/cm^2. The large change in I_r upon neutron irradiation is due to the fact that a large number of Frenkel pairs are created and unoccupied. Moreover, defect states are introduced upon neutron irradiation and they act as generation-recombination (g-r) centres [11]. These provide e-h pairs that are drawn by the applied reverse field contributing to the increased I_r [13]. It is pointed out that increase in I_r due to the minority charge carriers is a consequence of defects induced by the irradiated neutrons both at the surface and in the bulk of the diode. The increase in I_r is gradual, reaching a maximum value of ~ 5.7×10^{-4} A, for the diode irradiated to a fluence of 1×10^{16} n/cm^2.

The behaviour of I_r at full depletion voltage which is ~ 100V, in the present experiment is shown in figure 6.10 as a function of ϕ. This behaviour is comparable to that reported by S.Moloi et al. [14] but does not follow a linear behaviour as reported by Hasegawa et al. [15] and Lemeilleur et al. [13]. Incidentally, a plot of I_r for lower V_r (20V), shows the same trend as V_r of 100V. The behaviour shown in figure 6.10 implies that change in minority carriers is very large for the lowest fluence and thereafter the change is minimal. The curve tends to flatten indicating that the material is already radiation hard [14].

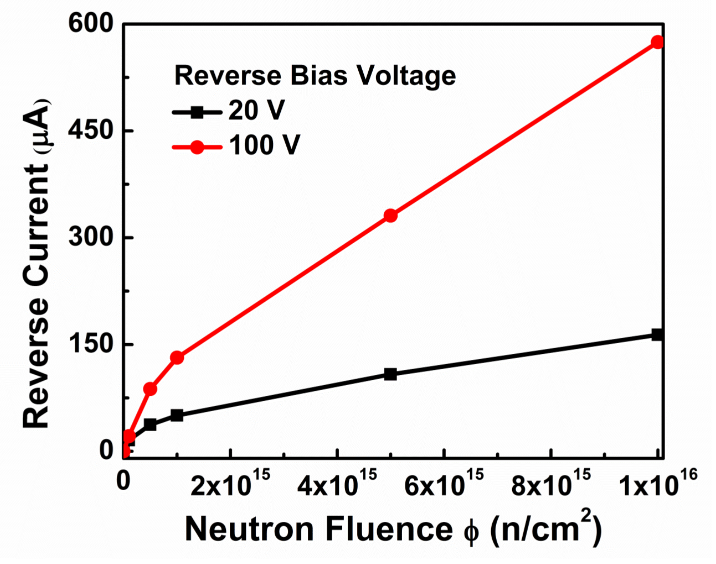

Figure 6.10. Reverse leakage current at bias voltage of 20V and 100 V as a function of neutron fluence ‘ϕ’ (n/cm^2).

A qualitative behaviour of the effect of exposure of the diodes to neutrons can also be inferred from the ‘gap’ between the I_f and I_r for both virgin and irradiated diodes. The progressive convergence of ‘gap’ between the forward and reverse profiles (I_r-I_f) with increase in ϕ is shown in figures 6.11 (a-c) for a few representative specimens, namely virgin, $1x10^{14}$ n/cm^2 and $5x10^{15}$ n/cm^2 .The progressive decrease in the gap shown in figures 6.11, is indicative of the change in behaviour from a diode like to ohmic behaviour and compares well with the reported behaviour [14]. The forward and reverse currents are almost equal and vary linearly with applied voltage for higher irradiation fluences.

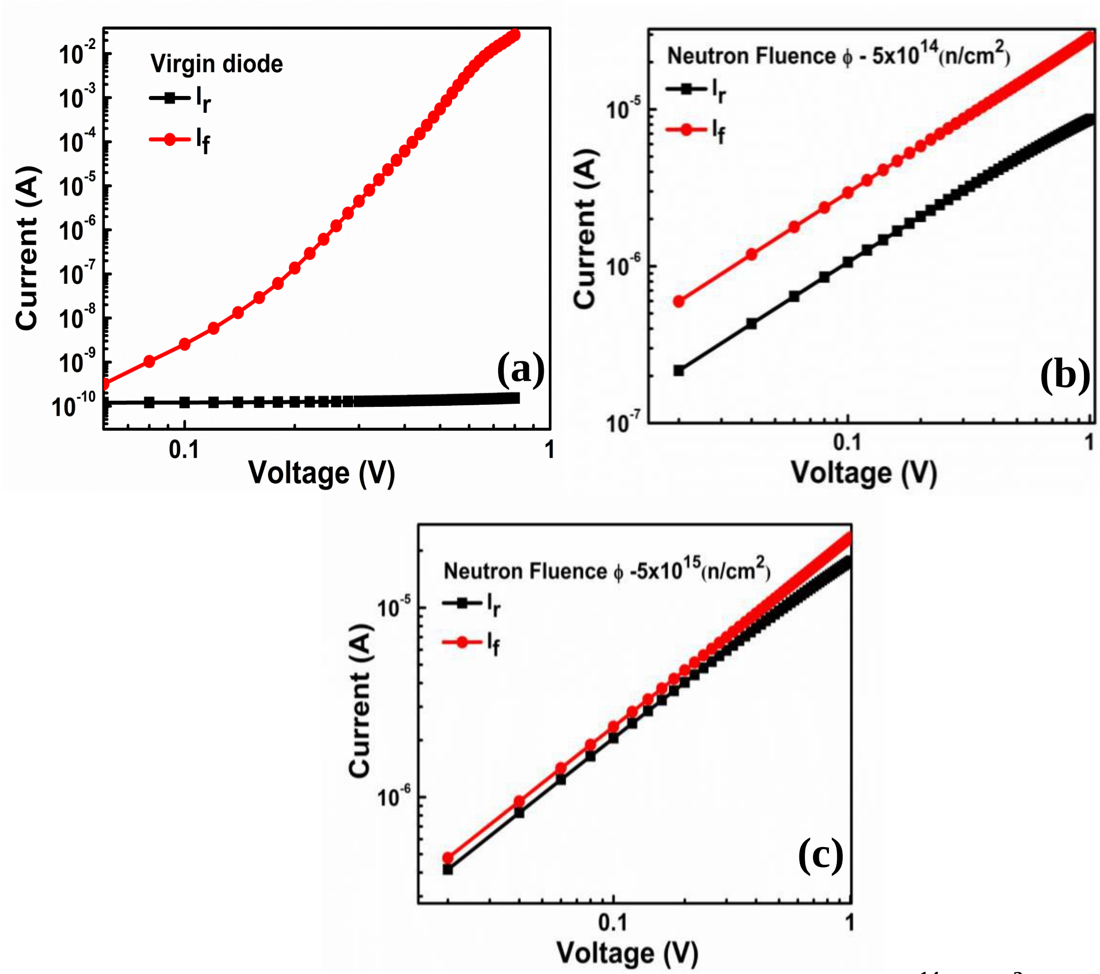

Figure 6.11. Low voltage gap between I_f and I_r for (a) virgin (b) $5x10^{14}$ n/cm^{2}and (c) $5x10^{15}$n/cm^2 showing the progressive decrease in gap between I_f and I_r with increasing fluence.

The variations in the I-V characteristics are readily brought out by ‘rate of change’ in the knee voltage ‘V_{knee}’ and reverse current I_r obtained from figures 6.7 and

6.10, respectively. These rates of change are shown in log-log scale in figures 6.12 and 6.13. The reference current and voltage for forward and reverse bias measurements were taken to be 17.5 mA and 100 V, respectively. For the evaluation of slope of V_{knee} with fluence, the data was limited between $1x10^{14}$ to $1x10^{15}$ n/cm^2, as beyond this fluence, the V_{knee} saturates. Whereas in case of I_r the slope was evaluated for the full data range, i.e. between the virgin diode and diode irradiated with $1x10^{16}$ n/cm^2 fluence. The 'rate of change' of V_{knee} and I_r with fluence are 0.6 and 0.7 respectively, as obtained from figures 6.12 and 6.13, respectively. The magnitudes of the slopes in the present experiment are nearly comparable and differ from that reported by Moloi et al. [14], where the slope of the reverse bias is reported to be twice that in the forward bias case. The difference in the slopes from ref. [14] is owing to the fact that in the present work the slopes were estimated for low neutron fluence as saturation in V_{knee} was observed at higher fluence.

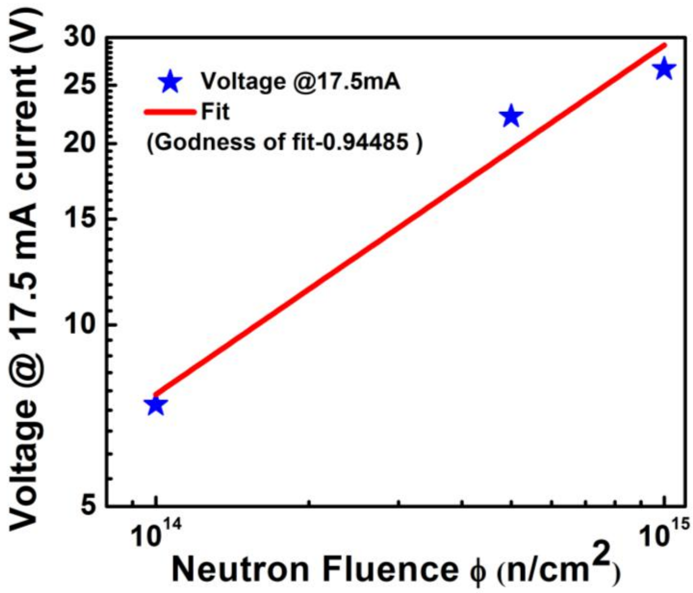

Figure 6.12. 'Rate of change' of knee voltage at forward current of 17.5mA with neutron fluence in log-log scale.

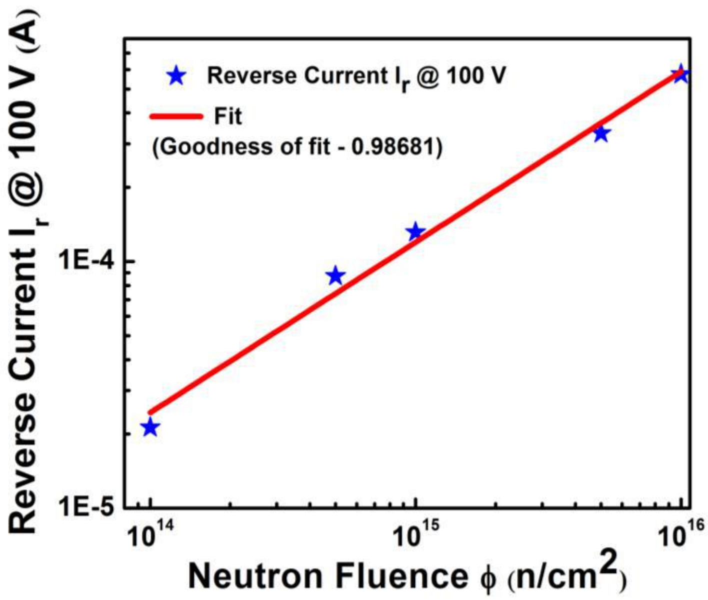

Figure 6.13. 'Rate of change' of reverse current with neutron fluence in log-log scale.

In order to verify whether Si PIN Diode had undergone transmutation due to the thermal neutrons or in other words whether type inversion had occurred in diode, the X-Ray fluorescence (XRF) studies on virgin and highest neutron irradiated Si- PIN diode (neutron fluence-1x 10^{16}) was carried out, it showed minute difference in phosphorous concentration. This showed that silicon had not undergone substantial transmutation upon interaction with thermal neutrons.

6.3 Damage Constant

The damage constant 'α' or volume reverse leakage current I_r/V_l, in the reverse bias conditions is taken as a measure of the damage caused by irradiation [16] and it is used to evaluate the radiation hardness property of the diode [16,17]. The constant 'α' is defined through the relation, $\Delta I=\alpha V_l$, where, ΔI is the difference in the reverse leakage current for the irradiated and virgin diode for the full depletion voltage of 100V and V_l is the volume of the depletion region in the diode. The lateral dimension of the PIN diodes used in the experiments is 5mm x 5mm and the width of the depletion region was computed from a measurement of capacitance in reverse bias conditions (C-V). Figure

6.14 shows the reverse C-V measurement of virgin Si PIN diode in which the capacitance decreases with increase in reverse voltage and becomes constant beyond 60 V. The initial decrease in capacitance is attributed to the increase in depletion width of diode with voltage, while the invariance above a certain voltage (~60V) indicates a complete depletion of the diode. The depletion region width estimated from the C-V measurement is ~300μm [18].

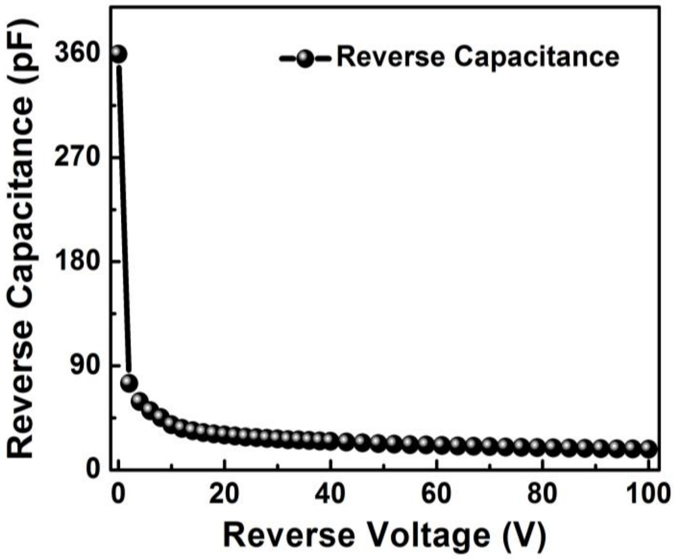

Figure 6.14. Reverse capacitance voltage characteristics of virgin diode.

The difference in the I_r per unit volume estimated at the reverse bias voltage of 100V for all the five irradiated diodes is shown in figure 6.15. From a linear fitting of ΔI vs ϕ, the damage constant α is estimated to be 1.7683 x 10^{-18}(A/cm).The damage constant 'α' in this experiment is lesser compared to that reported in ref. [15]. This is due to the use of a wide spectrum of incident neutrons energy rather than a mono energetic neutron beam.

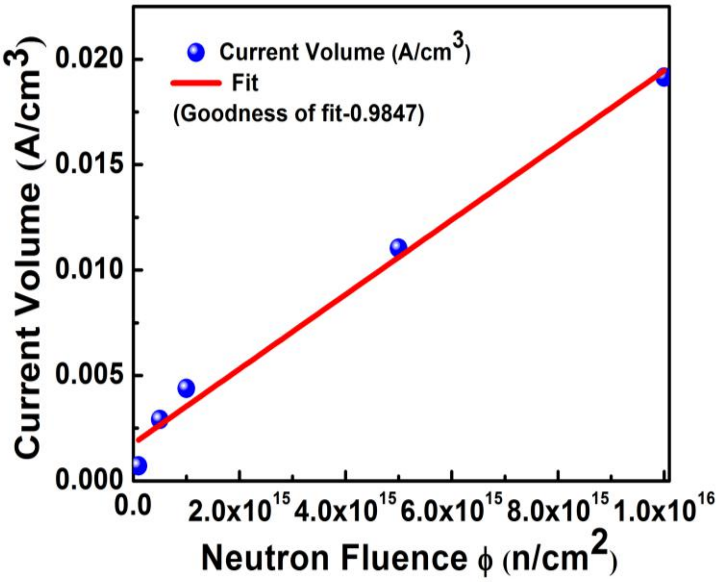

Figure 6.15. Variation of current density with neutron fluence and slope showing the damage constant 'α'.

6.4 Rectification Ratio

It is well known that the I-V characteristics, which demonstrate the rectifying behaviour, are crucial for device applications. In the context of diodes, rectification is monitored and quantified in terms of rectifying ratio 'RR', which is expresses as the ratio of the I_f to the I_r. Mathematically, RR is

$$\boldsymbol{RR = \frac{I_{fV_{f,max}}}{I_{rV_{f,max}}}} \qquad (2)$$

In the above expression, $V_{f,max}$ is the maximum forward voltage of the diode which can be applied within the permissible limits of operation and is used as the reference voltage for calculation of the RR. In the present experiment, as seen from figure 6.3(a), V_{fmax} varies with the neutron irradiation fluence.

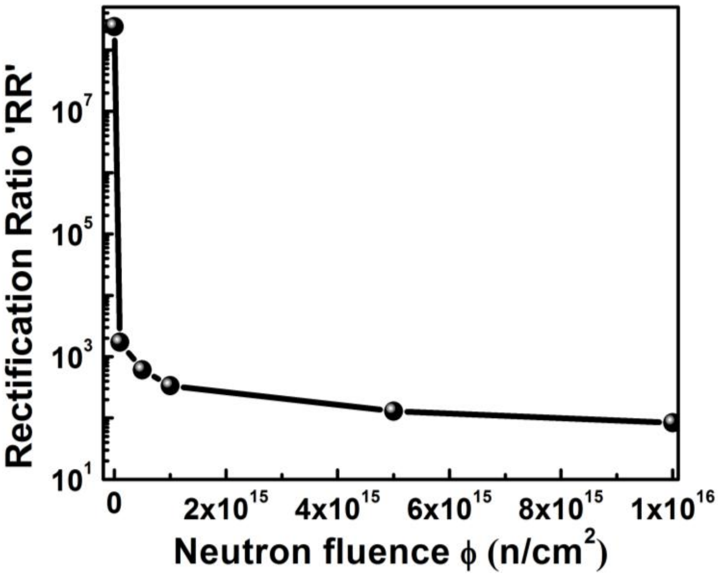

Figure 6.16. Variation of rectification ratio RR of virgin and neutron irradiated diodes as function of neutron fluence 'ϕ' (n/cm^2).

As seen from the graph (see figure 6.16), the virgin diode has the highest rectification ratio RR of ~10^8, with the current conduction in one direction only. This high value of RR is owing to the fact that the I_f is in the mA range, while the reverse leakage current in the reverse bias condition is in the nA range. Large RR has also been reported in all printed organic diodes [19] and metal induced lateral crystallization in a-Si: H in solar cell application [20].

In the present experiment, RR decreases drastically to ~ 10^3 and ~84 for diodes exposed to ϕ of $1x10^{14}$ n/cm^2 and $1x10^{16}$ n/cm^2, respectively as shown in figure 6.16. This decreasing trend is consistent with the observation by Bosetti et al. [21], although the magnitudes vary. The decrease in RR clearly indicates that the neutron irradiated diodes progressively lose their rectifying behaviour with increasing ϕ. The reason for the loss of rectifying behaviour is the decrease (increase) in the concentration of majority (minority) charge carriers. It is well known that irradiation induces defects and leads to loss of crystallinity, thereby resulting in decreased lifetime and mobility [4] .Such defect centres are known to increase the reverse leakage current and consequently resulting in loss of rectification [21].The variation of RR vs ϕ has been studied in literature and a critical fluence was observed [21] in which the RR is equal to zero. However, in the present experiment, it is found that the RR is ~ 84 even for a fluence of $1x10^{16}$ n/cm^2, which is higher than that reported in ref [21].

The quantities, RR and η_i are inverse to each other and the same are shown in figure 6.17. A large RR results in nearly ideal diodes where the η_i is ~1 in the recombination region. It is pertinent to note that the ideality factor of an ideal diode is 1(2) in the recombination (diffusion) region with the concomitant RR being very large (typically 10^8 or more). Figure 6.17 indicates a clear change in the behaviour of the diode from a rectifying one to ohmic one. This is a consequence of deceasing (increasing) forward (reverse) current with increasing fluence. Such a correlation has also been reported for nanocrystalline pn diodes [20].

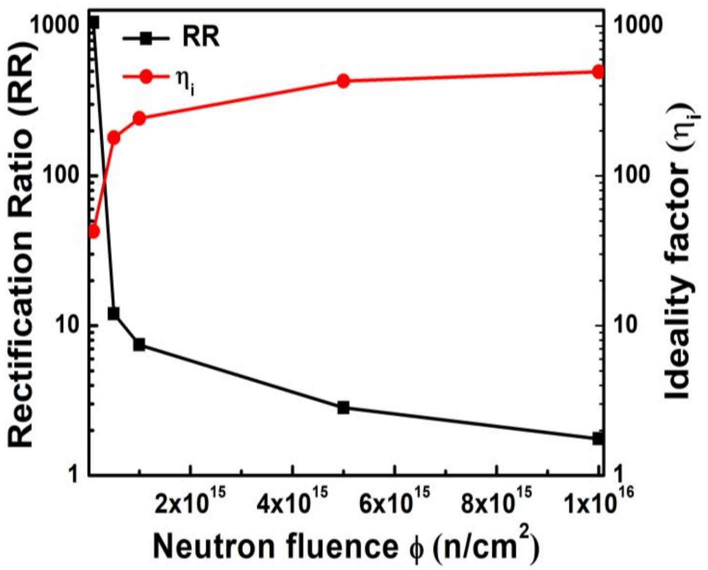

Figure 6.17. Variation of rectification ratio RR and ideality factor (η_i) with neutron fluence ϕ (n/cm^2).

6.5 Conclusions

This chapter discussed the effect of neutron irradiation on the current -voltage characteristics of silicon PIN diodes in a typical thermal research reactor for fluences ranging from $1x10^{14}$ to $1x10^{16}$ n/cm^2. The measured forward I-V characteristics, is increasingly becoming shallow upon increased irradiation fluence. Moreover, the knee voltage increases from 0.5V for the virgin Si PIN diode to ~ 36.3 V for diode irradiated to a fluence of ~ $5x10^{15}$ n/cm^2 and thereafter saturates. The shift and increase in knee voltage is attributed to increased trap density [22], which in turn leads to the recombination of the majority carriers, thereby decreasing the concentration of the intrinsic charge carriers. The increase in knee voltage indicates that diodes can be operated at higher voltages [23].The ideality factors extracted from the fit of the forward I-V characteristics to diode equations in the low/high voltage regions varied from a typical value of ~ 2 for the virgin case to ~ 496 for the highest irradiated fluence. The large ideality factors observed in this study are caused by the defects that are created upon irradiation.

With increase in neutron fluence, the reverse leakage currents also increased by almost four orders of magnitude owing to the production of a large number of defect states that act as generation-recombination (g-r) centres upon neutron irradiation. Another important consequence of the increase in fluence of irradiation is the transformation of diode properties from a rectifying to ohmic one, which was inferred from the progressive decrease in gap between the forward and reverse currents. Further, quantitatively, the rectification ratio decreased from 10^8 for virgin diode to 84 for the maximum neutron irradiated fluence of $1x10^{16}$n/cm^2. The damage constant evaluated from the reverse leakage current indicates that the diode hardness property is still in intact after the irradiation. The quantitative behaviour of diodes in terms of rectification ratio shows that its rectification property has been degraded drastically with the increase in neutron fluence.

References

[1] A. Bar-Lev, Semiconductor and electronic devices, Prentice-Hall, 1993.

[2] V.R.V. Pillai, S.K. Khamari, V.K. Dixit, T. Ganguli, S. Kher, S.M. Oak, Effect of γ-ray irradiation on breakdown voltage, ideality factor, dark current and series resistance of GaAs p–i–n diode, Nucl. Instrum. Methods Phys. Res. Sect. Accel. Spectrometers Detect. Assoc. Equip. 685 (2012) 41–45. doi:10.1016/j.nima.2012.05.062.

[3] C.Sah,R.N. Noyce,W. Shockley, Carrier Generation and Recombination in p-n Junctions and p-n Junction Characteristics. Proceedings of the IRE 45 (1957) 1228-1243. http://dx.doi.org/10.1109/JRPROC.1957.278528

[4] I. Anokhin, O. Zinets, A. Rosenfeld, M. Lerch, M. Yudelev, V. Perevertaylo, M. Reinhard, M. Petasecca, Studies of the Characteristics of a Silicon Neutron Sensor, IEEE Trans. Nucl. Sci. 56 (2009) 2290–2293. doi:10.1109/TNS.2009.2024150.

[5] W. Shockley, W.T. Read, Statistics of the Recombinations of Holes and Electrons, Phys. Rev. 87 (1952) 835–842. doi:10.1103/PhysRev.87.835.

[6] O. Breitenstein, P. Altermatt, K. Ramspeck, A. Schenk, The Origin of Ideality Factors N> 2 of Shunts and Surfaces in the Dark I-V Curves of Si Solar Cells, 21st European Photovoltaic Solar Energy Conference., 2006.

[7] M. Brötzmann, U. Vetter, H. Hofsäss, BN/ZnO heterojunction diodes with apparently giant ideality factors, J. Appl. Phys. 106 (2009) 063704. doi:10.1063/1.3212987.

[8] J.R. Srour, D.M. Long, D.G. Millward, R.L. Fitzwilson and W.L. Chadsey, Radiation damage of silicon junction detectors Enhancement of Electronic Materials, (Noyes Publications), 1984.

[9] J.P. Raymond, E.L. Petersen, Comparison of Neutron, Proton and Gamma Ray Effects in Semiconductor Devices, IEEE Transactions on Nuclear Science. 34 (1987) 1621–1628. doi:10.1109/TNS.1987.4337526.

[10] J.M. Swartz, M.O. Thurston, Analysis of the Effect of Fast-Neutron Bombardment on the Current-Voltage Characteristic of a Conductivity-Modulated p-i-n Diode, J. Appl. Phys. 37 (1966) 745–755. doi:10.1063/1.1708249.

[11] M. McPherson, B.K. Jones, T. Sloan, Effects of radiation damage in silicon p - i - n photodiodes, Semicond. Sci. Technol. 12 (1997) 1187. doi:10.1088/0268-1242/12/10/003.

[12] Y. Murakami, T. Shingyouji, Separation and analysis of diffusion and generation components of pn junction leakage current in various silicon wafers, J. Appl. Phys. 75 (1994) 3548–3552. doi:10.1063/1.356091.

[13] F. Lemeilleur, M. Glaser, E.H.M. Heijne, P. Jarron ,E. Occelli, Neutron-induced radiation damage in silicon detectors,IEEE Transactions on Nuclear Science, 39, 1992 551-557.

[14] S.J. Moloi, M. McPherson, The current and capacitance response of radiation-damaged silicon PIN diodes, Phys. B Condens. Matter. 404 (2009) 3922–3929. doi:10.1016/j.physb.2009.07.123.

[15] M. Hasegawa, S. Mori, T. Ohsugi, H. Kojima, A. Taketani, T. Kondo, M. Noguchi, Radiation damage of silicon junction detectors by neutron irradiation, Nucl. Instrum. Methods Phys. Res. Sect. Accel. Spectrometers Detect. Assoc. Equip. 277 (1989) 395–400. doi:10.1016/0168-9002(89)90768-7.

[16] G. Lindström, M. Moll, E. Fretwurst, Radiation hardness of silicon detectors – a challenge from high-energy physics, Nucl. Instrum. Methods Phys. Res. Sect. Accel. Spectrometers Detect. Assoc. Equip. 426 (1999) 1–15. doi:10.1016/S0168-9002(98)01462-4.

[17] F.Honniger, Radiation Damage in Silicon - Defect Analysis and Detector Properties, Ph.D dissertation submitted in 2007.

[18] V.Mishra, Study of Silicon Detectors, Ph.D dissertation submitted in 2002 , Mumbai University.

[19] S. Ali, J. Bae, C.H. Lee, Organic diode with high rectification ratio made of electrohydrodynamic printed organic layers, Electron. Mater. Lett. 12 (2016) 270–275. doi:10.1007/s13391-015-5202-y.

[20] J.D. Hwang, K.S. Lee, A High Rectification Ratio Nanocrystalline p–n Junction Diode Prepared by Metal-Induced Lateral Crystallization for Solar Cell Applications, J. Electrochem. Soc. 155 (2008) H259–H262. doi:10.1149/1.2840618.

[21] M. Bosetti, N. Croitoru, C. Furetta, C. Leroy, S. Pensotti, P. Rancoita, M. Rattaggi, M. Redaelli, A. Seidman, Study of current-voltage characteristics of irradiated silicon detectors, Nucl. Instrum. Methods Phys. Res. Sect. B Beam Interact. Mater. At. 95 (1995) 219–224. doi:10.1016/0168-583X(94)00439-0.

[22] V. Sopko, B. Sopko, D. Chren, J. Dammer, Study of PIN diode energy traps created by neutrons, J. Inst. 8 (2013) C03014. doi:10.1088/1748-0221/8/03/C03014.

[23] A. Chilingarov, T. Sloan, Operation of heavily irradiated silicon detectors under forward bias, Nuclear Instruments and Methods in Physics Research Section A: Accelerators, Spectrometers, Detectors and Associated Equipment. 399 (1997) 35–37. doi:10.1016/S0168-9002(97)00940-6.

Chapter-7

Summary, Conclusion and Scope for future research

7.1 Summary

The present thesis presented three aspects of research on semiconductor neutron detectors, namely, simulations for optimization of thickness of converter material to achieve maximum neutron detection efficiency, fabrication of a prototype semiconductor neutron detector in collaboration with IISc and investigation on neutron radiation damage of Si PIN diode. The summary and important conclusions from the thesis are discussed below.

7.2 Conclusions

As mentioned in the previous chapters of the thesis, a Monte Carlo simulation is of paramount importance ahead of the semiconductor neutron detector fabrication. The objective of GEANT4 simulation was to find out the optimized critical geometrical parameters for various detector configurations in order to obtain the maximum neutron detection efficiency. The two neutron sensitive converter materials used for the simulation in the present work were Boric acid (H_3BO_3) and Depleted Uranium Oxide (DUO_2). In particular, for the boric acid converter material (CM) case, the efficiency was estimated for various ^{10}B enrichment levels. Different geometrical configurations such as planar, stack, cylindrical perforation, embedded spherical design and cuboidal trench were investigated using GEANT4 simulation toolkit. Besides estimation of maximum efficiency, histogram plots to study the energy deposition in Si detector medium were also studied for different detector configurations.

Along with GEANT4 simulation studies, an experimental effort was attempted to detect the thermal neutron using Boron Based Material (BBM) coated Si PIN diode was successfully accomplished using the standard nuclear read out electronics chain. The thesis also focused on experimental study on the behaviour of the electrical characteristics of Si PIN diodes before and after neutron irradiation in a typical thermal research reactor for neutron fluences ranging from $1x10^{14}$ to $1x10^{16}$ n/cm^2.

Any simulation methodology necessitates commensurate benchmarking as a prelude for validation of results generated by the simulation. In line with this, detailed benchmarking simulations were carried out for 100% enriched ^{10}B as converter material and Si as detector material for two test problems, viz., planar and stack geometries and compared with literature. The GEANT4 simulation result showed an excellent agreement with the literature results.

GEANT4 simulation for the boric acid as neutron sensitive converter material having 100% enrichment of ^{10}B in planar configuration revealed a maximum efficiency (η_{max}) of 0.73% for thermal neutrons at a critical thickness of 5 μm . Improvements in efficiency (η) were affected by adopting stack, embedded sphere, cylindrical perforation and cuboidal trench structured detectors. In the case of stack configuration, it was found that the η can be enhanced by increasing the number of detector units. For instance, 30 detector units in stack configuration leads to η_{max} 15.96% at a critical thickness of 3.5 μm having 100% enriched ^{10}B content in boric acid. It is clear that, the efficiency is much higher than the planar configuration. In the case of a single layer embedded sphere configuration, the η_{max} obtained from the simulation was 0.91% at a critical diameter of 9 μm. Improvement in efficiency was brought about by stacking single layer embedded spheres to 18.89% for 30 layers.

For a cylindrical perforation and cuboidal trench configuration, the optimum critical diameter and width was found to be ~8 μm respectively. It was also found that in both the configurations efficiency (η) increased with increasing depth. The typical efficiencies at same dimension of 8 μm diameter and width at a maximum depth of 275 μm were 16.21% and 13.02 % for cylindrical perforation detector and cuboidal trench detector, respectively. These efficiencies values are significantly higher than that of planar configuration.

Although boric acid is a preferred converter material (CM) in terms of its simplicity in coating on Si PIN diode, it has a low Q-value, thereby preventing setting up of higher LLD values for background gamma rejection. Therefore, in a typical nuclear reactor where background radiations are typically in high MeV range, boric acid as a converter material for neutron detection is not a preferred choice. Hence, an alternative converter material such as Depleted UO_2 (DUO_2) was explored. The simulations were performed for geometric configurations similar to boric acid except for the direct configuration mode. As DUO_2 is semiconducting in nature, it can be used in the direct configuration mode too.

From the GEANT4 simulation studies it was found that DUO_2 based semiconductor neutron detectors can be used for detecting dual neutron energies of thermal and fast neutrons, with good gamma discrimination, which is a distinct and indispensable advantage over other conventional converter materials. Efficient background discrimination is an inherent feature of this converter material, as the energy possessed by the generated fission products (in range ~200 MeV) are significantly above the background radiation. Efficiencies of DUO_2 based converter material detectors in both planar (direct and indirect) and three dimensional (3D) (cylindrical perforations and trench structures) configurations were studied. The simulation studies revealed that, for a typical thickness of ~1000 μm, η for thermal neutron (0.025 eV) and fast neutron (typically 10 MeV) detection for planar direct (indirect) configurations are 0.45% and 0.24% (0.0008%and 0.0004%), respectively. Even though the η of DUO_2 in planar direct configuration mode is significantly larger than the indirect configuration, synthesis and fabrication of controlled stoichiometry UO_2 is still a formidable task and poses a major challenge. It is shown that η of planar indirect configuration detectors can be further enhanced by creating 3D structures in Si detector. The simulations of 3D configurations of both cylindrical perforation and trench structure showed an enhancement in η over planar indirect configurations by two (one) orders for thermal (fast) neutrons. Therefore, as inferred from the simulations, for applications in high background environments which require good background discrimination, it is prudent to use DUO_2 in the 3D indirect configuration mode as a better choice of converter material.

In collaboration with IISc a BBM converter material coated on Si PIN diode planar neutron detector was fabricated. The critical thickness of BBM for maximum efficiency (η_{max}) was obtained from GEANT4 simulation and same was coated on Si PIN diode. The BBM coated Si PIN diode was exposed to the calibrated thermal Am-Be neutron source. Several noise sources were encountered in the neutron detection measurement and steps were taken to minimize the effect of noise on the measurement. A point to note that in order to study the background radiation contribution, an uncoated Si PIN diode was also exposed to the calibrated thermal Am-Be neutron source. Before exposing the BBM coated diode to thermal neutron source, the electrical characterization in terms of reverse I-V and C-V were measured to ascertain the effect of coating on diode. It was found from the I-V and C-V measurements that the coating had not affected the electrical functionality of diode. It is also to note that in the present work the functionality of read out electronics was tested by performing alpha spectroscopy experiment on uncoated Si PIN diode. The other objective of alpha spectroscopy was to check the sensitive of Si PIN diode to charged particles.

The last part of thesis focused on the electrical characteristics of neutron irradiated Si PIN diodes. From the studies it was found that the measured forward I-V characteristics, is increasingly becoming shallow upon increased irradiation fluence. Moreover, knee voltage increases from 0.5V for the virgin diode to ~ 36.3 V for diode irradiated to a fluence of ~ 5×10^{15} n/cm^2 and thereafter saturates. Whereas, the ideality factors extracted from the fit of the forward I-V characteristics to diode equations in the low/high voltage regions varied from a typical value of ~ 2 for the virgin case to ~ 496 for the highest irradiated fluence. The large ideality factors observed in this study are caused by the defects that are created upon irradiation. With increase in neutron fluence, the reverse leakage currents also increased by almost four orders of magnitude owing to the production of a large number of defect states that act as generation-recombination centres upon neutron irradiation. Another important consequence of the increase in neutron fluence of irradiation is the transformation of diode properties from a rectifying to ohmic one, which was inferred from the progressive decrease in gap between the forward and reverse currents. Further, quantitatively, the rectification ratio decreased from 10^8 for virgin diode to 84 for the maximum neutron irradiated fluence of 1×10^{16} n/cm^2. The quantitative behaviour of diodes in terms rectification ratio shows that it rectification property have been degraded drastically with the increase in neutron fluence.

7.3 Scope for future research

1. In the present GEANT4 simulation work, the dead layer contribution on efficiency was not included. The dead layer effect should be included in GEANT4 simulation which will give a more accurate estimate of efficiency.

2. The three dimensional (3D) detector configuration simulation result needs to be validated with the experiments for different converter materials.
3. The depleted UO_2 semiconductor device can be fabricated and tested for its detection of neutron in radiation environment.
4. Other alternate radiation hardened semiconductor like SiC, GaAs can be explored since Si detector electrical performance degrades at higher neutron irradiation fluence.
5. A portable nuclear readout electronics needs to be designed which can be integrated with the semiconductor detector.